REPORT NO. P76-448
HAC REF. NO D2617

CR151336

NAS 9-14273

# SHUTTLE IMAGING RADAR (SIR) CALIBRATION STUDY

FINAL REPORT

November 1976

ADVANCED PROJECTS LABORATORIES
ADVANCED PROGRAMS DEVELOPMENT
RADAR SYSTEMS GROUP

HUGHES

HUGHES AIRCRAFT COMPANY
CULVER CITY, CALIFORNIA

MAY 1977
RECEIVED
NASA STI FACILITY
INPUT BRANCH

# CONTENTS

# LIST OF ILLUSTRATIONS

## LIST OF ILLUSTRATIONS (Continued)

# 1.0 INTRODUCTION

This is the second preliminary design report by the Hughes Aircraft Company on the Shuttle Imaging Radar (SIR). The first, entitled "Earth Resources Shuttle Imaging Radar," was published in October 1975. It included designs for both the space radar and the ground processor. The baseline design is a two-frequency radar, X-band and L-band with dual polarization (horizontal and vertical) at each frequency. The ground processor subsystem produces four images of four looks each, one for each frequency and polarization combination; e.g., an X-band horizontally polarized image and an X-band vertically polarized image.

All SIR designs include radar calibration for measuring the radar backscattering characteristics of the imaged terrain. Such measurements have been made with SAR imagery in the past, but with nowhere near the accuracy required for the SIR applications. To achieve the required accuracy for the backscattering coefficient measurement (about 2 dB with 80 percent confidence), the space hardware design must include a means of monitoring the state parameters of the radar. For example, the transmitter output power is sampled and a replica of its output waveform is circulated through the receiver. These are recorded digitally and are used on the ground to determine such radar parameters as the transmitter power and the receiver gain. This part of the data is needed by the ground processor to measure the terrain backscattering characteristics.

This report contains a description of this radar calibration subsystem and discussions of its performance and implementation.

## 1.1 THE MEASURED QUANTITY

The SIR system can measure the radar cross section for each image resolution cell. If available knowledge of the radar and propagation were perfect, this measurement would depend on the contents of the resolution cells and the viewing angle. A resolution cell containing a man-made structure, such as part of a metal frame building or a radar corner reflector, could have a large radar cross section over a wide range of viewing angles (Figure 1). In this case, the radar cross section would afford indication of the material and structures within the resolution cell. But, no interest in such radar cross section measurements of cultural objects for earth resources has been expressed; so, although the SIR design provides the capability for making these measurements, it was not studied here.

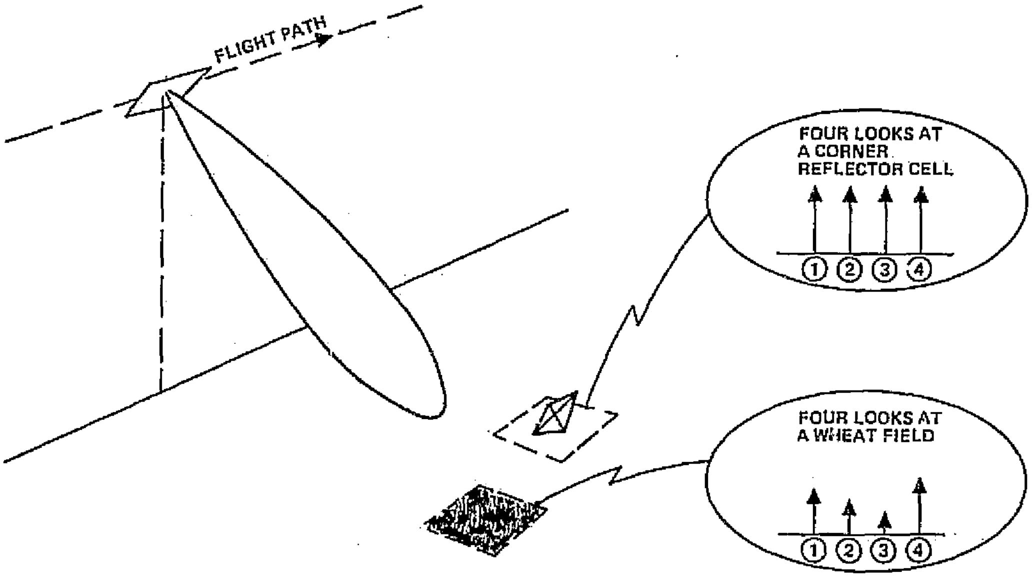

Figure 1. Dependence of radar cross section on resolution cell contents and direction of viewing

Measurements of diffuse backscattering were considered. A resolution cell containing diffuse backscattering elements such as a field of wheat or just bare terrain has a radar cross section that is highly dependent on the direction from which it is viewed. Because of this dependence, the average rather than the individual radar cross-section measurement is of interest. Also, the average radar cross section of the cell is almost always normalized by the cell area, so that it represents the radar cross section per unit area of terrain. The preliminary design analyses and the results presented here are concerned with this normalized, average cross section (denoted $\sigma_0$).

## 1.2 APPROACH TO MEASUREMENT

A single, high accuracy measurement of the average backscattering coefficient requires many — more than 30 — individual measurements of resolution cell radar cross section. Since SIR forms four images at each frequency and polarization, (i. e., each mode involves four looks) only four radar cross-section measurements are available for each resolution cell; while the image can be improved significantly by averaging the four looks, four samples are plainly inadequate for a single average backscattering measurement. To obtain the needed radar cross-section estimates, resolution cells from a region of ground extending over several resolution cells must be used (Figure 2).

The extent is a function of single-to-noise ratio; for a single-to-noise ratio of 8 dB, about 64 looks or samples are needed. A ground region 100 by 100 m is covered by 16 resolution cells (25 x 25 m). Since each resolution cell has four looks, this region of ground would provide the needed 64 looks.

For the baseline design discussed in this report, the final $\sigma_0$ measurement for the 100 x 100 m region would have an accuracy of 2.5 dB, with a confidence of 80 percent. Thus, a high accuracy measurement of the average backscattering coefficient is obtained by spatially combining several resolution cells. If the measurements of these resolution cells were plotted

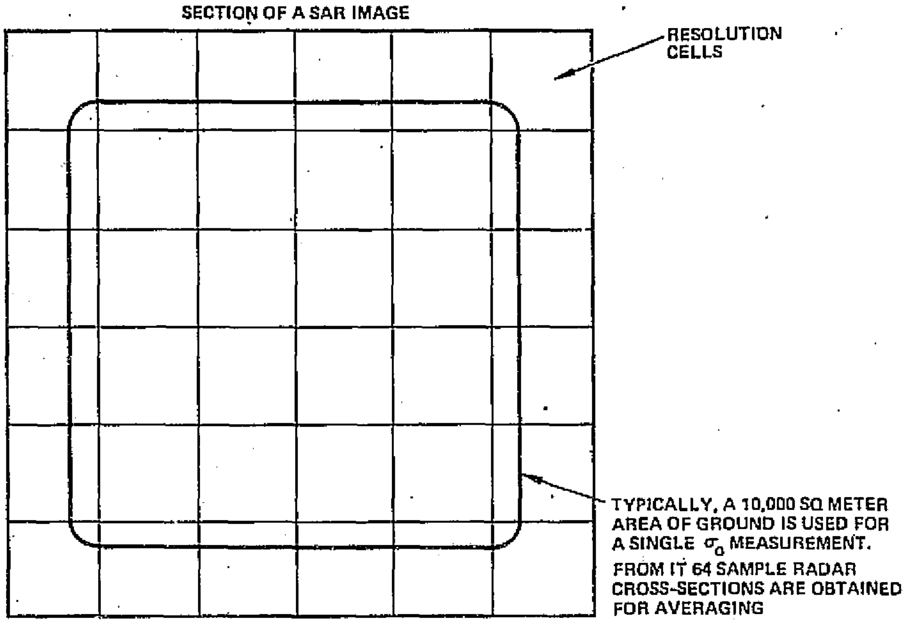

Figure 2. Accurate average required for many radar cross section measurements

for a $\sigma_o$ map, the result would be of lower resolution than the 25 x 25 m of SIR; in the preceding example it would be 100 x 100 m.

In this report, only single $\sigma_o$ measurements are discussed. The experimenter is presumed to be at the ground processor, where he indicates that region of image from which the resolution cells are to be taken. He uses a probe to circumscribe that region of ground from which the cells for the measurement are to come; with this probe he can also delete any cells in this region not wanted. The end result or output would then be a single $\sigma_o$ measurement, accompanied by an estimate of the signal-to-noise ratio, the accuracy of the measurement, and the number of samples used in the estimate.

There are other approaches to the $\sigma_o$ measurement. For example, a $\sigma_o$ map could be made for an entire 85 x 85 km image frame instead of for a selected region. Typically, such a map would have a resolution of 100 x 100 m, which is considerably more complex than what has been above. Such a map would make it more difficult for the experimenter to control the kind of data used. In the approach presented here, the experimenter does part of the estimation. He can eliminate contamination such as farm buildings, power lines, and other extraneous elements from the input region. This would be more difficult to accomplish with a $\sigma_o$ map.

The approach taken here can be extended in various ways; one of the more important is to provide a "constant - $\sigma_o$" test. When the experimenter circumscribes a region for a $\sigma_o$ measurement, the system assumes that $\sigma_o$ does not vary within the region. Knowledge of the statistical characteristics for the class of backscatterers to which the region presumably belongs can provide a basis for developing a test of this constancy. Such tests are best developed when experimental data are available for verification.

The Hughes approach to measurement was selected because a basic algorithm was needed for making $\sigma_o$ estimates with the ground processor. With the evolution of that algorithm, it was easier to determine the required data base and to isolate certain critical radar parameters to which $\sigma_o$ measurements might be sensitive.

The first operation the processor executes in making a backscattering measurement ($\sigma_o$ - measurement in Figure 3) is to form an image of the area of interest. The experimenter then centers a cross hair in the region of interest, which results in re-centering the displayed region on this point and also expanding it. The experimenter then designates the specific region of the display for which a $\sigma_o$ measurement is to be made. The original radar data are then reprocessed to form a new image.

Reprocessing is necessary because the four SAR looks used in making the $\sigma_o$ - measurement must be symmetrically located in the antenna pattern. If they are not, the final accuracy of the measurement will be quite sensitive to the known accuracy of the antenna pattern.

After the four SAR looks are centered and the image is reformed, the amplitudes of those pixels circumscribed by the experimenter are used to calculate the average backscattering coefficient, $\sigma_o$. In making this calculation, certain variables other than those provided by the radar system are needed: propagation loss, land altitude, and land slope. The importance

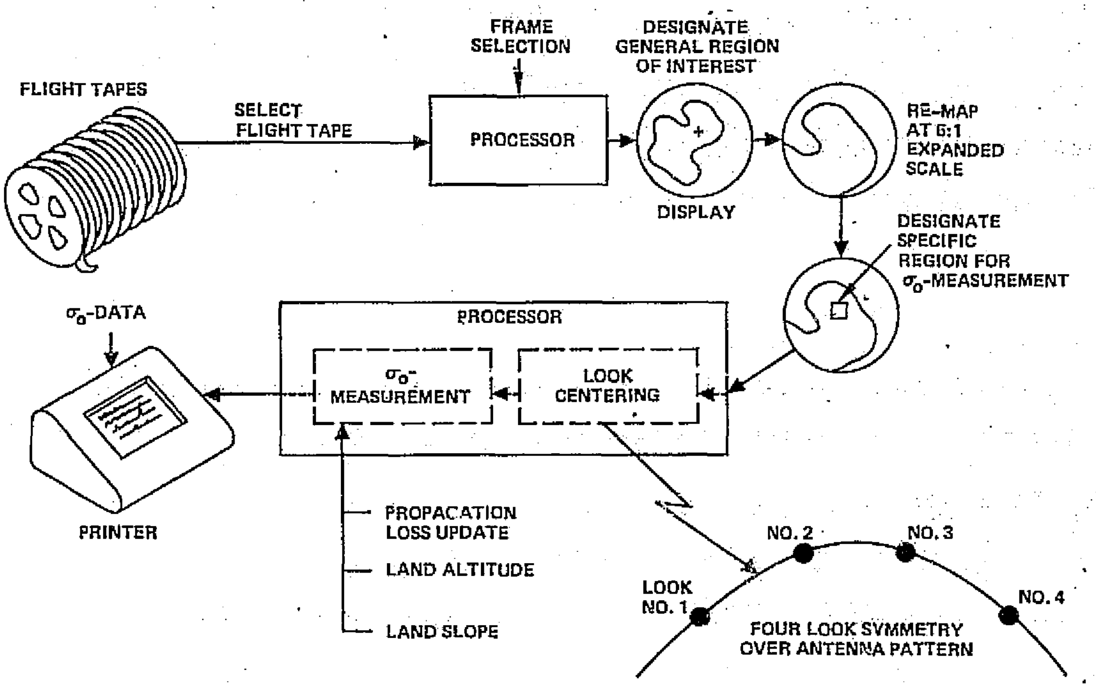

Figure 3. $\sigma_o$ measurement sequence

of these is about the same for L- and X-band, except for the propagation loss, where the extent of data needed for the L-band loss is much less than for X-band.

After the processor completes the $\sigma_o$ - calculation the result is printed at the output terminal.

## 1.3 CALIBRATION APPROACH

Calibration is the determination of those quantities needed to form an SAR image with pixel amplitudes equal to the square root of the backscattering coefficient (or the backscattering coefficient times a known constant). The pixel amplitudes of an uncalibrated SAR image are affected by the state of the radar and the state of the troposphere. The receiver gain can increase and cause an increased image amplitude for a fixed pixel backscattering coefficient. Similarly atmospheric attenuation can be less at one geographical point than another and cause the image amplitude for the same backscattering coefficient to be greater in one instance than the other.

Fortunately, these variations in the tropospheric and radar states are fairly slow, so the image patterns are not distorted. The variations, however, do present difficulties when making measurements of the radar backscattering characteristics of the terrain within a pixel. Since the pixel amplitudes are used in estimating the radar backscattering coefficient, an image must be produced with pixel amplitudes equal to the backscattering coefficient (times a known constant). In this SIR system, a conventional uncalibrated image is formed first and then converted to a calibrated image.

The quantities needed to make a calibrated image are determined by estimating the effects of the radar components and the environment on image amplitude. Such effects are mostly multiplicative; only one, noise, is additive. The major radar and environmental contributors are seen by tracing the flow of energy from the transmitter to the image (Figure 4). First, the RF energy is generated by the transmitter and radiated, then, atmospheric propagation loss, the receiving aperture, receiver gain, and finally the data transmission medium and ground processing. Each of these can vary, and each is measured in the calibrated radar system. For transmitter-power and receiver gain, the measurement is direct. To determine the antenna gain contribution, the location of the pixel (i. e., resolution cell) in the gain pattern must be known, therefore, antenna pointing measurements are made, and the pixel position is accurately located.

Atmospheric loss for L-band can be estimated by using a very simple seasonal and geographical model. However, to achieve a high accuracy of calibration, the atmospheric loss model for X-band should include estimates of existing meteorological conditions.

In the preceding, the antenna gain and antenna pattern were assumed and did not vary significantly. These facts are necessary to calibration, and the assumption appears correct. However, some question exists as to whether antenna gain and pattern can be predicted adequately from ground measurements. Measurements can be made on the ground for antennas as large as those of the Shuttle Imaging Radar, but experience is needed in making the desired predictions from these measurements. The antenna will be effected both electrically and thermally by interactions with its environment; since the gain and pattern must be known with very high accuracy, it

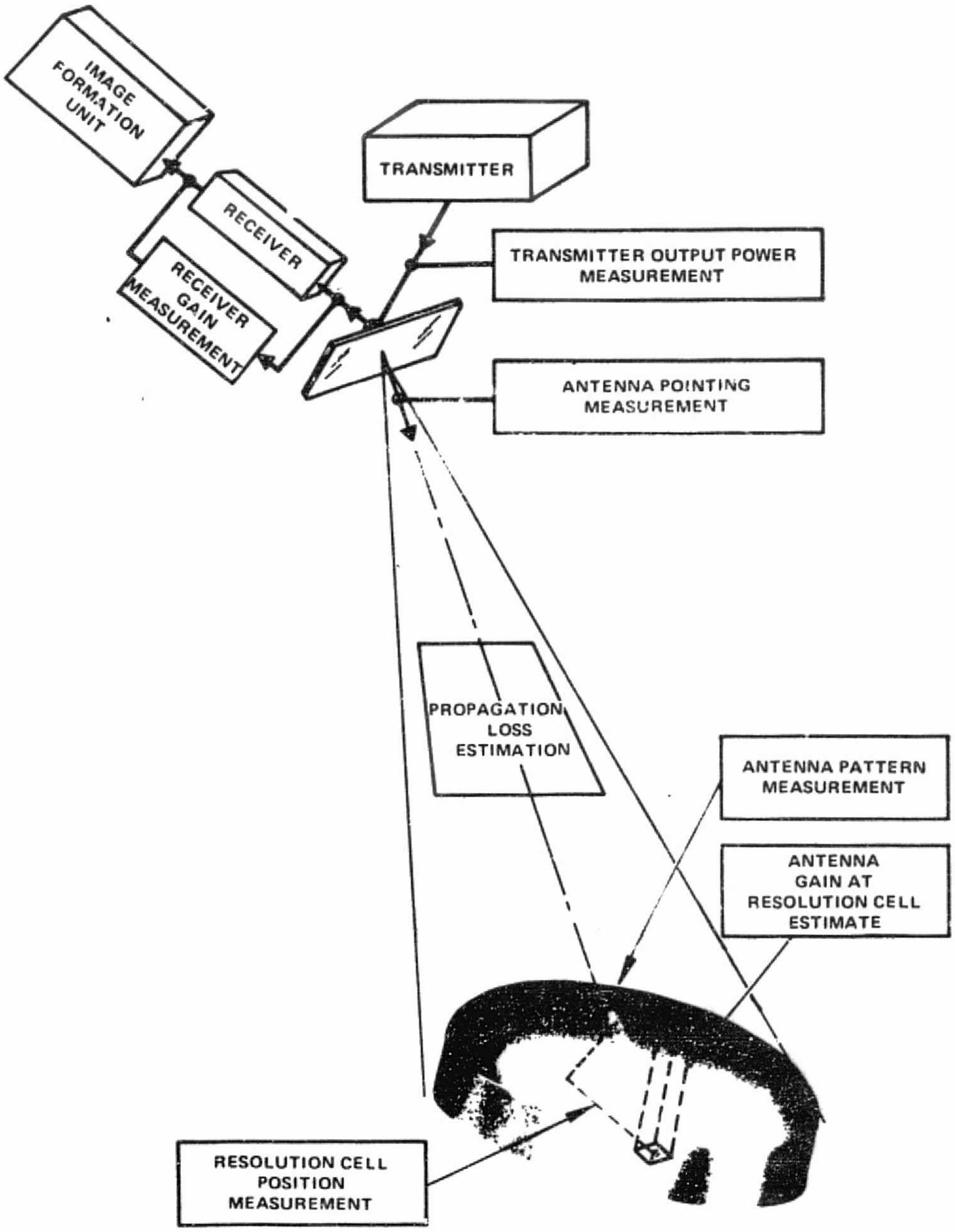

Figure 4. Primary functions in SIR calibrations

is not certain that these interactions can be adequately accounted for from the ground. For this reason it is recommended that a corner reflector farm be used during SIR to make gain and pattern measurements.

## 1.4 CALIBRATION ACCURACY

The SIR sensor can be calibrated to an absolute accuracy of about 0.65 dB RMS, exclusive of propagation effects. The calibration precision at X-band wavelengths with moist cloud cover is estimated to be about 0.70 dB RMS. The calibration accuracy is obtained by frequent use of precision pilot signals that are proportional to transmitter power-receiver gain products and infrequent use of an array of 16 corner reflectors for calibrations which include antenna gain, pattern, and propagation loss factors.

The calibration precision for SIR includes a "fixed" component of about 0.5 dB, the mean uncertainty of calibration over the duration of a mission, and a "temporal" component of about 0.45 dB, which is the deviation of calibration. The fixed and temporal components are given in Table 1.

TABLE I. ERROR STRUCTURE ASSUMPTIONS

| Fixed Errors | Temporal Errors |
|---|---|
| Antenna Gain Pattern | Antenna Pattern Orientation (0.3 dB budgeted error) |
| Transmitter Power, Receiver Gain Product | Terrain Incidence Angle (typically 0.6 dB/deg at an incidence angle of 10 degrees) |
|  | Propagation Path Loss (typically total loss 0.3 dB at X-band) |

The temporal component is highly correlated for durations of about 10 seconds, corresponding to distances of about 75 km, and essentially independent over much greater time intervals or distances. It represents the "relative" calibration accuracy for $\sigma_o$ - measurements made at the same place but on different orbits or at widely spaced distances, either on the same orbit or on different orbits.

The calibration errors establish the limiting measurement accuracies for cases in which $\sigma_o$ applies to very large areas. These areas are large enough for the removal of scintillation errors by averaging measurements from many individual cells. The limiting measurement accuracies are customarily expressed in dB at an 80 percent confidence level as shown in Figure 5. The calibration limited measurement accuracies, with a normal distribution of calibration errors, are given below:

| Error Category | Standard Deviation of Error, dB | Limiting Accuracy at 80 Percent Confidence, dB |
|---|---|---|
| Absolute | 0.65 | 1.8 |
| Relative | 0.45 | 1.2 |

## 1.5 MEASUREMENT ACCURACY

Measurement accuracies of 2.5 dB at 80 percent confidence can be obtained with the SIR sensor, both at X- and L-band, for general conditions exclusive of precipitation, with four looks and smoothing over an area of 150 by 150 m (36 resolution cells at two-dimensional resolutions of 25 m). Measurement accuracies for a given area are limited by the three components of error, as shown by

$$\frac{\epsilon_\omega}{\sigma_o} = \epsilon_M + \epsilon_{10\,sec} + \epsilon_I$$

Examples of contributing error sources are given in Table 2.

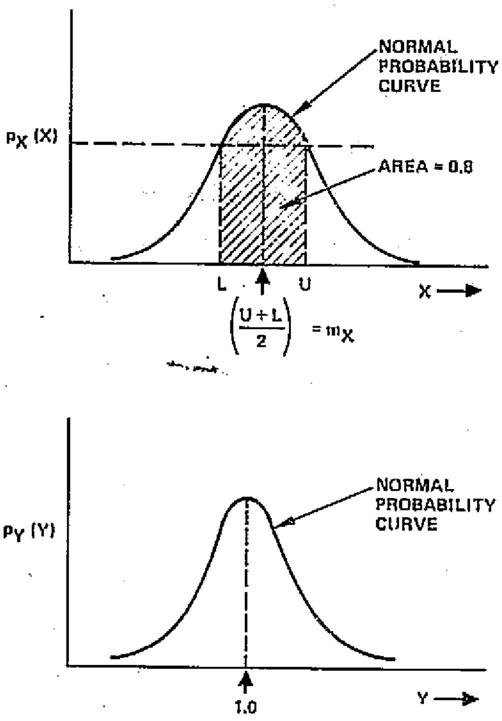

LET: $\int_U^L p(X)\,dX = 0.8$

AND

$$Y = \frac{X}{\left(\frac{U+L}{2}\right)}$$

THEN: (1) $m_Y = 1$

$$(2) \quad \sigma_Y = \frac{\sigma_X}{\left(\frac{U+L}{2}\right)} = \frac{\sigma_X}{m_X}$$

$$(3) \quad \left(\frac{U}{L}\right) = \frac{1 + 1.282\,\sigma_Y}{1 - 1.282\,\sigma_Y}$$

$$(4) \quad \sigma_Y = \frac{\left(\frac{U}{L}\right) - 1}{1.282\left(\frac{U}{L} + 1\right)}$$

$\sigma$- ERROR IN dB = $10 \text{ LOG } (1 + \sigma_Y)$

80% CONFIDENCE INTERVAL IN dB = $10 \text{ LOG} \left(\frac{U}{L}\right)$

Figure 5. 80 percent confidence interval and standard deviation

TABLE 2. $\sigma_o$ MEASUREMENT ACCURACY STRUCTURE

| Error Component | Period of High Correlation | Contributing Errors |
|---|---|---|
| $\epsilon_M$ | 1 mission | 1. Antenna gain and shapes<br>2. Transmitter power-receiver gain |
| $\epsilon_{10\ \mathrm{sec}}$ | 10 seconds | 1. Receiver noise measurement<br>2. Antenna pointing<br>3. Large area propagation loss |
| $\epsilon_I$ | 0 (little correlation between measurements) | 1. Short term variation in propagation loss<br>2. Scintillation in ground return<br>3. Ground slope and object area altitude |

Measurement accuracies are given in Table 3 for areas of 1 hectare (100 x 100 m) and 2.25 hectares (150 x 150 m). Measurement accuracies are given for the baseline $\sigma_o$ - measurement algorithm, and for an algorithm of near optimum performance. The baseline algorithm is computationally simple, but the measurement has accuracy limitations caused by the correlations between nearby measurement cells and the overlapped multi-looks (the four looks are overlapped 45 percent to improve antenna illumination characteristics). Measurement accuracies are improved with the near optimum $\sigma_o$ - measurement algorithm which is more efficient at the expense of computational complexity. The improvement for small area measurement is apparent (2.7 dB with the optimum as opposed to 4.0 dB with the baseline algorithm for an area of 1 hectare, 100 x 100 m). Signal-to-noise ratio is 8 dB in all cases.

The independent component of measurement error $\epsilon_I$ is included in the table. This error has a dominant term because of the scintillation component in the ground return. This error is reduced by smoothing the measurement from larger areas of terrain. It may be noted that the advantage of the near optimum algorithm is pronounced for the smaller area (0.6 versus 1.0 dB), but its advantage relative to the baseline is relatively minor for the larger area. The error is expressed in terms of the standard deviation of error for this term, as it is for the $\epsilon_{10\ sec}$ (temporal) term and for the $\epsilon_{MIS}$ (fixed) error term. The latter errors are functions only of the calibration accuracies.

## 1.6 CRITICAL CALIBRATION AND MEASUREMENT ISSUES

The accuracy of $\sigma_o$ - measurement depends on the area of terrain whose mean $\sigma_o$ is sought, the measurement algorithm, signal-to-noise ratio, calibration accuracy, terrain altitude, terrain slope and, at short wavelengths ($\lambda < 5$ cms), atmospheric losses.

The critical issues with respect to calibration are listed below:

1. What facilities are required to determine adequately antenna peak gain and pattern (beamwidths) factors?
2. What measures are needed to determine the stability of antenna gain and pattern factors (between calibrate updates)?

TABLE 3. BASELINE ACCURACY FOR 8 dB SN

| $\sigma_o$ Measurement Algorithm | Ground Region Dimension (R x W) | $\sigma_o$ Measurement Variances for Both L and X-Bands, dB | | | |
|---|---|---|---|---|---|
| | | $\left(\sqrt{\mathrm{Var}\left(\overset{W}{\sigma}_o\right)}\right)$ 80% Confidence | $\left(\sqrt{\mathrm{Var}\ (\epsilon_{MIS})}\right)$ $\sigma$-Error in dB | $\left(\sqrt{\mathrm{Var}\ (\epsilon_{10\ sec})}\right)$ $\sigma$-Error in dB | $\left(\sqrt{\mathrm{Var}\ (\epsilon_{I})}\right)$ $\sigma$-Error in dB |
| Baseline | (100 x 100 m) | 4.0 | 0.5 | 0.4 | 1.0 |
| Baseline | (150 x 150 m) | 2.5 | 0.5 | 0.4 | 0.5 |
| Near Optimum | (100 x 100 m) | 2.7 | 0.5 | 0.4 | 0.6 |
| Near Optimum | (150 x 150 m) | 2.4 | 0.5 | 0.4 | 0.5 |

3. What facilities are needed for accurate determination of transmitter-receiver gain products?

Antenna peak gain and pattern stability begin with an antenna design that has approximately predictable performance characteristics for the shuttle environment, including thermal stresses. A promising approach to the antenna is a planar array deployed for an unobstructed view of the terrain and carefully designed with respect to thermal stresses encountered in the shuttle imaging missions. Antenna designs and ground tests that provide the basis for performance analysis are required. The facilities for accurate calibration from space are needed.

Accurate measurement of antenna gains and patterns from space is the most critical issue of calibration. A single calibration measurement with a precise standard for gain and pattern measurement is not sufficient because of substantial uncertainties associated with finite signal-to-measurement noise, antenna pointing errors, and target position errors with respect to image processing coordinates. The study proposes that an array of 16 precise standard cross-section (corner reflector) targets be employed (separate arrays for dual L-, X-band systems, a common array for dual C-, X-band systems). The selected array geometry and processing algorithms for calibration should have the objective of minimizing overall calibration errors, including errors of geometry and target cross-sections.

Ideally, several calibration cycles with corner reflector farms should be performed for each SIR mission to provide accurate measurements of calibration stability. However, a return to a fixed calibration farm is impractical because of the short duration of the initial SIR missions (5 to 7 days). Further, the considerable expense of providing adequate facilities makes the duplication of calibration farms questionable. Thus, corner reflector calibration data obtained on a single pass must be as dependable as possible. The standard targets should be portable and must be rugged; they can then be used at two or more locations to provide data with some indication of calibration stability during a single mission. It may be possible to use several calibration points by moving them to suitably chosen and monitored locations that will be accessible on later orbits.

Frequent calibrations of transmitter power-receiver gain product are possible. These may be made by using appropriately designed generators of pilot signals that are precisely proportional to transmitter power.

Design approaches addressed to the critical calibration issues are discussed in the following sections. Appropriate algorithms for effective use of calibration facilities are also discussed.

The accuracy of the SIR $\sigma_o$ measurement increases with the size of the data set used in computation. However, there is a practical limit of the number of multiple looks and to the terrain area used in measurements. For 25 m resolutions, four multiple looks at a single resolution cell can be made to smooth measurement errors. This limitation is imposed by antenna illumination considerations. The accuracy obtainable with a given small area (e.g., 1.0 to 2.25 hectares or 16 to 36 cells, 25 m resolution each) is a critical measurement issue.

A nearly optimum measurement algorithm for accuracy is possible, and an algorithm that approaches the theoretical limit of accuracy (the Cramer-Rao lower bound) is developed and presented.

This nearly optimum measurement algorithm is somewhat more complex and requires more computations than the baseline algorithm, which performs simple power averages on the individual cell image outputs. The baseline algorithm is selected because of its simplicity and relative computational efficiency. However, it does require a somewhat larger area (e.g., about 2.25 hectares as compared to 1.0 hectare for the nearly optimum algorithm).

The $\sigma_o$ measurement accuracy is dependent in part on geometry and the atmospheric propagation losses. Consideration of geometry is an issue that requires some provision for processing with local terrain profile data to meet stringent accuracy requirements. Provisions for processing with meaningful models of current atmospheric propagation losses permit the attainment of reasonable accuracies at short wavelengths with the cloud cover penetration capabilities of the SIR remote sensor.

# 2.0 CALIBRATION DESIGN CONCEPT

SAR image output data will be used in measurements of terrain and vegetation canopy reflectivity. Reflectivities are used to deduce moisture content of soil, type and vigor of farm crops, bio-mass of forage crops, land use for animal husbandry, etc. To obtain these vital agronomic data, the SAR sensor must be calibrated for the accurate measurement of the reflectivity factor $\sigma_o$.

A parameter calibration design concept for the accurate measurement of $\sigma_o$ with SIR remote sensor data is presented. The concept involves three major elements of the SIR measurement process:

1. The two-way link between the antenna and the imaged terrain, including the intervening atmosphere with its propagation properties.
2. The transmitter-receiver electronics in the shuttle.
3. The image formation process with appropriate measurement algorithms.

These elements and their primary constituents were illustrated in Figure 4.

The discussion is specifically addressed to the shuttle imaging radar with on-board data recording and ground processing for image formation. The considerations apply to space processing as well, with, at most, a difference in emphasis. For example, automation of calibration algorithms and procedures is essential to real time processing in space, whereas operator intervention and multiple data passes are practical with ground processing.

Calibration consists of the determination of radar parameters $K_{rad}$, a set of gain parameters $g_i$ related to antenna pattern and orientation, and a receiver noise power $N_o$, each necessary for $\sigma_o$ measurement, as illustrated in Figure 6. The $\sigma_o$ measurement inputs are un-normalized amplitudes $y_i^u$ obtained from terrain backscatter data identified with the specific resolution cell i. These complex (voltage) amplitudes have the following structure:

$$y_i^u = X_i^u + Z_i^u \text{ (terrain plus noise)} \qquad (1)$$

The expectancy (variance) for the terrain component $X_i^u$ is

$$E\left\{ \left| X_i^u \right|^2 \right\} = K_{rad}\, g_i^2 \sigma_o \qquad (2)$$

and for the additive receiver noise component $Z_i^u$,

$$E\left\{ \left| Z_i^u \right|^2 \right\} = N_o^u \qquad (3)$$

where:

$g_i$ is the normalized antenna power for coordinates appropriate to each look at cell i, $\sigma_o$ is the terrain backscattering coefficient to be measured, and

$$K_{rad} = \frac{P_T G_o^2 \lambda^2 d_a d_r \Gamma_r}{(4\pi)^3 R_S^4 L_{at} L_{sys} \sin\phi}\; N_{pc}^2 N_{pulses}^2 \qquad (4)$$

In Equation (4), the symbols stand for SAR parameters:

$P_T$ = transmitter peak power (watts)

$G_o$ = antenna peak power gain

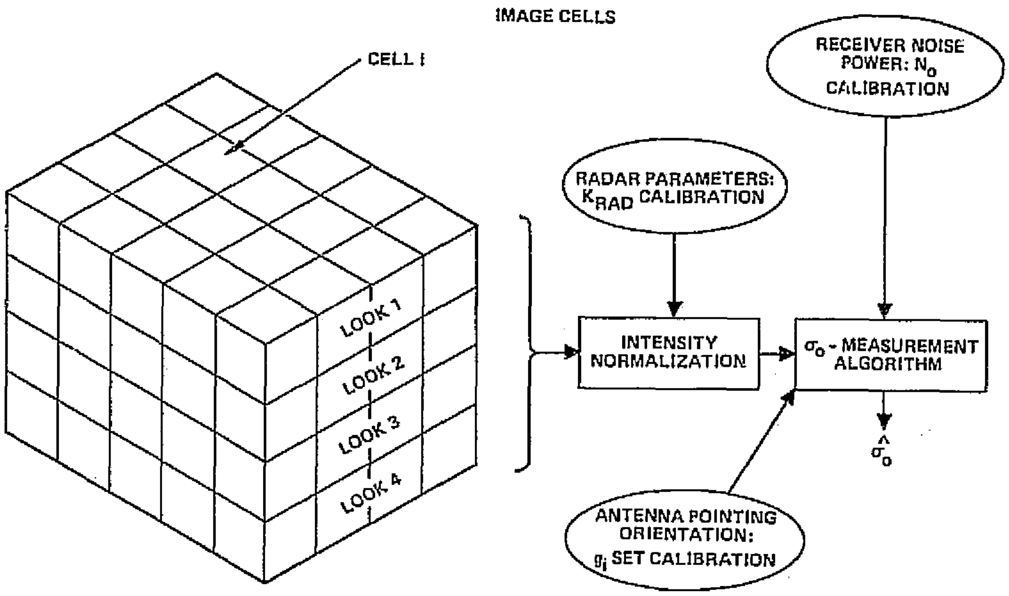

Figure 6. $\sigma_o$ measurement

$d_a d_r$ = dimensions of resolution cell ($m^2$)

$\Gamma_r$ = receiver power gain

$R_s$ = slant range (m)

$L_{sys}$ = system loss (loss between reference planes for $P_T$ and $G_o$ plus the loss between reference planes for $G_o$ and $\Gamma_r$)

$L_{at}$ = two-way propagation loss in the medium between the antenna and the reflecting terrain

$\phi$ = local incidence angle at the terrain

$\lambda$ = wavelength (meters)

$N_{pc}$ = $k_s BT$, sum for pulse compression (B is bandwidth and T the duration of the transmitted waveform), $k_s > 1$

$N_{pulses}$ = $f_r T_a$, sum for azimuth (time) compression ($f_r$ is the pulse repetition frequency and $T_a$ the synthetic aperture integration time).

The radar parameter $K_{rad}$ is the product of three terms:

$$K_{rad} = C_S C_G C_{R,\phi} \tag{5}$$

where:

$$C_S = P_T \Gamma_r N_{pc}{}^2 N^2{}_{pulses}, \text{ factor depending on the space SAR;} \qquad (6)$$

$$C_G = \left(\frac{\lambda G_o}{4\pi}\right)^2 \left(\frac{1}{4\pi L_{sys}}\right), \text{factors which vary very slowly with time;}^*$$

$$C_{R,\phi} = \frac{d_a d_r}{L_{at} R_s{}^4 \sin\phi}, \text{ factors depending on resolutions, range,}$$

incidence angle, propagation loss.

The calibration design concept involves the following procedures:

1. For space factors $C_s$, $N_o$.
   a. Produce calibrate record data for
      (1) Pilot image maps of the product of transmitter power and receiver gain (Figure 7)
      (2) Sensor noise image maps of receiver noise power (Figure 8)
   b. Implement processor algorithms for calibration measurements $\overline{C}_S$ for $C_S$ and $\overline{N}_o$ for $N_o$
2. For antenna gain $G_o$ and antenna pattern $g_i$-sets
   a. Provide a field of standard targets (corner reflector farm)
   b. Implement a modified image processing mode for calibration measurements $\overline{G}_o$ for $G_o$ and $\overline{g}_i$-sets for the pattern factors $g_i$. **

---

*The estimate $\overline{C}_G$ for $C_G$ will properly include compensation for time variations due to known thermal and related environmental factors.

**The calibration algorithm for the corner reflector farm data is end-to-end and includes the $C_s$ parameter of space calibration; thus the algorithm for measurement of $C_s$ is updated in conjunction with appropriate space calibration data of the $K_{rad}$ parameters.

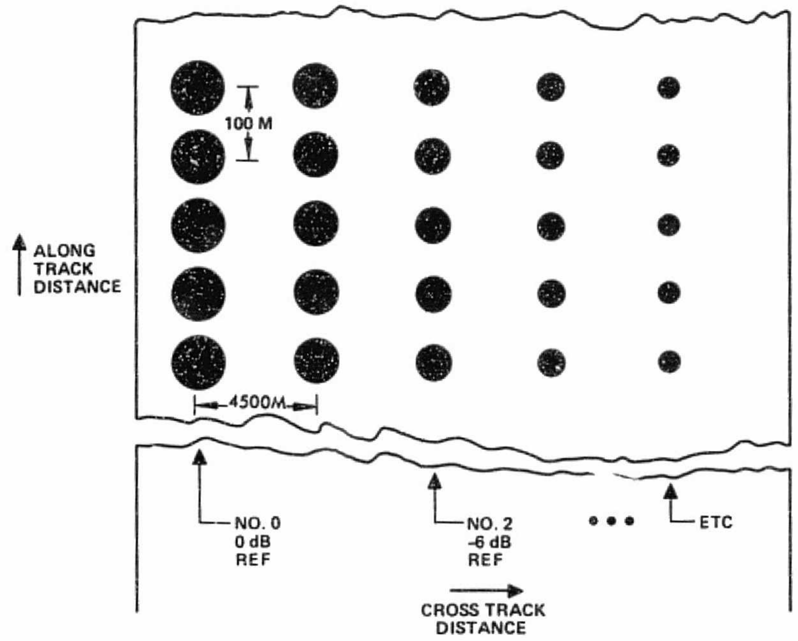

Figure 7. Pilot image map

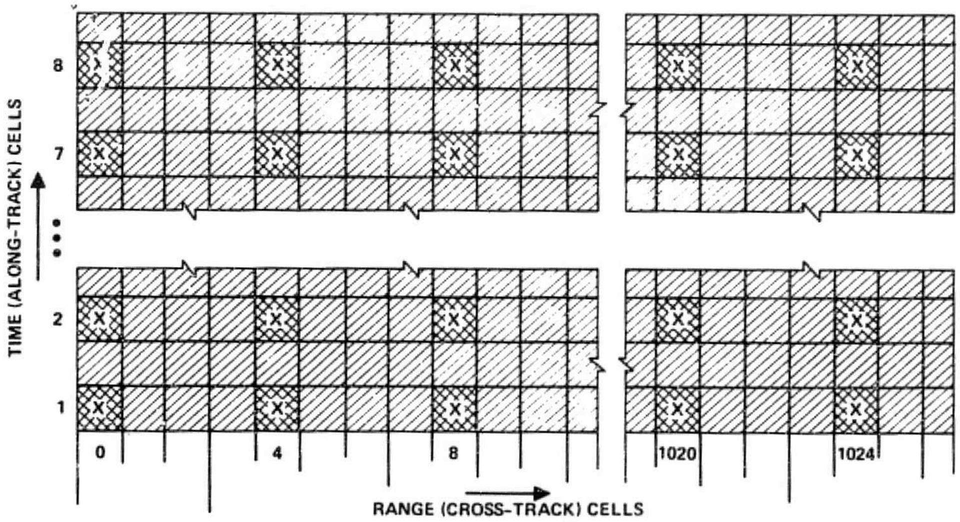

Figure 8. Noise image map (noise measurements are made in 8 time x 256 nonoverlapping cells)

## 2.1 SPACE CALIBRATION FUNCTIONS

Radar calibrations are made at the beginning and end of each mapping sequence. The three steps in space calibration are discussed in this section.

The first step in the calibration and measurement sequence is a 5-minute warm-up and power measurement period, illustrated in Figure 9. The transmitter waveform is sampled with a calibrated coupling device at a point very near the antenna corporate feed, then the power in the pulsed waveform is measured with a precision instrument and the measurements recorded. Power reflected because of imperfect matching of the transmitter coupling to the antenna feed system is also measured and recorded. Critical voltages, temperatures and parameter data (PRF, pulse duration, bandwidth, etc.) are included in the data recorded to establish the technical status of the transmitter function.

The second step is to record pilot signal data. A replica of the transmitter waveform is sampled at a "Pilot Signal Generator" port (the exciter

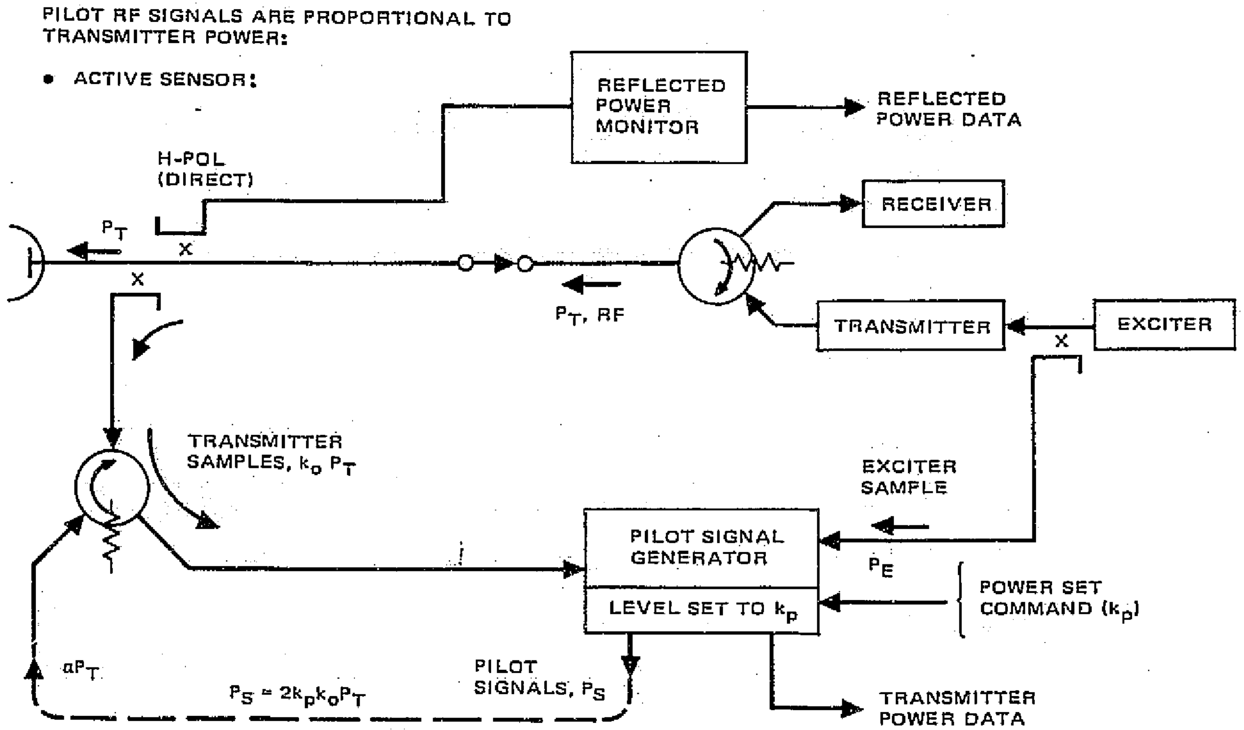

Figure 9. Sensor pilot mode transmitter power determination

RF drive signal sample "$P_E$" in Figure 9) and attenuated to match precisely the power of the transmitter samples ($k_T P_E = k_o P_T$).* The pilot signals are set to a command level $k_p$ relative to the transmitter sample power $k_o P_T$ for the pilot mode calibrate data record function.

Receiver RF pilot signals are coupled over a path that includes as much of the relevant system RF coupling to the antenna feed structure as is practicable (Figure 10). The pilot signal mode is a passive mode; the transmitter is de-activated (modulation of the gridded power amplifier is interrupted) and the antenna coupled to the receiver in an operational configuration to provide a normal external noise environment.

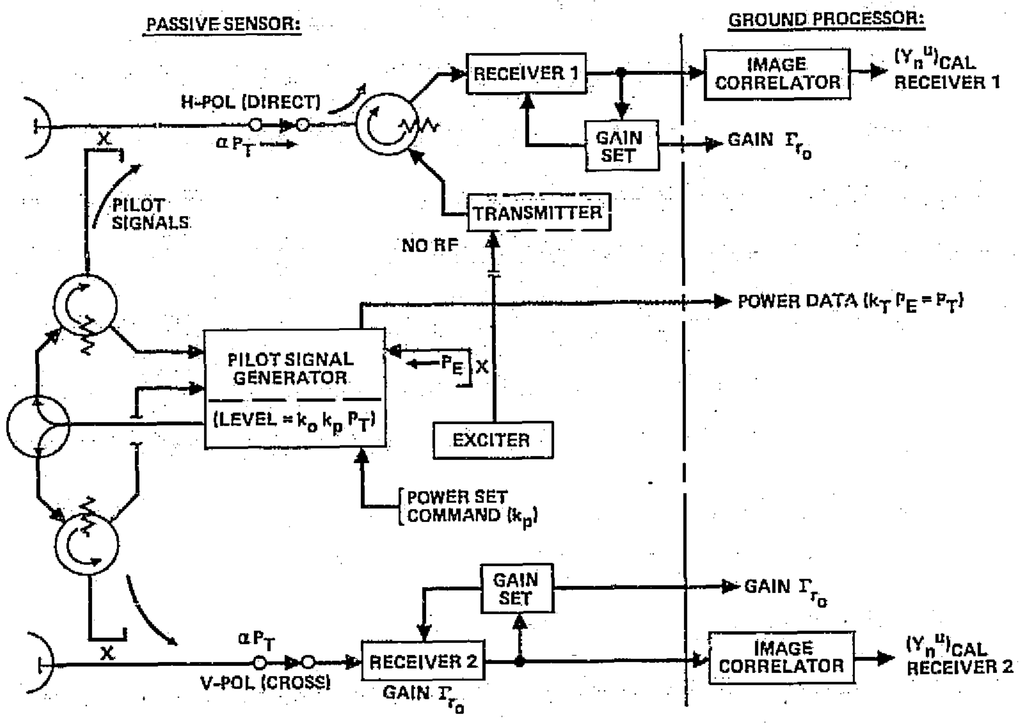

Figure 10. Pilot mode

---

*The samples $P_E$ may be coupled at the output of the transmitter and the transmitter coupling switched to an internal dummy load for the subsequent pilot signal record sequence to be described. However, this step requires the addition of the high power switch and dummy load as well as provision of at least 150 dB receiver isolation to permit sensitive pilot signal calibrate record data at zero time delay. These considerations recommend the use of the exciter RF drive samples $P_E$.

The pilot signals form a sequence of logarithmically decremented signals, precisely proportional to the transmitter power.* The conceptual approach for the pilot signal generator pulse train is shown in Figure 11; each RF waveform sample is circulated M times in a loop with a delay element (delay $T_D$, approximately 30 μs) and with a gain of precisely -3 dB. Thus, successive pulses decrease in power level by 3 dB decrements, and receiver calibrate data are provided over a range of 36 dB for 12 successive range samples. The receiver structure is illustrated in Figure 12. Pilot signal data are recorded for 3 seconds at the beginning and end of each SAR data set.

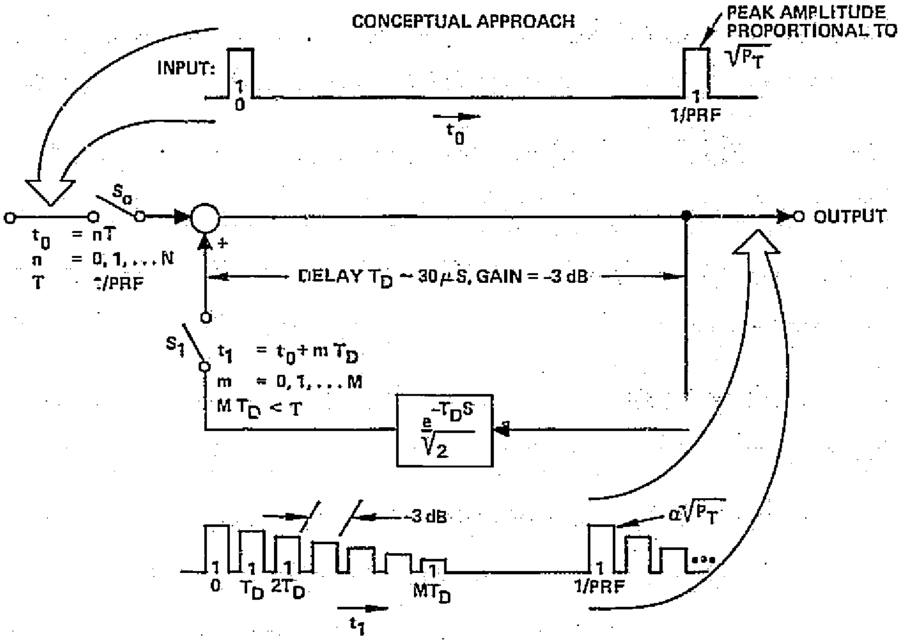

Figure 11. Pilot signal generator

---

*The power data of the sampled reference $P_E$ is continuously monitored to detect any alteration during the calibration sequence and to correct for any subsequent change in transmitter power during data recording intervals.

FOR EACH RADAR ACTIVATION:

| RADAR ACTIVITY | DURATION | STRUCTURE |
|---|---|---|
| PILOT RECORD BEGINNING AND END | 3 SECS | 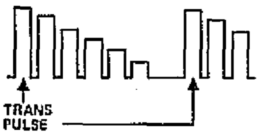 |
| NOISE RECORD BEGINNING AND END | 4 SECS | 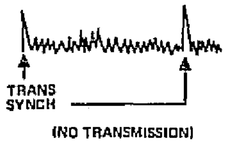 |
| TERRAIN RETURN RECORD | 5-20 MIN | 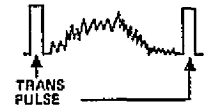 |

Figure 12. Receiver output structure

The third step in space calibration is to record receiver noise. Receiver noise record data are provided at stipulated receiver gain settings $\Gamma_r$ with the pilot signal generator RF turned off. The receiver output noise signals are measured at periodic range intervals (Figure 12) and at periodic time intervals (Figure 8). A 4-second sequence of data obtained at the beginning and end of each radar activation provides a quantity of data that is ample for noise measurement accuracy.

## 2.2 ANTENNA GAIN AND PATTERN MEASUREMENT FUNCTIONS

In calibrating antenna peak gain ($G_0$) and pattern parameters (the antenna beamwidth portion of the $g_i$-sets), calibration facilities external to the radar sensor proper are used. Standard cross section targets (corner reflectors) are adapted to this purpose, as required by the baseline calibration design concept.*

---

*One alternative approach makes use of calibrated field intensity recording devices at suitable ground sites. For pattern measurements, this approach is straight forward. Simultaneous transmitter power measurements of very good absolute precision aboard the passing shuttle are required for peak antenna gain measurement accuracy using this alternative approach.

The two-way, end-to-end, calibration with standard cross section targets (corner reflectors) is preferred. The alternate approach is a practical supplement; for example, a field intensity calibration site near each group of corner reflectors would usefully augment the utility of the calibration test range.

Antenna gain and pattern measurements are included in the radar parameter calibration. These measurements require a field of standard cross section targets. Corner reflectors are suitably dispersed in range and azimuth for imaging during the passage of the shuttle, as illustrated in Figure 13. Four groups of four corner reflectors each are appropriately oriented in an object field of about 1 by 50 km. The groups are spaced 10 to 15 km apart in the cross-track dimension of the imaged swath to permit measurements at four points in the elevation beam for each group.*

Azimuth beamwidth factors are measured at each elevation angle with 16 data points (four looks at each of four corner reflectors). The corner reflectors for this purpose are spaced 250 - 350 m for the baseline system at a nominal 25 m resolution, effectively decoupling the individual measurements.

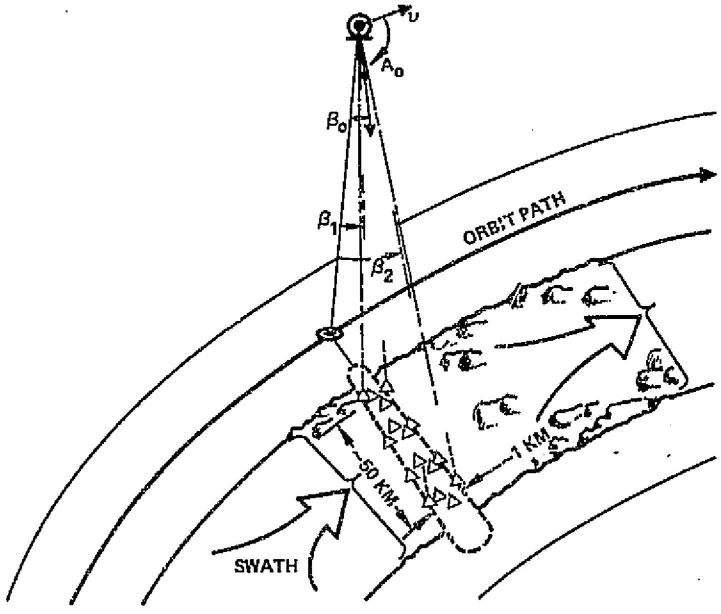

Figure 13. Standard target fields for calibration

---

*Ideally, the corner reflector farm would be revisited periodically for calibration updating. However, it is anticipated that a single visit in a 5 to 7 day mission may be a practical limit. Thus, calibration precision adequate for absolute calibration of the sensor function on a single visit basis is a design goal.

The antenna peak gain $G_o$ and the set of $g_i$'s belonging to the antenna pattern for the measurement geometry are measured with an algorithm that minimizes mean square error, described in Section 3.2.

## 2.3 GROUND CALIBRATION AND MEASUREMENT FUNCTIONS

The ground processor performs the following calibration and $\sigma_o$ measurement functions by:

1. Image correlation common to calibration and $\sigma_o$ measurement
2. Calibration algorithms for
    a. Sensor radar parameter computation ($K_{rad}$ and $N_o$) with the sensor pilot mode calibration data
    b. Antenna gain and pattern computations with the corner reflector farm calibration data
3. $\sigma_o$ measurements using generated calibration parameters ($K_{rad}$, $g_i$-sets, $N_o$) for data normalization, including the suppression of the bias-term arising from receiver noise.

Ground processing functions are illustrated in Figure 14. They are listed below.

1. Data Region Selection and Centering - An observer interacts with the display to designate the position and size of a region for $\sigma_o$ measurement or calibration, as appropriate.
2. Ancillary data separation - Radar mode, platform angle data (magnitudes and rates), and contoured AGC data are stripped from the sensor data recordings with a "data separator."
3. AGC Inversion - The contoured AGC data are used for AGC inversion to restore the precise range dependent receiver gain required for data normalization with $K_{rad}$.*
4. Determination of Image Coordinates and Orientating the Antenna Pattern - Ancillary data (e. g., average terrain altitude) and ephemeris data, together with platform and clutter derived angle data, are used by a "geometry solver" to determine image coordinates (latitude, longitude), antenna pattern orientation, range R, range rate $\dot{R}$, and acceleration $\ddot{R}$ terms as required.

---

*See Earth Resources Shuttle Imaging Radar, Report No. P75-415, Contract NAS-8-14273, Hughes Aircraft Co., October 1975, Sections 4.1 and 4.2 (esp pp 4-1 through 4-24). A digital contoured AGC for the baseline SIR radar which ensures 50 dB instantaneous dynamic range with 5 bits (I&Q) recorded data is described.

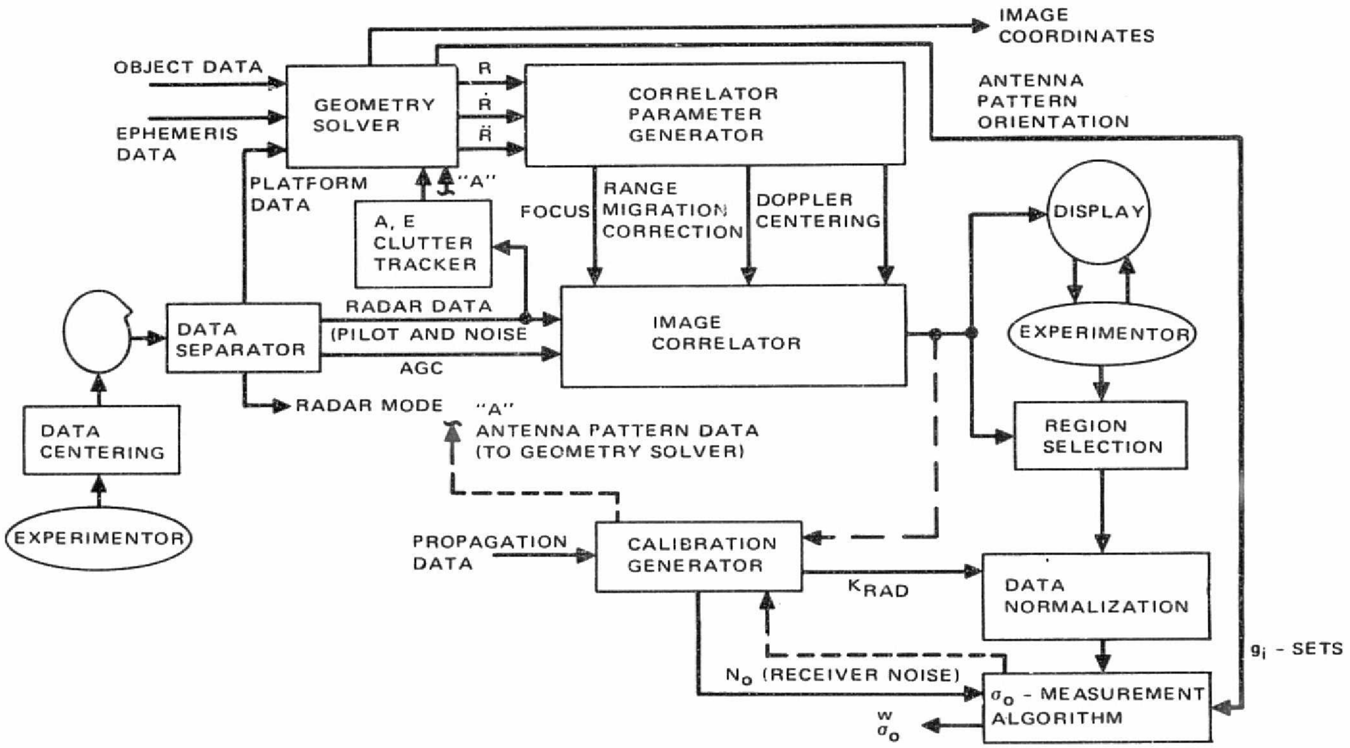

Figure 14. Ground processing block diagram

5. Image Correlation - Range and azimuth compression functions are performed with the "Image Correlator", properly focused and positioned in cross track range (range migration correction) and along-track range (doppler centering) by the "Correlator Parameter Generator".

6. Generation of Calibration Parameters - The "Calibration Generator" develops calibration parameters $K_{rad}$ and receiver noise measurements $N_o$ appropriate to the $\sigma_o$ measurements. In calibration modes (dashed lines), the parameters are generated from appropriate image correlator data (e. g., pilot signals in the case of the routine pilot mode calibration sequence; corner reflector farm data in the infrequent calibration sequence using standard cross section targets). The $\sigma_o$ measurement modes (solid lines) and the current radar parameter calibrations are supplied for data normalization with the "$\sigma_o$ Measurement Algorithm"; the "Geometry Solver" supplies antenna pattern orientation data ($g_i$-sets).

7. Multi-look Overlap - The "antenna pattern orientation" data are used in the $\sigma_o$ measurement algorithm to form suitable overlap of the multi-look imagery.

8. Overlay and Registration - The geometry solver computes image coordinates, which are employed to register multi-look imagery and to transform sensor image coordinate space to object field (terrain) coordinate space. This post-correlator function is not explicitly shown in Figure 14.

## 3.0 CALIBRATION DESIGN

The baseline calibration system is comprised of shuttle sensor calibration facilities, at least one corner reflector farm, a ground processing facility and appropriate computational algorithms.

The designs of shuttle facilities for transmitter power measurement and for data records of transmitter power-receiver gain products are discussed in Section 3.1. The space calibration data records, after ground processing, are image maps of the two-dimensional impulse function responses for the SAR. For this purpose the pilot signal generator produces signal records with precisely controlled power levels proportional to the products of transmitter power and receiver gains at discrete ranges. A surface acoustic wave (SAW) device is the crucial element of this facility. In addition, the space calibration design provides data records for noise image maps. These noise image maps are processed for the bias compensation needed for precision in measurement of backscattering coefficients.

Ground processing for calibration is discussed in Section 3.2. The space calibration data records for determining radar parameters accessible to the space calibration facilities are processed routinely; the critical parameters of transmitter power and receiver gains are developed from the pilot signal generator data records. The corner reflector farm data records are processed when available to develop antenna gain and pattern parameter calibrations.

The design of the corner reflector farm is discussed in Section 3.3. The corner reflector farm contains strategically arranged multiple corner reflectors. The baseline design uses 16 precisely calibrated standard radar cross-section targets, grouped by fours, to provide the accuracies needed for calibrating antenna peak gain and pattern parameters. The corner reflector farm is important in that it provides for measurement of critical SAR parameters in addition to antenna factors; these include propagation in the troposphere, registration, overlay of multiple looks, impulse functions, range migration compensations and antenna pointing data functions.

## 3.1 SPACE CALIBRATOR DESIGN

Space calibrator functions are designed for execution in three time sequences:

1. Power and Gain Set Sequence - In this sequence, transmitter power is measured and recorded. The pilot generator levels are set to designated fractions of the transmitter power, and receiver gains are set to values assigned at the beginning of a data run or used at the end of a data run. A 5-minute warm-up period precedes the start of data runs in this sequence of the space calibration function. Thus operating parameters can be stabilized before data are recorded.
2. Pilot Data Record Sequence - During this 3-second sequence, transmitter power-receiver gain data are recorded with use of the pilot signal generator replicas of the transmitter waveform; the receiver dynamic range is sampled at 4.5 km range intervals and at 3 dB logarithmic decrements per step.
3. Noise Data Record Sequence - During this 4-second sequence, sensor noise data are recorded with passive radar functions (transmitter and pilot signal generator in standby modes). The antenna is configured as for normal operation, and the system is sensitive to all external sources of noise and interference of significance to measurement. Receiver gains are set to values appropriate to sensitive measurement of relevant SIR sensor noise (i.e., receiver gains are increased by approximately the average signal-to-noise ratio for data records with nominal A/D converter quantization and saturation noise contributions).

Pilot mode sequences of the sensor calibration functions are given in Table 4, with time lines addressed specifically to initial calibration data records (before a data run). Critical components of the calibration function are activated 5 minutes and 12 seconds before data recording is scheduled to start. During the 5-minute warm-up period:

1. Transmitter power output and waveform characteristics stabilize
2. Receiver gains are AGC'd to nominal levels corresponding to terrain characteristics, antenna patterns and geometry

## TABLE 4. PILOT MODE SEQUENCE

| SENSOR UNIT \ STATUS | BEFORE DATA RECORD INITIATE AT DESIGNATED TIME $T_D$: | | | | | | | | |
|---|---|---|---|---|---|---|---|---|---|
| | TIME TO $T_D$ → | | | | | | | | SIR DATA |
| | 5.2 MIN | 7.61 SEC | 7.3 SEC | 7.2 SEC | 4.2 SEC | 4.1 SEC | 0.1 SEC | ••• 0.000 | |
| TRANSMITTER | ON | → | OFF | — | — | → | ON | → | → |
| RECEIVER: | ON | — | — | — | — | — | — | — | → |
| GAIN $\Gamma_r$ | AUTO | SET | RECORD | → | RE-SET | RECORD | RESET | RECORD | → |
| EXCITER | ON | — | — | — | — | — | — | → | → |
| PILOT GENERATOR: | ON | — | — | — | — | → | STANDBY | — | → |
| REF POWER $k_TP_E$ | AUTO | SET/RECORD | | → | CONFIRM/RECORD | | CONFIRM/RECORD | | → |
| PILOT LEVEL SET $k_P$ | SET | CONFIRM/RECORD | | → | OFF | — | → | SET BIT MODE | → |
| RECORDER(S)† | STANDBY | ON | — | — | — | — | — | — | → |
| TRANSMITTER POWER DATA | RECORD* | RECORD† → | $k_TP_E$ → | → | RECORD† | — | — | — | → |
| REFLECTED POWER DATA | RECORD* | RECORD† | OFF | — | — | → | RECORD† | — | → |
| PILOT DATA RECORD | STANDBY | → | START | ON | OFF | — | — | — | → |
| NOISE DATA RECORD | OFF | — | — | → | START | ON | OFF | — | → |
| DATA RECORD | OFF | — | — | — | — | → | START | ON | → |

NOTES:

† HIGH DENSITY TAPE RECORDER(S) FOR SIR MISSION DATA (WIDE BANDWIDTH)

* NARROW BANDWIDTH (ENGINEERING PURPOSES) DATA RECORDERS

3. The pilot generator develops a stable reference power level in an automatic level set mode of operation.
4. Data records for engineering purposes (narrow bandwidth data) are produced; these records include transmitter power, reflected power from antenna feed, critical voltages, temperatures, parameters status (PRFs bandwidths, pulse durations, reference commands, etc.)
5. The high-density tape recorder(s) stabilize before the recording of wide-bandwidth data begins.

Pilot data records begin 7.3 seconds before SIR data records; the transmitter is turned off, the pilot generator reference level ($k_TP_T$) is set to equal the transmitter power reference level ($k_TP_T$), and each receiver gain is set to an appropriate reference level for calibration. The pilot reference power level ($k_TP_E$) is monitored throughout the data record interval to account for any (unexpected) reference power drift.

Noise data records begin 4.2 seconds before SIR data records; the pilot generator outputs are set to zero, and each receiver gain is re-set to the reference level for noise calibration.

The transmitter is returned to active operation 100 ms before SIR data records begin. Transmitter power monitoring is initiated in a BIT (Built-In-Test) mode to account for any significant power level drifts during SIR data records.

SIR data records begin 100 ms after return of the transmitter to its normal operating mode.

A Built-In-Test (BIT) mode is active and provides for continuous monitoring throughout the data record sequence (i. e., 2 to 20 minutes), Transmitter power is monitored with the pilot power measurement function. Receiver gain may be monitored at zero range (coincident with RF transmission) with an IF signal coupled into the receiver for that purpose. A practical mechanization is to use an IF pilot signal offset 1/2 PRF from the transmitter leakage. Transmitter power reflected from the imperfectly matched antenna is monitored to account for the corresponding loss in radiated power and to detect significant changes in antenna feed and/or antenna condition.

Ancillary data comprising critical voltages, temperatures, system and subsystem parameters (including PRFs, pulse durations, transmitter waveform bandwidth, etc.) will also be recorded. Data are included that are either essential to correct for known systematic variations (e. g., thermal factors in antenna pattern or gains, waveguide losses, etc.) or useful for diagnostics in the event of anamolous results.

The space sensor implementation for the pilot signal calibration approach is illustrated in Figure 15. Samples of the transmitter amplitudes and precise pilot signal replicas of the transmitter waveforms are coupled at a common point in the sensor waveguide feed very near the radiating antenna port (point 1 in Figure 15). The transmitter waveform samples of power $P'_T = k_o P_o$ are used to monitor transmitter power and to set the proportional levels of the pilot replicas. Thus, the pilot data used in the calibration process is precisely proportional to the product of transmitter power $P_T$ and receiver gain $\Gamma_r$ at a point very near the reference plane for antenna

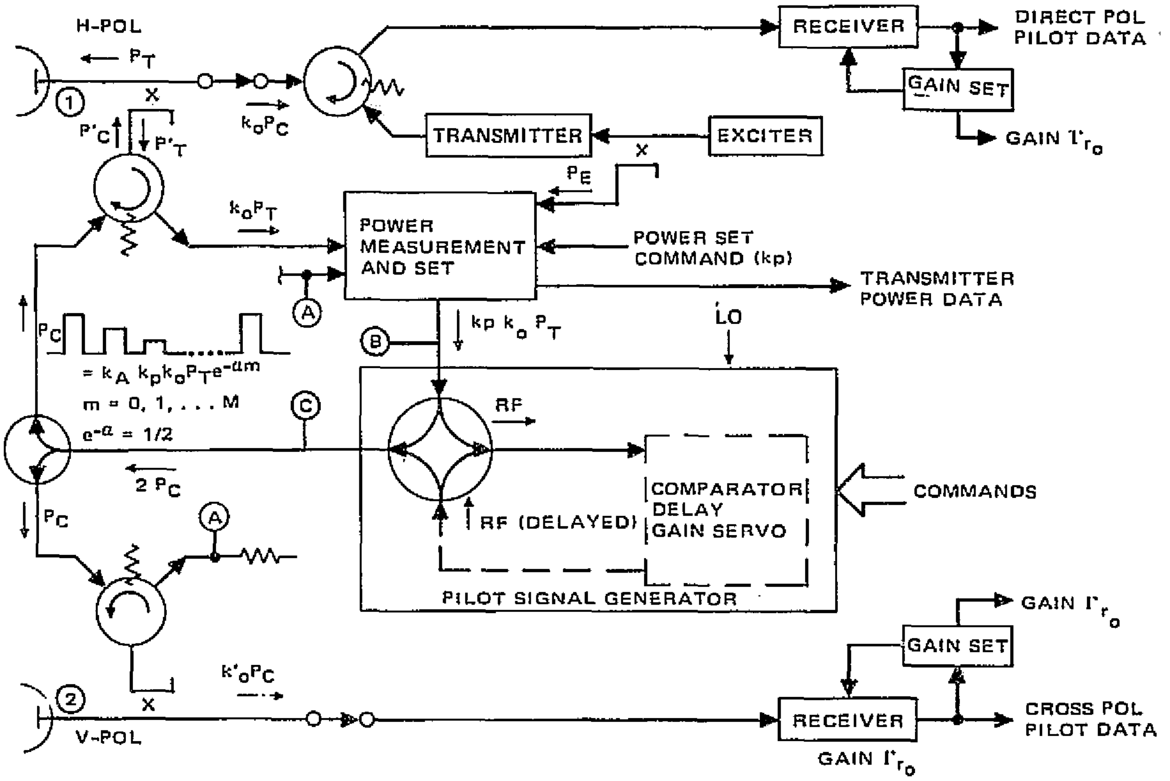

Figure 15. Pilot signal calibration approach, functional implementation

peak gain $G_0$; common losses between the transmitter, receiver and the reference plane (point 1) are included in the calibration. The coupling factor $k_o$ is measured as a function of frequency and temperature. The response characteristics of the power measurement and pilot signal generator should be measured before and after each mission to determine with precision the critical ratio $P_T/P_C$. This ratio must be adjusted to correct for known thermal factors involved in space sensor measurements.

Calibration is executed in sequential steps of active (radiating) and passive (nonradiating) sensor operation.* The RF references $P_E$ are used as source of pilot signals during the passive pilot mode for calibration. The

---

*Passive modes are used to avoid the possible contamination of calibration data with active sensor returns and to permit processing of calibration signals at zero relative range.

power measurement and pilot level set functions are performed with attenuated samples ($k_T P_E$) matched to corresponding samples ($k_1 k_o P_T$) of the transmitter waveform. The waveform of $P_E$ is a replica of the transmitter waveform obtained by either coupling to the exciter RF drive signal for the transmitter or to the transmitter output with the transmitter switched to a dummy load.*

The coded power level set command $k_p$ is used to select an attenuation level appropriate to the pilot data used for calibration. The zero-range calibrate signal (m = 0 in Figure 15) is coupled into the direct-polarization receiver at port 1 and the cross polarization receiver at port 2. A ganged high-power switch is used to select either horizontal or vertical linear polarization for direct polarization. The transmitter sample input to the "Power Measurement and Set" is unique to horizontal or vertical polarization with the selector switch between the coupling port (1 or 2) and the transmitter, as shown. The receivers are identified with direct or cross polarization, using this switching configuration.**

Range delayed pilot data are obtained for calibration by recirculating a portion of the "Pilot Signal Generator" RF inputs (point B in Figure 15) through a delay medium. The RF outputs (point C in Figure 15) are in the form of a logarithmically decremented pulse train repeated at PRF intervals; the delay medium includes a net loss of 3 dB per circulation.

---

*The implementation provides pilot data at zero relative range (i. e., concurrently with the transmitter waveform). Doppler offset of the $P_E$ samples is used to discriminate between them and the inevitable portions of transmitter signals that leak into the receiver; for example, a $0/\pi$ biphase modulator in the input for $P_E$ is alternately switched at the PRF to effect a 1/2 PRF offset for the calibrate signals. Thus, at the cost of a modulator, a high power switch and a dummy load, the transmitter itself is usable as the source of pilot calibration signals.

**In an alternative arrangement, a three-position switch might be used in the transmitter-to-circulator coupling link; the third position coupling to a dummy load. A second circulator with attendant loss (.2 to .4 dB at X-band) would be required in the path of the cross polarization receiver.

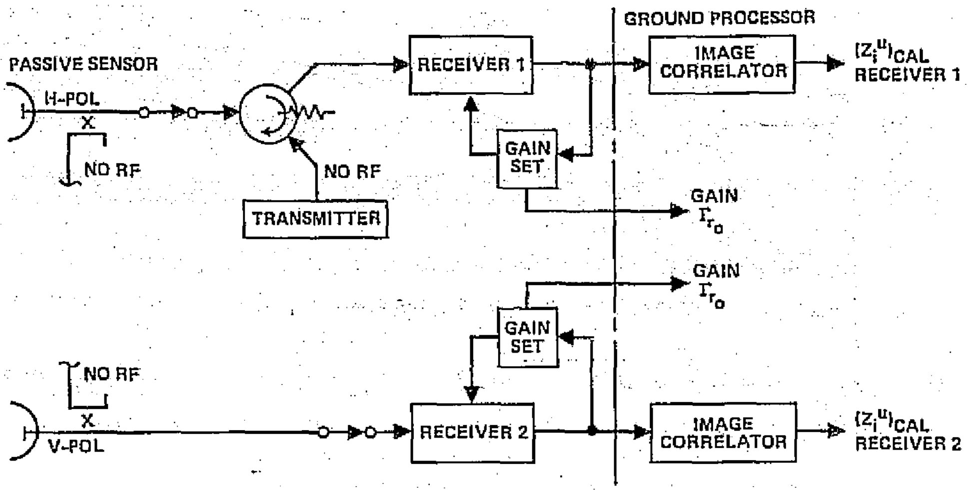

Figure 16. Sensor noise mode

The noise calibration sequence is effected by operating the sensor system in a passive mode (no external radiation). Implementation of the noise calibration sequence is simply a command function, involving only rudimentary hardware provisions.[*] The sensor configuration is shown in Figure 16.

## Power Measurement and Level Set Design

The objectives for power measurement and level set design are

1. Precision: ±3 percent (0.13 dB) or better, $1\sigma$[**]
2. Stability: ±1 percent (0.04 dB) or better, $1\sigma$[**]

The precision and stability of a reference power ($kT P_E$, in Figure 17) relative to a transmitter power level ($P'_T$ in the figure) are of most interest. The product of transmitter power and receiver gain is a fundamental parameter for space calibration determination. Thus, the function of first importance is to produce the pilot signals $P'_c$ (Figures 15 and 17) precisely proportional to transmitter power.

---

[*] For example, the transmitter may be operated in a passive mode by interrupting grid modulation for the final power amplifier. Receiver gain is set according to prearranged schedule, using existing circuit functions.

[**] Exclusive of directional couplers at coupling ports 1 and 2 of Figure 15.

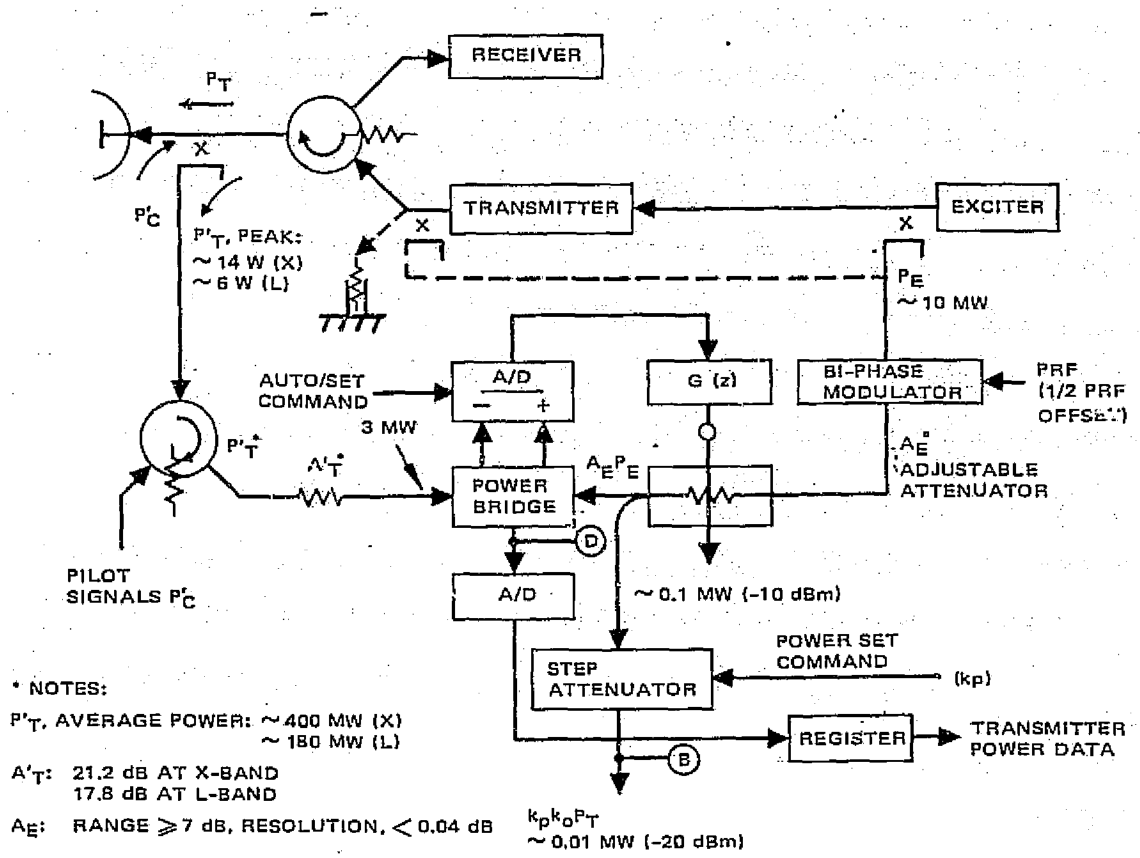

* NOTES:

$P'_T$, AVERAGE POWER: ~400 MW (X)
~180 MW (L)

$A'_T$: 21.2 dB AT X-BAND
17.8 dB AT L-BAND

$A_E$: RANGE $\geqslant$7 dB, RESOLUTION, $<$ 0.04 dB

Figure 17. Power measurement and pilot signal level set functional block diagram

The critical elements of the approach shown in Figure 17 are given below:

1. A reference power source is slaved to match the transmitter power samples ($A_E P_E = A'_T P'_T$ in Figure 17)
2. The transmitter power level is monitored with common elements of the power comparison scheme (transmitter power data derived at point D in Figure 17).
3. A precision step attenuator is used to establish pilot power level per command (power level at B = $k_p (k_1 k_o) P_T$, with $k_p$ precisely known and $k_1 = A_T$).

Two critical requirements must be satisfied in the physical design:

1. Thermal drift effects of critical elements must be controlled; in particular, the attenuators ($A_T'$ and $A_E$), the power bridge with related circuits, the step attenuator and control circuits must must be thermally isolated and controlled to a temperature range of 20 to 40°C, or better.
2. The VSWR of the bridge elements and sources must be controlled to 1.18 and 1.12 or less, respectively, over the temperature range (20 to 40°C) and a bandwidth of ±2 percent centered on the assigned carrier frequencies.

The power bridge should satisfy the following constraints:

1. It should be self-balancing or contain an automatic, self-zeroing calibration source
2. Accuracy should not be degraded by prime power fluctuations of ±15 percent.

Additionally, the "power measurement and set" device should include a biphase (0-π) phase modulator readily adapted to synchronization from a PRF strobe. This facility is adaptable to 1/2 PRF frequency offset to discriminate against receiver/transmitter cross-coupling.

The device is operated in two modes (Figure 17):

1. AUTO - a digital sampled data control loop slaves the reference power $A_E P_E$ to the input power $A'_T P'_T$
2. SET - the device is operated open loop as a fixed attenuator.

Transmitter power $A'_T P'_T$ is monitored for transmitter power data in the AUTO-mode; the reference power $A_E P_E$ is monitored in the SET-mode.

The input reference power $P_E$ in Figure 17 is coupled from the exciter RF drive signal for the transmitter. Alternatively, this sample may be coupled from the output of the transmitter and the transmitter switched to a dummy load during the pilot mode record data phase. Biphase (o/π) modulation at the PRF is used in this latter instance to discriminate the pilot signal from transmitter leakage into the receiver.

## Pilot Signal Generator Design

Range delayed replicas of the transmitter waveform (point C in Figure 17) are generated by the pilot signal generator. The basic objective of design is to produce stable amplitude characteristics; the device performance can be measured in a laboratory with excellent precision. Furthermore, the input signal (point B in Figure 17) is also a zero-delay calibrate signal; hence a stable reference of the amplitude of recirculated signals is provided.[*]

The pilot signal generator, shown in Figure 18, employs a time delay element operating at IF to circumvent practical difficulties in achieving adequate time delay at the L-band and X-band carrier frequencies of SIR. The selected delay length of 30 $\mu$s is greater than the transmitter pulse duration for SIR (about 25 $\mu$s maximum). The suggested design avoids the

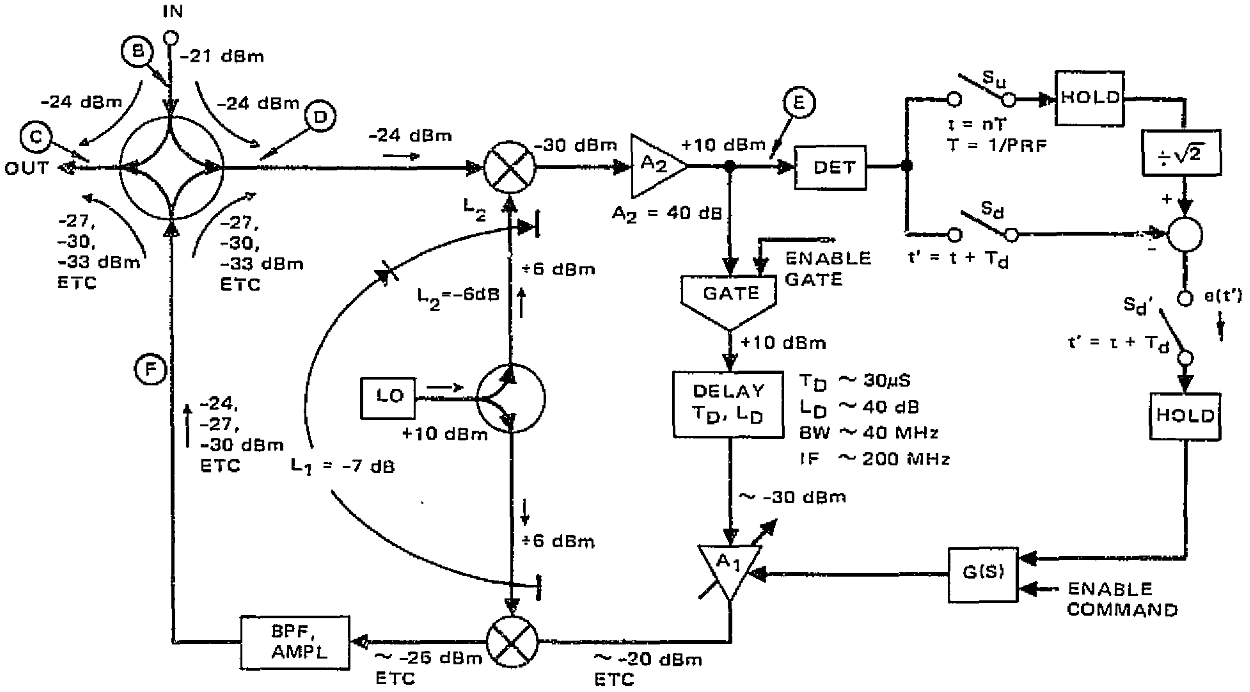

Figure 18. Recirculating pilot signal generator functional block diagram with levels, gains and losses

---

[*] Pilot signal record data at zero delay are important for this reason.

considerable complexity in the discriminant required for accommodation of pulse overlap.

The delay element is the most critical design item for the device because of the large time-bandwidth product of the transmitter waveform (e. g., 25 μs duration at 25 MHz bandwidth for 25 m ground range resolution at look angles near 10 degrees). A delay element with at least 40 MHz bandwidth is shown in Figure 18. To satisfy this requirement, a surface-acoustic wave (SAW) device is used. In particular, a minimum diffraction cut lithium tantalate substrate SAW is recommended. For such a device at 30 μs delay, a bandwidth of 40 MHz is practical at a carrier frequency of 200 MHz with an insertion loss of 40 dB maximum. Designs of a delay element with a $LiTa0_3$ substrate having frequency dispersion losses and spurious responses better than -40 dB are practical. Delay sensitivity is about 3 μs/cm at 65 ppm/°C. A moderate degree of thermal control (e. g., ±10°C) for critical elements of the pilot signal generator, including the delay device, the amplifiers, converters, and gain control circuits, is advisable.*

The recirculated train of pulses is decremented logarithmically at 3 dB per circulation by servo adjustment of loop gain to precisely -3 dB. The gain control discrimination is accomplished at a common point in the loop (point E in Figure 18). The discriminator samples the input amplitude at zero time delay, takes the difference between the stored result divided by root 2 and the amplitude of the first circulated signal, time delayed $T_D$ (30 μs). The process is repeated at PRF intervals, and the amplifier gain $A_2$ adjusted as a consequence until the first delayed replica has an amplitude of -3 dB relative to the input. The replicas recirculated two or more times also have amplitude ratios of -3 dB for a linear system. (The discriminant, in principle, can be cascaded for K pairs of circulations per PRF; however, since the PRF (≈1500 Hz) sampling rate is large in comparison to fluctuation bandwidths of practical amplifier designs, it is not necessary.)

---

*The critical elements of the pilot signal generator and the power measurement and set device should be isolated thermally in an enclosure controlled to a temperature range of $T_0^{o}$ ±10°C (e. g., $T_o = 30^{o}C$, a range of 68 to 104°F).

It is evident that the sampled data discriminant can be placed at any point in the common signal path of the input signal and its replica, i. e., anywhere between points D and F of Figure 18. Point E is chosen for the discriminant to operate the detector in its linear amplitude region with the large voltages sampled at this point. The line schematic of Figure 19a is helpful in appreciating the general scheme of this device.

Gain control analysis for the pilot signal generator is facilitated by the simplified schematics of Figure 19. A zero-order hold circuit for the discriminant is practical because inputs are very nearly constant, and the amplifier $A_1$ has a stable design. The moderately high sampling rate (at PRF = 1500 Hz) permits a stable sampled data control loop design with excellent precision and a moderately short settling time.

The gain control loop is balanced at a loop gain of -3 dB. The condition for zero error (discriminant node voltage $e(t') = 0$ in Figures 18 and 19) at the n-th sampling instant ($t' = nT + T_d$, $T = 1/PRF$) is given by

$$e(t') = r(nT)K_2(nT)\left[1/\sqrt{2} - K_1(t')K_2(t')\right] = 0 \qquad (7)$$

which is satisfied if:

$$K_1(t')K_2(t') = \sqrt{2} \qquad (8)$$

where:

$K_2(t') = L_2A_2(t')$

$K_1(t') = L_1L_oA_2(t')$

$A_2(t') = A_oG(t')$

and $G(t')$ is the loop gain control (voltage).

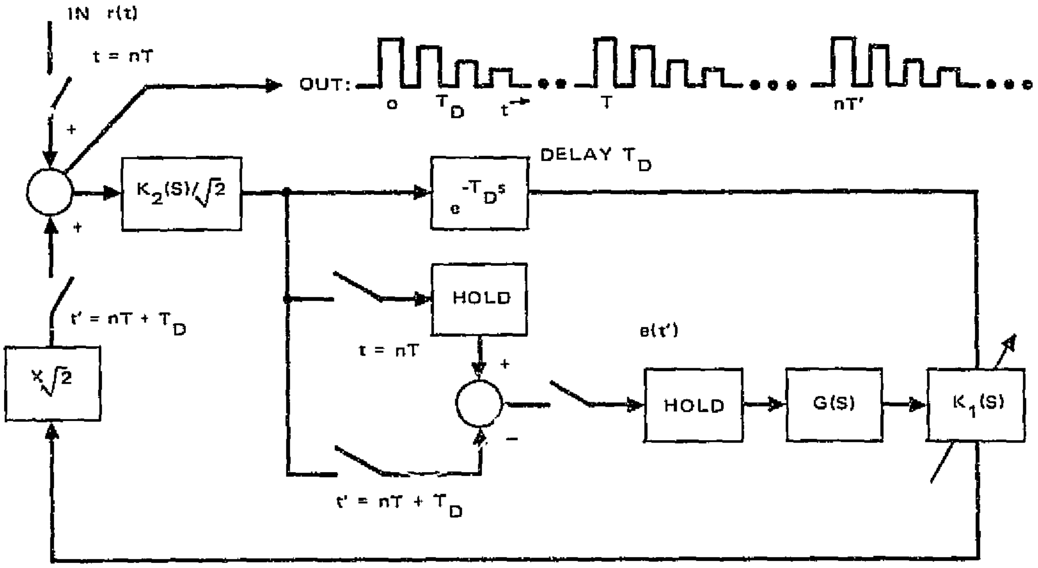

a. Simplified schematic

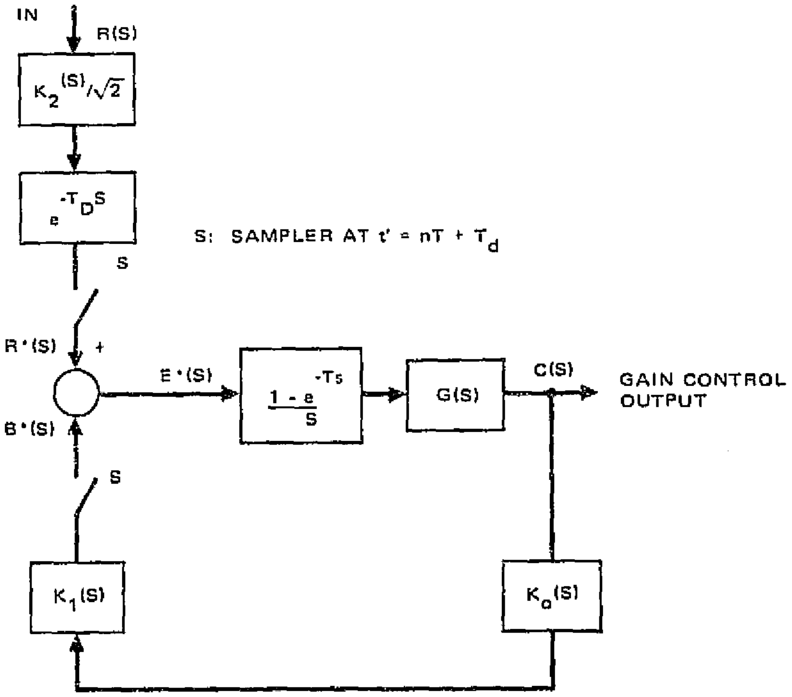

b. Equivalent transform representation

Figure 19. Equivalent circuits for gain control analysis of pilot generator

Gain control loop design emphasis is directed at precision and stability of response to step input gain errors. A design with a simple analog integrator is chosen:

G(s):

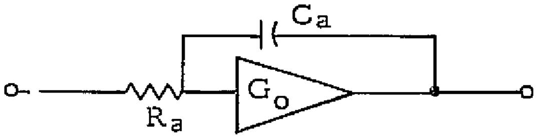

; $T_a = R_aC_a$, $G_o > 10^4$

$$K_oK_1T_aG(s) = \frac{1}{S};\ K_oK_1T_a = 16/\mathrm{PRF} \qquad (9)$$

For practical cases, $K_oK_1 \simeq 1$ and the integrator time constant $T_a$ is approximately 10 ms. The control loop is assymptotic to a unit step input without overshoot and with a 63 percent response time less than 11 ms (16 samples at a PRF of 1500 Hz). The loop settles to better than 0.1 percent gain error in less than 90 ms. The control loop gain provides effective response to slowly fluctuating inputs below about 16 Hz. Gain error is bounded to ±1 percent for drift rates confined to ±10 percent per second.*

The pilot signal generator is controlled by enable command and enable gate signals. The OFF state is enforced by near open circuit conditions at the SAW delay element input and output; the input gated driver (GATE in Figure 18), and the output amplifier (the gain controlled amplifier "$A_2$" in the figure) are operated at cut-off parameters. The "ON" state is established with enable command and enable gate signals applied simultaneously in the gain control loop for $A_2$ and to the delay line input gate, respectively, as indicated in Figure 18. The enable gate signals are applied in synchronism with the PRF, thus generating a controlled number of range delayed transmitter replicas each PRF and squelching multiple echoes at ranges greater than the interpulse period. The time relationships of these functions are shown in Figure 20.

---

*A moderate degree of thermal control for circuits subject to drift is advisable, as discussed above.

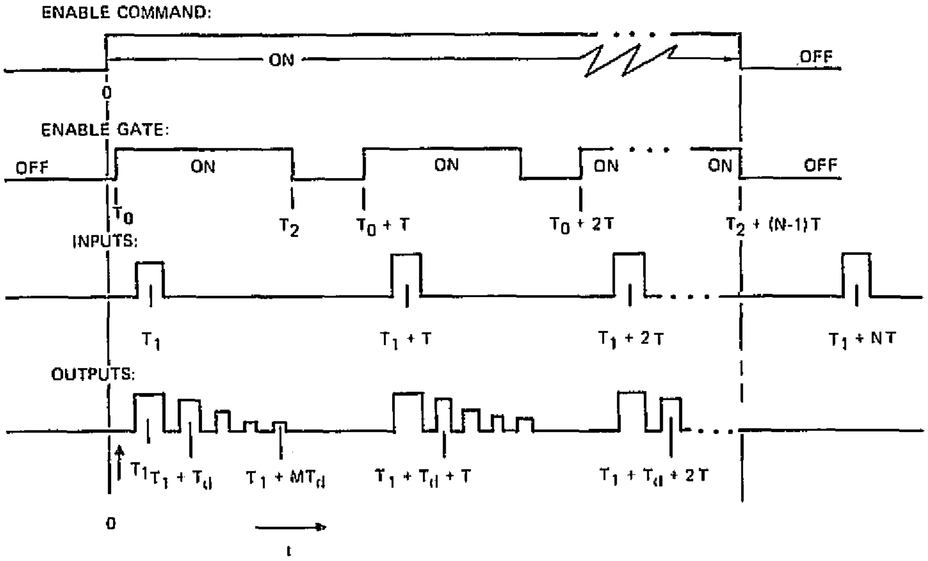

Figure 20. Control signals for pilot signal generator

The initial operation of the pilot signal generator is at a nominal loop gain established by the quiescent state of the gain control G(s). The quiescent loop gain is preset to -3 dB approximately, minimizing the settling time for the gain control response.*

The levels, losses, and gains shown in Figure 18 are recommendations based on the following design considerations:

1. Practical values of amplitudes for the pilot data records

---

*A design option is to gain control amplifier $A_1$ and fix the gain of $A_2$:

1. "OFF" state, $A_2$ cut-off, gain less than -50 dB,
2. "ON" state, $A_2$ gain nominal, about ±10 dB.

Automatic gain control of $A_1$ during the "OFF" state necessarily would be referenced to the input signal only; i.e., a logic state signal would switch the gain control discriminant:

a. "OFF" state, coupled at the undelayed sample and hold output ("$S_u$-HOLD" in Figure 18) and referenced to a fixed level;
b. "ON" state, coupled at the difference sample and hold output ("$S_d$-HOLD" in Figure 18).

The amplifier $A_1$ in this option could be operated at a fixed nominal gain (about 40 dB) in the "OFF" state. The amplifier $A_1$ must have a reasonable gain to operate the amplitude detector well within its linear input-output characteristic

2. Operation of mixers at values consistent with linearity and signal-to-noise ratio considerations
3. Mixer noise at down conversion (i. e., at $L_2$) dominant in re-circulating signals
4. Linearity for signal amplitude detection
5. Reasonable delay line driver requirements.

The local oscillator signal for the down-conversion and up-conversion of signals may be derived from the sensor LO.[*] The local oscillator stability should be comparable to that of the system LO, though maximum delay is less than 60 μs (pulse width plus delay). The LO mixer injection level must be well above maximum signal levels for linear conversion. The mixers should be image rejection types. The RF combiner network at the input/output junctions should be chosen carefully for low loss and thermal stability. The RF circuits should be included in a thermally stabilized enclosure, in conjunction with other critical RF elements of the power measurement and set device, as discussed above.

The pilot signal generator should be well tested, calibrated and certified before use. Calibrations, in situ, should be performed before and after shuttle missions to establish a firm experimental base for system calibration error budgets.

## 3.2 GROUND PROCESSING FOR CALIBRATION

The calibration parameters for the baseline SIR measurement system are developed through the ground processing of data records. Pilot signal and receiver noise image maps are processed routinely to provide current calibration parameters $K_{rad}$ and $N_o$. The sensor pilot signal data records are processed at the beginning and end of each data record set. Data records of transmitter power are monitored during image processing and calibration parameter $K_{rad}$ corrected for any significant drift in radiated power. Antenna peak gain and antenna pattern factors, (i. e.,

---

[*] A system first IF of about 200 MHz is recommended so that LO's may be common. In other cases, the pilot signal generator LO may be derived with an injection lock oscillator with a stable offset frequency.

beamwidths) are calibrated with data records for standard radar cross-section targets. The standard RCS targets are provided by one or more corner reflector farms as available.

All important aspects of SIR measurement are involved in developing the calibration parameters from corner reflector farm data. Thus the critical functions of antenna pointing, range migration compensation, focus, overlay, etc., are evaluated and the calibration parameter data set is updated. A "steepest descent" algorithm is used to develop the calibration parameter set with optimum accuracies. This algorithm provides current calibration of the geometry solver and the clutter tracking functions that produce the antenna orientation sets $g_i$ required for $\sigma_o$ measurement. The steepest descent algorithm is described next.

The measurement of calibration parameters begins with un-normalized intensities $Y_i^u$, as shown in Figure 21. The image intensities $Y_i^u$ have the following structure:

$$Y_i^u = X_i^u + Z_i^u \text{ (terrain plus noise)}$$

$$E\left\{\left|X_i^u\right|^2\right\} = K_{rad} g_i^2 \sigma_o$$

$g_i$: normalized antenna pattern (i. e., $G_i/G_o$)

$\sigma_o$: terrain backscatter coefficient (to be measured)

$$K_{rad} = \frac{P_t G_o^2 \lambda^2 d_a d_r \Gamma_r}{(4\pi)^3 R_s^4 L_{at} L_{sys} \sin\phi} N^2_{pc} N^2_{pulses}$$

$$E\left\{\left|Z_i^u\right|^2\right\} = N_o^u \text{ (receiver noise power appearing at i-th cell, same for all cells)}$$

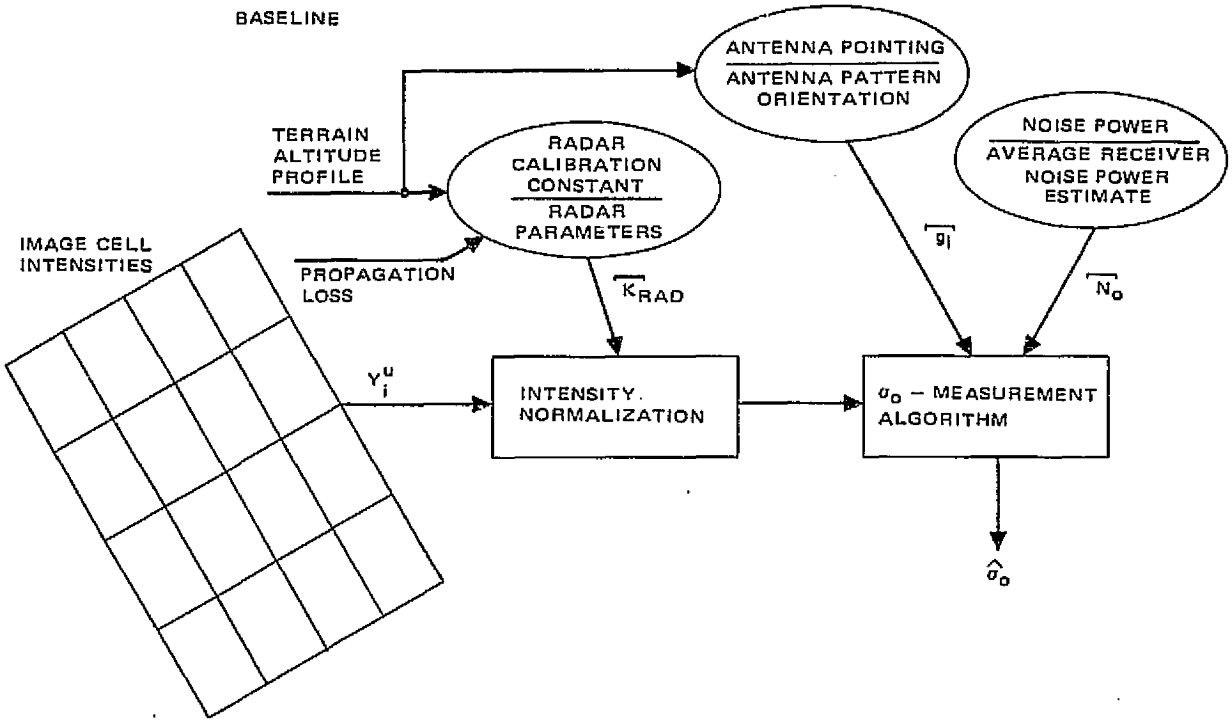

Figure 21. Measurement of calibration parameters

## Receiver Noise Parameter $N_o$ Measurement

$N_o$ measurement is made with noise record data ($X_i^u = 0$) where the receiver gain is $\Gamma_{r_o}$. The basic algorithm is

$$N_o^u = \left(\frac{1}{K_{rad}}\right)\left(\frac{\Gamma r}{\Gamma r_o}\right) \text{NOISE} \tag{10a}$$

where:

$$\text{NOISE} = \frac{1}{M_o}\left[\sum_{m=0}^{M_o} \left|(Y_m^u)\right|^2\right], \text{ at gain } \Gamma_{r_o}, \tag{10b}$$

$K_{rad}$ and ( $\Gamma r / \Gamma_{r_o}$) are the radar parameter and the receiver gain ratio for $\sigma_o$ measurements, respectively. The number of independent measurements $M_o$ is chosen to be large (e. g. , $M_o = 2048$) to provide negligible error in the measurement accuracy for NOISE. This is accomplished, for example, by making measurements with a noise image map of 256 range cells by 8 along track (azimuth) cells. The standard deviation of the measurement is accordingly:

$$[\mathrm{VAR\ (NOISE)}]^{1/2} = \frac{N_o^u}{\sqrt{2048}} \simeq 0.095 \text{ dB}$$

The receiver gain $\Gamma_{r_o}$ for noise measurement is selected to produce a mean power level at the A/D converter which is the same as the expected power level with terrain signal; i. e.:

$$E\left[\left|Y_i^u\right|^2\right] \approx E[\mathrm{NOISE}] = (N_o^u)_{CAL}$$

$$\text{and } \Gamma_{r_o} \approx \Gamma_r/\mathrm{SNR}.$$

Thus A/D converter, processor roundoff and truncation noise contributions are effectively the same for $\sigma_o$ measurement and $N_o$ measurement. The overall accuracy for noise compensation is a function of the gain scaling ($\Gamma_r / \Gamma_{r_o}$). Data records of receiver gain $\Gamma_r$ are supplied concurrently with image data records; the gain scaling should be accomplished with an RMS error less than 0.15 dB.

### Radar Parameter $K_{rad}$ Measurement

The parameter $C_S$ is measured with data records of pilot signal image maps and the parameter $K_{rad}$ calculated using current calibrations for parameters $C_G$ and $C_{R,\phi}$:

$$K_{rad} = C_S\, C_G\, C_{R,\phi} \qquad (11a)$$

$$C_S = P_t\, \Gamma_r N^2_{pc}\, N^2_{pulses} \qquad (11b)$$

$$C_G = \left(\frac{\lambda G_o}{4\pi}\right)^2 \left(\frac{1}{4\pi L_{sys}}\right) \tag{11c}$$

$$C_{R,\phi} = \frac{d_a d_r}{L_{at} R_s^4 \sin\phi} \tag{11d}$$

where the parameters transmitter power $P_t$, receiver gain $\Gamma_r$, pulse compression sum $N_{pc}$, azimuth (time) compression sum $N_{pulses}$, antenna peak gain $G_o$, range $R_s$, etc., are as defined in Section 2. The parameters $C_G$ and $C_{R,\phi}$ are estimated with $\overline{C}_G$ and $\overline{C}_{R,\phi}$ respectively, based on the calibrations of the parameters $G_o$, $L_{sys}$, $d_a$, $d_r$, $L_{at}$, $R_s$, and $\phi$.

The pilot signal image data are measured as calibrate variates $(Y_i^u)_{CAL}$:

$$(Y_i^u)_{CAL} = (X_i^u)_{CAL} + (Z_i^u)_{CAL}$$

where

$$E\left\{\left|X_i^u\right|^2\right\} = k_{CAL} P_t \Gamma_{r_o} N_{pc}^2 N_{pulses}^2 = k_{CAL} C_S \tag{12}$$

and

$$E\left\{\left|(Z_i^u\right|^2\right\} = (N_o^u)_{CAL}.$$

The receiver gain is recorded with the data, and $K_{rad}$ scaled as required for the receiver gain $\Gamma_r$ corresponding to the image data records. The calibrate gain is chosen to equal the image data gain where possible, and scaling in most instances is nominal or unity. The parameter $k_{CAL}$ is the calibrated transfer characteristic for the pilot signal data mode; generally it is a function of range (decreasing at 3 dB per range step) and may be varied in calibrated increments, which are encoded on the image data tape records.

The parameter $C_S$ is determined by averaging a large number of measurements of image intensities:

$$C_S = \frac{1}{M_1} \sum_{i=1}^{M_1} \frac{\left[\left|Y_i^u\right|^2_{CAL} - (N_o^u)_{CAL}\right]}{k_{CAL_i}} \tag{13}$$

Precision is improved by continuing measurements at the various values of $k_{CAL_i}$ over $M_1$ intensities corresponding to about 3 seconds of data.

Antenna Gain and Pattern Measurements

Radar parameters, including antenna gain and pattern factors, are calibrated with target image data obtained by processing corner reflector farm records. The baseline system determines the calibration of the parameters by ground processing.

Ground processing procedures for the measurement of antenna peak gain and pattern factors include:

1. Detection and designation of the standard target signals to be processed
2. Generation of parameters to optimize focus and range migration compensation at the range and angle coordinates of the target
3. Positioning processor coordinates to nearly center the target coordinates in the corresponding resolution cell
4. Determination of calibration parameters which minimize mean square calibration error.

The detection and designation of the standard target functions are facilitated by the large signal-to-noise ratios of the discrete targets and the readily recognized pattern of the target array, respectively. The processor focus and range migration compensation functions are then performed, as necessary, to optimize image formation of the individual targets. Calibration errors due to quadratic phase errors or motion of the target during image formation are thus minimized.

Ideally, target coordinates are centered in an image cell, since the slope of the symmetrical impulse function responses are zero at this point. The calibration errors caused by imprecision in target position data degrade rapidly with target distance from the center of the resolution cell coordinates. For this reason, the ground processor is asked to re-position the image cell center at the apparent target coordinates in range and azimuth. An RMS accuracy of at least ±15 percent the resolution cell dimensions, or ±3.8 m at 25 m resolution, is needed for this positioning function, including the limitations caused by finite signal-to-total noise ratio (about 20 dB, typically).

The SAR multilook images should be processed with symmetrical illumination of the antenna pattern in the azimuth plane. This need arises to minimize measurement errors caused by imprecision in the antenna pointing data. The target image data should be reprocessed as needed to provide symmetry equivalent to ±5 percent the azimuth beamwidth of the antenna. The adjustment for symmetry is a simple (time) shift in the initial inputs for synthetic aperture formation.

Records of SIR sensor data may be repeatedly processed with the ground processor facility. The calibration operations are especially crucial with respect to accuracies for the early missions with SIR. Only a very few such operations are performed with corner reflector farm data records for each mission. Thus the need to reprocess for the best possible calibration accuracy is a relatively minor inconvenience and expense.

The target data for calibration operations may be processed in groups of resolution cells (e. g., the sum of energies from four, five, or nine neighboring cells containing the target) and, at the expense of signal-to-noise ratio, the sensitivity to target position and motion in the cell may be reduced. A calibration approach of this sort will obviate the need for repeated processing of calibration data and can be exercised in real time processing. When SAR sensor experience has developed through the early shuttle missions, it is anticipated that routine calibration operations of an essentially single pass character will have evolved.

The antenna peak gain and antenna pattern factors are determined with a steepest descent algorithm, together with other radar sensor parameters subject to calibration. This algorithm is described below.

The antenna pattern factors are determined in the conventional orthogonal azimuth and elevation planes. This convenience and custom are especially suited to the types of rectangular planar array anticipated for SIR. The antenna pointing angles and beamwidths for separable arrays are designated in the algorithm. Figure 22 illustrates the antenna configuration relationships involved in the $g_i$-calibration sets used for $\sigma_o$ measurement.

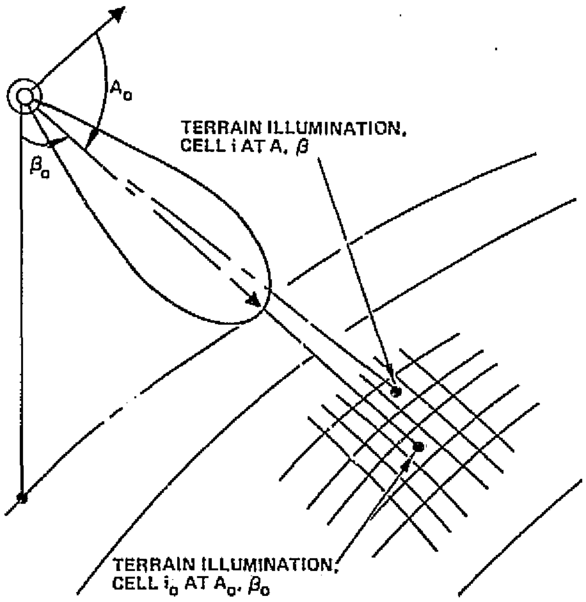

Figure 22. $g_i$ set determination

$$g_{i_o} = \frac{G(A_o, \beta_o)}{G_o} = 1$$

$$g_i = \frac{G(A - A_o, \beta - \beta_o)}{G_o}$$

$$g_i = g_1(A - A_o) + g_2(\beta - \beta_o)$$

## Algorithms

The problem of determining the antenna gain and the antenna gain pattern parameters from the calibration data is a nonlinear parameters estimation problem. Thus, it is implied that the solution cannot be determined easily in closed form. This section is a description of a numerical technique that simultaneously finds the maximum likelihood estimate of all the antenna parameters from the standard target returns. This technique is one of many standard multidimensional optimization numerical routines available is most computer system libraries.

A steepest descent algorithm for calibration is used to determine the maximum likelihood estimate for all the antenna gain pattern parameters.

From estimation theory:

1. The Cramer-Rao bound is a lower bound on the mean square estimation error.
2. For an estimator to achieve the Cramer-Rao bound, it must be efficient; an efficient estimator need not always exist.
3. If an efficient estimator exists, it must necessarily be the maximum likelihood estimator.

A test can determine whether an estimator is efficient; however, in this case the actual form of the estimator is not known (the parameters are obtained numerically) and, therefore, they cannot be tested for efficiency.

Therefore, Hughes can claim only

1. The estimates for the antenna parameters are optimal in the maximum likelihood sense;
2. If an efficient estimator for the antenna parameter can be found, it will be the Hughes estimator and thus have the best performance possible.

The maximum likelihood estimate method for $\sigma_0$ measurement takes advantage of statistical relationships between resolution cells and multiple looks. The near optimum $\sigma_0$ estimator is the maximum likelihood estimator (also efficient) for the region of interest (SNR $\geq$ 8 dB, ground area $\geq 10^4$ square meters). Since the maximum likelihood estimator is efficient for this problem, it achieves the smallest possible mean square estimation error. On the other hand, the baseline and marginal estimator require much more area to achieve the same performance. Thus to compensate for lack of knowledge of the statistical structure, the area of ground return must be increased.

The antenna parameters consist of the antenna peak gain $G_o$, azimuth beamwidth $\Delta A$, elevation beamwidth $\Delta\beta$, and azimuth and elevation pointing angles $A_1$, $\beta_1$ relative to the ground coordinates $\bar{x}$, $\bar{y}$ for the centroid of the imaged area. Equivalently, a single five dimensional parameter vector can be defined and the antenna calibration problem reduced to determining an optimal antenna parameter vector from the calibration data. Because the calibration data are non-deterministic, the optimal antenna parameter vector can be chosen to be the maximum likelihood estimate of the parameter vector. That is, given the outputs of the resolution cells $\{z_i, i = 1, 2, \ldots, N\}$, the vector that will maximize the log likelihood functional can be found.

$$f(\underline{\alpha}) = \ln p(\underline{z} \mid \underline{\alpha})$$

where:

$$\underline{z} = \begin{vmatrix} z_1 \\ z_2 \\ \cdot \\ \cdot \\ \cdot \\ z_n \end{vmatrix}$$ is the observed set of resolution cell outputs

$$\underline{\alpha} = \begin{vmatrix} G_o^2 \\ \Delta A \\ A_1 \\ \Delta\beta \\ \beta_1 \end{vmatrix}$$ is the parameter vector

$p(\underline{z}|\underline{\alpha})$ is the probability density of the set of resolution cell outputs given the parameter vector

$G_o^2$ = peak antenna gain squared

$\Delta A$ = azimuth beamwidth

$A_1$ = azimuth pointing angle relative to the patch centroid ($\bar{x}$)

$\Delta\beta$ = elevation beamwidth

$\beta_1$ = elevation pointing angle relative to the patch centroid ($\bar{y}$)

The calibration data can be modeled as*

$$z_k = g_k(\underline{\alpha})\ (m_k + c_k) \qquad (k=1, \ldots, N) \tag{14}$$

where:

$m_k$ = kth cell output component due to the standard cross-section target**

$c_k$ = clutter contribution to the kth cell output

In vector notation

$$\underline{z} = D_g\ (\underline{\alpha})\ (\underline{m} + \underline{c})$$

where:

$$(D_g(\alpha))_{ij} = \begin{cases} g_i(\underline{\alpha}) & i=j \\ 0 & i \neq j \end{cases}$$

$$\underline{m} = \begin{vmatrix} m_1 \\ m_2 \\ \cdot \\ \cdot \\ \cdot \\ m_N \end{vmatrix} \quad ; \quad \underline{c} = \begin{vmatrix} c_1 \\ c_2 \\ \cdot \\ \cdot \\ \cdot \\ c_N \end{vmatrix}$$

---

*Thermal noise is neglected at this point to simplify the problem and because it is comparatively negligible.

**The same resolution cell has a different index for a different look.

The random vectors $\underline{m}$ and $\underline{c}$ are assumed to be statistically independent, but the vector components of each vector are statistically correlated. Assuming Gaussian statistics, the log of the likelihood functional can be written as

$$\ln[p(\underline{z} \mid \underline{\alpha})] = -\underline{z}^{*}\Lambda^{-1}(\underline{\alpha})\underline{z} - \ln\left(\text{determinant}\left[\Lambda(\underline{\alpha})\right]\right) \tag{15}$$

where:

$\Lambda(\alpha) = D_g(\underline{\alpha})\,\Lambda\,D_g(\underline{\alpha})$

$\Lambda = mM + \sigma_o R$

$\underline{z}^{*}$ = transpose of the complex conjugate vector $\underline{z}$

$m$ = power reflected by the standard target

$M$ = covariance matrix of the set of standard target samples

$\sigma_o$ = clutter power reflected by the diffuse terrain

$R$ = covariance matrix of clutter

The above quantity must be maximized or its negative minimized with respect to the parameter vector $\underline{\sigma}$. This is done numerically by a steepest descent algorithm.

The steepest descent algorithm is one standard numerical technique utilized in optimization theory. The algorithm will determine simultaneously all the required antenna parameters that will maximize the log likelihood functional. The algorithm is summarized in Table 5.

It should be noted that to determine the maximum of the log likelihood functional, the gradient must satisfy

$$\nabla_{\underline{\alpha}} \ln[p(\underline{z} \mid \hat{\underline{\alpha}})] = 0$$

This implies that once the optimal parameter vector is found, it must necessarily satisfy the condition given in step 3 of Table 5.

## TABLE 5. STEEPEST DESCENT ALGORITHM

**Step 1**

Given

1. The observation vector $\underline{z}$
2. The initial parameter vector $\underline{\alpha}^o$, i. e., the antenna parameter vector updated by the most recent calibration or ground pattern measurements.

**Step 2**

Assume one has the $n^{th}$ iteration parameter vector $\underline{\alpha}^{(n)}$ to generate the $(n+1)^{th}$ parameter vector utilize the following recursive form:

$$\underline{\alpha}^{(n+1)} = \underline{\alpha}^{(n)} + t^{(n+1)} \cdot \nabla_{\underline{\alpha}} \ln [p(z|\underline{\alpha}^n)]$$

where:

$t^{(n+1)}$ = step size that is determined by the Golden section search method given at the end of this section.

$\nabla_{\underline{\alpha}} \ln [p(z|\underline{\alpha}^n)]$ = log likelihood functional gradient vector evaluated at $\underline{\alpha}^n$; its form is given in Table 6.

**Step 3**

Repeat step 2 until the following test is satisfied

$$\sum_{k=1}^{5} (\alpha_k^{(n+1)} - \alpha_k^{(n)})^2 = 0$$

If the test is satisfied, then set the optimal antenna parameter vector as

$$\hat{\underline{\alpha}} = \underline{\alpha}^{(n+1)}$$

## TABLE 6. COMPONENTS OF THE VECTOR $\nabla_{\underline{\alpha}}$ ln $[p(\underline{z} | \underline{\alpha})]$

| Vector Component Index k | Vector Component | $\nabla_{\underline{\alpha}} \ln [p(\underline{z} \mid \underline{\alpha})]$ Component |
|---|---|---|
| 1. | $G_o^2$ | $\frac{1}{G_o^2} \left( \sum_{i=1}^{N} \sum_{i=1}^{N} \frac{z_i^* a_j \Lambda_{ij}^{-1}}{g_i g_j G_o^2} - N \right)$ |
| 2. | $\Delta A$ | $\sum_{i=1}^{N} \sum_{j=1}^{N} \frac{z_i^* a_j \Lambda_{ij}^{-1}}{g_i g_j G_o^2} \frac{\partial}{\partial \Delta A} [\ln (g_i g_j)] - \sum_{i=1}^{N} \frac{\partial}{\partial \Delta A} \ln (g_i^2)$ |
| 3. | $A$ | $\sum_{i=1}^{N} \sum_{j=1}^{N} \frac{z_i^* z_j \Lambda_{ij}^{-1}}{g_i g_j G_o^2} \frac{\partial}{\partial A} [\ln (g_i g_j)] \sum_{i=1}^{N} \frac{\partial}{\partial A} \ln (g_i^2)$ |
| 4. | $\Delta \beta$ | $\sum_{i=1}^{N} \sum_{j=1}^{N} \frac{z_i z_j \Lambda_{ij}^{-1}}{g_i g_j G_o^2} \frac{\partial}{\partial \Delta \beta} [\ln (g_i g_j)] - \sum_{i=1}^{N} \frac{\partial}{\partial \Delta \beta} \ln (g_i^2)$ |
| 5. | $\beta$ | $\sum_{i=1}^{N} \sum_{j=1}^{N} \frac{z_i^* a_j \Lambda_{ij}^{-1}}{g_i g_j G_o^2} \frac{\partial}{\partial \beta} [\ln (g_i g_j)] - \sum_{i=1}^{N} \frac{\partial}{\partial \beta} \ln (g_i^2)$ |

Note: The matrix $\Lambda = mM, + \sigma_o R$ and $\Lambda_{ij}^{-1}$ is the (i. j) component of the inverse matrix $\Lambda^{-1}$.

The attractive features of the steepest descent algorithms are simplicity and efficiency. Its efficienty is reflected in its rate of convergence which is geometric. That is, the algorithm converges to the solution geometrically.[*] Other numerical techniques that are more efficient are also computationally more complex and therefore less attractive.

Neglecting receiver noise in the model of Equation (14) simplified the problem tremendously. With the proposed standard targets, the signal-to-clutter power ratio is about 20 dB minimum and clutter-to-receiver noise ratio is about 8 dB typically. This justifies the simplification. Although the negligible noise assumption is usually realistic, the antenna parameter vector $\underline{\alpha}$ with noise can still be solved. To include receiver noise, the following changes must be implemented. The log likelihood functional in Equation (15) is of the same form but the matrix $\Lambda(\underline{\alpha})$ becomes

$$\Lambda(\underline{\alpha}) = D_g(\underline{\alpha}) \Lambda D_g(\underline{\alpha}) + N_o R$$

where:

$N_o$ is the receiver noise power.

This implies that computing the log likelihood functional and its gradient requires a matrix inversion. In terms of the steepest descent algorithm, it is implied that $\Lambda^{-1}(\underline{\alpha})$ must be computed for each iteration. A large increase in the number of computations is created and the method becomes unattractive. The algorithm can be utilized for the simplified problem as described in this section to get an initial point for the numerical algorithm which solves for the antenna parameters and includes receiver noise.

---

[*] Aoki, Masanao, "Introduction to Optimization Techniques," The Macmillan Co., N. Y., 1971, pp 102-126.

## Golden Section Search Method

This one-dimensional search will determine the optimal step size of the descent algorithm in the desired direction. At the $n^{th}$ step of the descent algorithm, one is given $\underline{\alpha}^{(n)}$ and computes $\nabla_{\underline{\alpha}} \ln \left[ p(\underline{z} | \underline{\alpha}^{(n)}) \right]$. To determine the step size the following method is used:

Let

$(a_o, b_o)$ be the initial closed interval of search so that

$a_o \leq t^{(n+1)} \leq b_o$ and $a_o = 0$

$$\phi^{(n)}(t) = \ln \left[ p(\underline{z} | \underline{\alpha}^{(n)}) \right] + t \cdot \left( \nabla_{\underline{\alpha}} \ln \left[ p\,(\underline{z} | \underline{\alpha}^{(n)}) \right] \right)$$

Assume, the search interval at the $k^{th}$ step of the one-dimensional search has been reduced to $\left[ a_k, b_k \right]$. To generate the $(k+1)^{th}$ interval of search given $\left[ a_k, b_k \right]$, compute

$$t_{k+1} = 0.328\,(b_k - a_k) + a_k$$

$$t'_{k+1} = 0.618\,(b_k - a_k) + a_k$$

and perform the following test:

If $\phi(t_{k+1}) < \phi(t'_{k+1})$, then $a_{k+1} = a_k$

and $b_{k+1} = t'_{k+1}$

If $\phi(t_{k+1}) \geq \phi(t'_{k+1})$, then $a_{k+1} = t_{k+1}$

and $b_{k+1} = t'_{k+1}$

To end the one-dimensional search algorithm, determine if

$$\left| a_k - b_k \right| \leq \varepsilon, \ \varepsilon \simeq 0 \qquad (16)$$

If Equation (16) is satisfied, then the optimal step size at the $n^{th}$ iteration $t^{(n+1)}$ of the descent algorithm becomes $t^{(n+1)} = (a_i + b_k)/2$.

Otherwise, continue the one dimensional search until Equation (16) is satisfied and the corresponding step size determined.

## 3.3 ANTENNA GAIN AND PATTERN CALIBRATION DESIGN

Designs for a corner reflector farm and for a processing algorithm to be used for antenna gain and pattern calibration purposes are discussed above and in this section. The corner reflector farm provides standard radar cross section targets for absolute and relative gain measurements. The processing algorithm is a mathematical expression for nearly optimal parameter measurements with the recorded SAR data, including the error contribution caused by imprecise knowledge of antenna pointing angles and corner reflector position relative to resolution cells.*

The two basic objectives of measurements with the reference target data are given below:

1. To calibrate antenna peak gain $G_0$ and pattern beamwidths in azimuth and elevation
2. To provide overall "end-to-end" calibration measurements that update and supplement sensor calibration measurements of transmitter power, receiver gain and system losses.

The corner reflector farm design provides an array of 16 standard cross section targets for:

1. The smoothing of measurement errors to obtain precision in peak gain determination
2. The determination of antenna beamwidths in vertical and horizon horizontal planes of the pattern with data smoothing for accuracy.

---

*Optimal as used here implies minimum mean square error for the ensemble of parameter measurements obtained from each specific set of corner reflector farm SAR data.

Multiple corner reflectors are used to permit data smoothing for reduction of errors from the following sources:

1. Antenna pointing knowledge (sensor and tracking errors)
2. Target cross section variance (reference errors)
3. Target aspect knowledge (survey errors)
4. Target coordinate determination (discriminant position errors)
5. Target migration in resolution cell (focus and range migration compensation errors).

Corner reflector specifications should have provisions for the following properties:

1. Large Reference Cross Section - $\sigma_s \geq 1000\ m^2$ at assigned wavelengths to provide signal to background clutter ratios of at least 13 dB for 25 x 25 m resolution cells with background backscatter coefficients $\sigma_o \simeq .08\ m^2/m^2$ (-11 dB);
2. Accurate Reference Cross Section - The on-axis cross section of the corner reflectors should be known to an accuracy of at least ±0.5 dB, $1\sigma$ (±1.0 dB with 95 percent confidence);
3. Portability - the corner reflectors should be mounted to fixtures to enable:
   - a. Easy adjustment and survey of aspect angle relative to SAR imaging geometry
   - b. Convenient positioning and survey of target geographical coordinates
   - c. Target position and aspect stability
   - d. Easy inspection of reflectors for geometrical integrity in situ (dimensions, angle, flatness, surface smoothness)
   - e. Easy dismounting of reflectors for convenient storage and security;
   - f. The reflectors to clear surrounding terrain by about 1 meter and to be readily visible for detection and inspection (e.g., by aerial survey).

The reflectors should be located in an area of about 50 x 3 km. The terrain should be nearly homogeneous and should be characterized by generally low backscatter coefficients ($\sigma_o < -11$ dB). The immediate vicinity of the corner reflectors should be free of large discrete targets (farm buildings, machinery, vehicles, homes, grain elevators, etc.).[*]

A site with generally stable atmospheric conditions should be selected for the corner reflector farm, if practicable. Knowledge of the lower atmosphere conditions is needed to determine two-way propagation loss with an accuracy better than 0.2 dB ($1\sigma$), at the time of the shuttle passage, for calibration purposes.

The reflectors should be physically large for adequate signal-to-noise ratio, and must be fabricated with precision to ensure theoretical pattern properties. Significant parameters are as follows:

1. Lineal dimensions of a side (see Figure 23):

$$a = \left(\frac{3\lambda^2}{4\pi}\sigma_s\right)^{1/4} \pm 0.6 \text{ percent}, \quad \sigma_s = 1000 \text{ to } 5000 \text{ m}^2$$

2. Right angles at corner vertex: $\alpha = \pi/2 \pm 3$ mrad ($90 \pm 0.2$ degrees)
3. Flatness: all surfaces flat to within $\pm\lambda/20$ ($\approx$1600 microns at X-band)

A single corner reflector with a side a = 104 cms or 41 inches will provide a cross section of 1000 to 5000 $m^2$ from C-band (4.3 GHz) to X-band (to 9.6 GHz); adequate for a dual C/X-band SAR. However, a corner reflector of cross section $\sigma_s = 1000$ $m^2$ at L-band (1.71 GHz) is 165 cms (65 inches) on a side and has impractically large cross section of 31,500 $m^2$ at X-band (9.6 GHz). Separate corner reflectors are required for dual L/X-band systems. However, the corner reflectors may share a common site with a judicious choice of corner reflector location to avoid potential X-band calibration errors caused by interference from the larger corner reflector.[**]

---

[*] Multipath interference is not a problem for angles of incidence less than 45 degrees. At greater incidence angles multipath inteference due to terrain reflections near the corner reflector should be controlled by suitably designed and positioned shields or fences for that purpose. The corner reflectors should be mounted at a reasonable heighth (e.g., 1 m minimum) above the terrain.

[**] The disadvantage of large size for L-band corner reflectors can be offset by fabricating them with a wire mesh surface on a suitably rugged framework with mesh size very small in comparison to a wavelength (e.g., $< \lambda/50$); thus the weight and wind surface effects of very large metal reflectors can be reduced substantially.

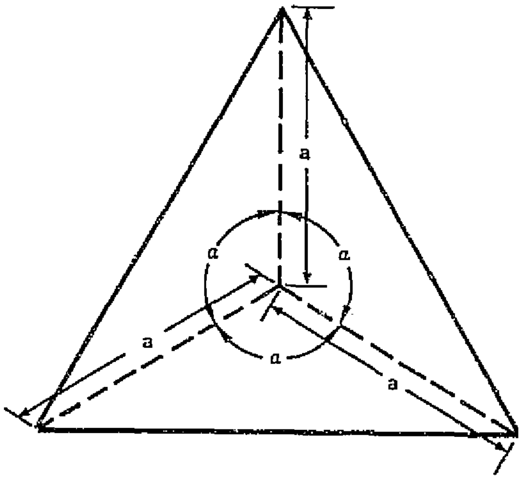

a. Geometry

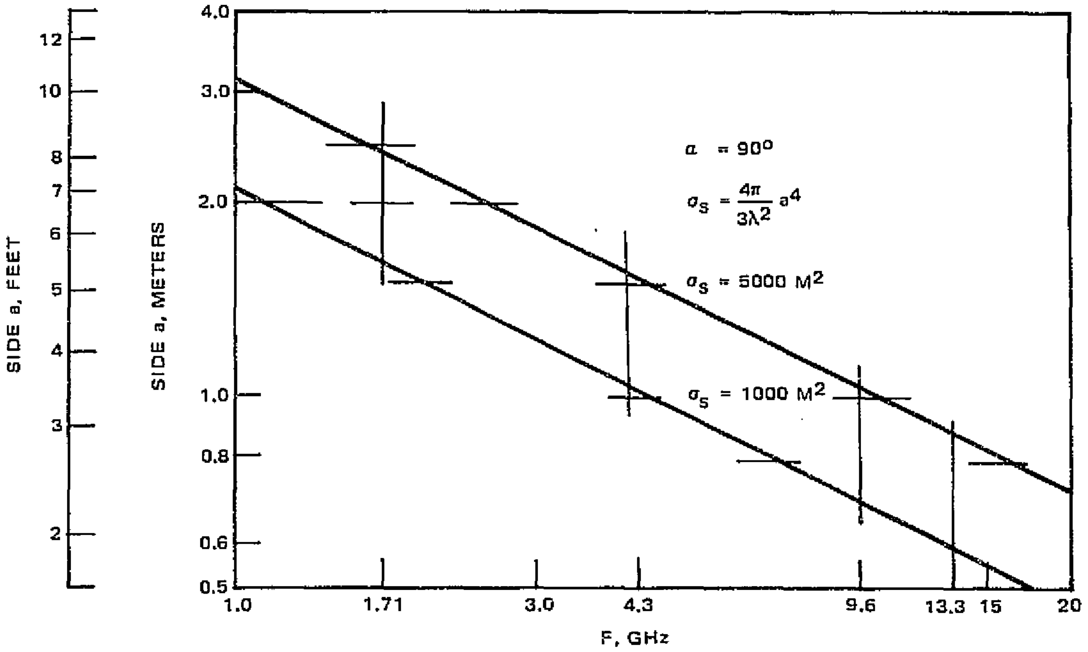

b. Maximum cross section versus size and frequency

Figure 23. Trihedral corner reflector

A possible corner reflector farm and an approach to corner reflector installation are shown in Figure 24. The 16 corner reflectors are dispersed in four groups of four corner reflectors each, located on a strip that is 74 km long and 750 m wide. The reflectors are arranged for passage of the shuttle at an altitude of 200 km above the terrain with the subshuttle path direction 50 degrees west of local north. The local incidence angle is 50 degrees, and the corner reflectors have been positioned with their symmetry axis tilted for SAR viewing at 90 degrees relative to the subsatellite path. The corner reflectors are mounted on sleds rimmed with absorptive shields to divert potential multi-path reflections from the corner.

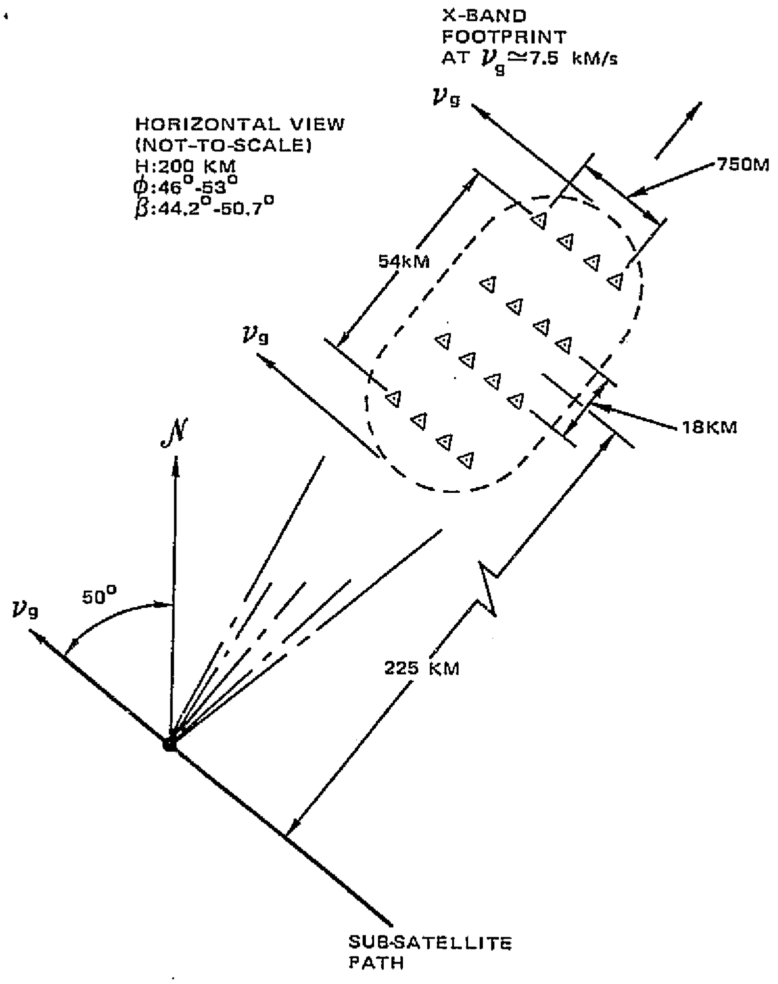

a. Reflector farm

Figure 24. Corner reflector array and mounting
(Sheet 1 of 2)

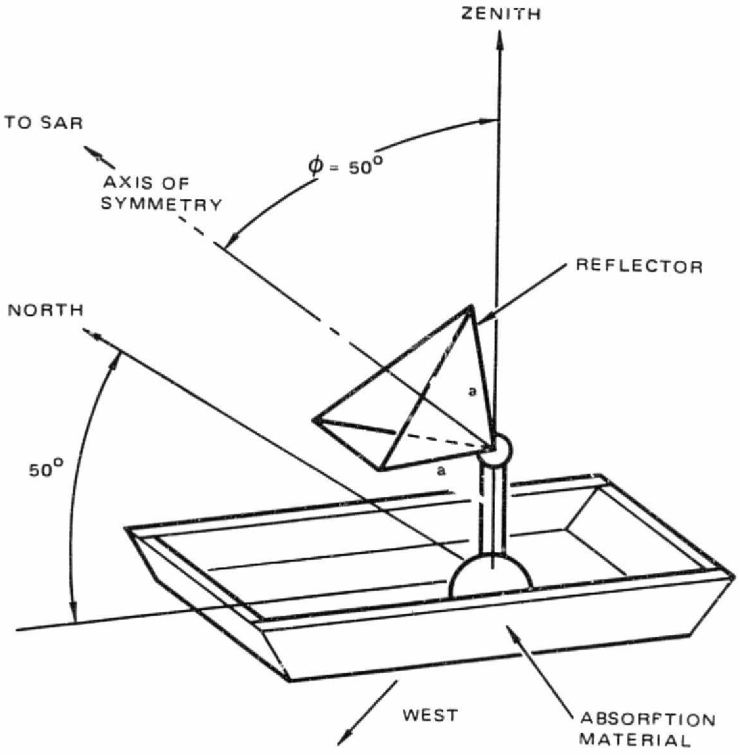

b. Sled-mounted reflector

Figure 24. Corner reflector array and mounting (Sheet 2 of 2)

# 4.0 MEASUREMENT AND CALIBRATION ACCURACY

The accuracy of SIR measurement and calibration systems are discussed in this section. The radar parameters requiring calibration, error sources and an error model are described in Section 4.1. The statistical performance of three measurement algorithms is discussed in Section 4.2. Error budgets for calibration and measurement accuracies are given in Section 4.3.

The calibration error budgets include estimates of performance for the space calibration functions and estimates of accuracy of calibration of the corner reflector farm targets by means of data records.

The measurement accuracies are estimated for the baseline measurement algorithm, which makes use of simple averages of squared amplitudes, and a nearly optimum algorithm. The later algorithm is more complex computationally but superior in performance when used for small areas; that is, at a given accuracy level, the nearly optimum algorithm has better resolution. In particular, it is estimated that the more effective algorithm gives results with an accuracy of 2.5 dB at 80 percent confidence for an area of $10^4$ square meters, while the baseline algorithm requires an area greater than $2 \times 10^4$ square meters for equivalent accuracy. The less complex algorithm was selected as the baseline algorithm because of its simplicity and moderate efficiency.

## 4.1 MEASUREMENT ERROR CONTRIBUTIONS

Measurement error, in the context of this study, is the difference between the measured value ($\overset{\omega}{\sigma}_o$) and the true value ($\sigma_o$) of the backscattering coefficient that characterizes imaged terrain areas. The imaged terrain areas, in general, consist of a number of resolution cells (e.g., 16 to 36 cells of 25 x 25 m each) which border one another. The number of cells is chosen to provide adequate smoothing of scintillation error or noise caused by the diffuse scattering surface, consistent with the required resolution area.

The algorithm used for measuring $\sigma_o$ provides an unbiased estimate $\overset{\omega}{\sigma}_o$:

$$E\left\{\overset{\omega}{\sigma}_o\right\} = \sigma_o \tag{17}$$

where E signifies expectation in the sense of mathematical statistics; i.e.,

$$E\left\{\overset{\omega}{\sigma}_o\right\} = \underset{NM\to\infty}{\text{limit}} \frac{1}{NM} \sum_{n=1}^{N} \sum_{m=1}^{M} \left(\overset{\omega}{\sigma}_o\right)_{n,m} \tag{18}$$

where N is the number of SAR sensors making measurements and M the number of measurements made with each SAR. The common measurement algorithm is used for the common backscatter coefficient $\sigma_o$.

The error in measurement is

$$\epsilon_\omega = \overset{\omega}{\sigma}_o - \sigma_o \tag{19}$$

and the normalized error is

$$\frac{\epsilon_\omega}{\sigma_o} = \frac{\overset{\omega}{\sigma}_o}{\sigma_o} - 1 \tag{20}$$

For purposes of this study, the normalized error is expressed in decibels.

$$\Delta_\omega = 10 \log\left(\frac{\overset{\omega}{\sigma}_o}{\sigma_o}\right) = 10 \log\left(1 + \frac{\epsilon_\omega}{\sigma_o}\right) \tag{21}$$

$$\simeq 4.34 \frac{\epsilon_\omega}{\sigma_o}, \ \epsilon_\omega << 1 \tag{22}$$

Measurement error in the context of a single mission (5 to 30 days duration) and a particular SAR sensor comprises fixed and temporal errors. It is defined below:

1. Fixed error — constant for an entire mission
2. Temporal error – varies within a mission.

It is useful to classify the error components in terms of their correlation period; three such components have been identified in this study (see Table 7):

$$\epsilon_{\omega_{\sigma_o}} = \epsilon_M + \epsilon_{10\ \mathrm{SECS}} + \epsilon_I \qquad (23)$$

The measurement errors are expressed in decibels and in terms of an 80 percent confidence interval based on the chi-square distribution or a Gaussian distribution model for the errors. The 80 percent confidence interval is expressed in decibels as 10 log (U/L), where U is the expected upper bound (the probability of a measurement larger than U is 10 percent)

TABLE 7. MEASUREMENT ERROR COMPONENTS

| Error Component | Period of High Correlation | Contributing Errors |
|---|---|---|
| $\epsilon_M$ | 1 Mission | 1. Antenna gain and shapes<br>2. Transmitter power/receiver gain |
| $\epsilon_{10\ \mathrm{SECS}}$ | 10 Seconds | 1. Receiver noise measurement<br>2. Antenna pointing<br>3. Large area propagation loss |
| $\epsilon_I$ | 0 (Little correlation between measurements) | 1. Short term variation in propagation loss<br>2. Scintillation in ground return<br>3. Ground slope and object area altitude |

and L is the expected lower bound (probability of a measurement smaller than L is 10 percent). The relations are shown in Figure 25 where $\sigma_y$ is the standard deviation of the measurement error:

$$\sigma_y^2 = E\left\{\left(\frac{\overset{\omega}{\sigma}_o}{\sigma_o} - 1\right)^2\right\} = \text{Variance}\left(\frac{\overset{\omega}{\sigma}_o}{\sigma_o}\right). \tag{24}$$

The decibel equivalent of the standard deviation is defined below:

$$\sigma_{y,\,dB} = 10 \log (1 + \sigma_y) \tag{25}$$

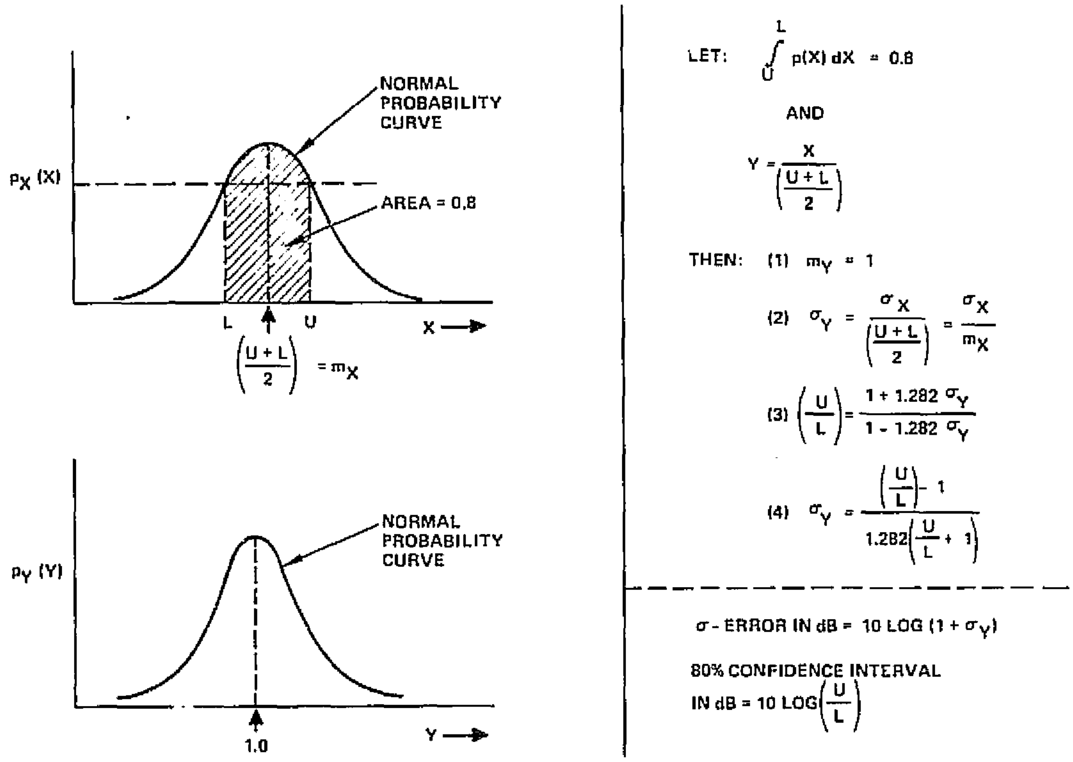

Figure 25. 80 percent confidence interval and standard deviation.

The broad categories of error sources are given below:

1. $\xi_\sigma$, the error in $\sigma_o$ due to scintillation in the backscatter from the diffuse surface and the receiver noise; varies from look-to-look and cell-to-cell
2. $\xi_K$, the error in the sensor parameter $K_{rad}$, relatively fixed, but includes a component ($C_{R,\phi}$) which may vary cell-to-cell because of propagation factors or geometry
3. $\delta_i$, the error in gain parameters $g_i$; will vary from look-to-look and cell-to-cell in a systematic manner, depending on antenna pointing and pattern errors
4. $\xi_N$, the error in the measurement for the noise power; this error is common to each set of N looks-and-cells.

The error sources are identified through the baseline measurement process, discussed in Section 3.2. Measurements are made with a normalized image variate $Y_i$ (complex):

$$|Y_i|^2 = \frac{|Y_i^u|^2}{K_{rad}}$$

where

$$E\left\{|Y_i|^2\right\} = g_i^2 \sigma_o + N_o$$

and $K_{rad}$ is the radar sensor parameter discussed in Section 2.1. The measurement is

$$\overset{\omega}{\sigma}_o = \frac{1}{N}\sum_{i=1}^{N} \frac{\left(|Y_i|^2 - N_o - \xi_N\right)(g_i + \delta_i)^{-2}}{\left(1 + \frac{\xi_k}{K_{rad}}\right)} \tag{26}$$

Let

$$\hat{\sigma}_{o_i} = (|Y_i|^2 - N_o)\, g_i^{-2}$$

$$\hat{\sigma}_o = \frac{1}{N}\sum_{i=1}^{N} \hat{\sigma}_{o_i} ; \quad \xi_\sigma = \hat{\sigma}_o - \sigma_o$$

then

$$E\left\{\hat{\sigma}_o\right\} = \sigma_o$$

There are four component errors in measurement, neglecting higher order terms than the first:

$$\xi_\omega = \overset{\omega}{\sigma}_o - \sigma_o = \xi_\sigma - \left(\sum_{i=1}^{N} \frac{g_i^{-2}}{N}\right)\xi_N - \hat{\sigma}_o \frac{\xi_k}{K_{rad}} \sum_{i=1}^{N} \hat{\sigma}_{o_i} \left(\frac{2\delta_i}{g_i}\right) \qquad (27)$$

The corresponding variances of the measurement errors (assuming statistical independence between component errors) are

$$E\left\{(\xi_\omega - \xi_\omega)^2\right\} = \mathrm{Var}\,(\hat{\sigma}_o) + \sum_{i=1}^{N} \frac{g_i^{-2}}{N}\,\mathrm{Var}\,(\xi_N) + \sigma_o^2\,\mathrm{Var}\left(\frac{\xi_k}{K_{rad}}\right)$$

$$+ \sigma_o^2 \left[E\left\{1/4 \sum_{k=1}^{4} \left(\frac{2\delta_k^A}{g_k^A}\right)^2\right\} + E\left(\frac{2\delta^E}{g^E}\right)^2\right]$$

where:

$$(g_k + \delta_k)^2 = (g^E + \delta^E)^2 \, (g_k^A + \delta_k^A)^2$$

$$\approx (g^E g_k^A)^2 \left(1 + \frac{2\delta^E}{g^E} + \frac{2\delta_k^A}{g_k^A}\right); \qquad (28)$$

i.e., the antenna pattern is separable in elevation and azimuth.

The first term in Equation (27) is the minimum expected error; it determines the best possible measurement accuracy with the baseline algorithm. The basic accuracy limitation is fixed by finite area ($N \ll \infty$) and the effective signal-to-noise ratio. The expected error is significant for all practical values of N ($N \ll 400$), even for very large effective signal-to-noise ratios ($SNR \gg 10$ dB):

$$\text{Var}\left(\frac{\hat{\sigma}_o}{\sigma_o}\right) \geq \frac{\left[1 + (SNR)^{-1}\right]^2}{N} \qquad (29)$$

where the equality applies for statistical independence among the N observations. Conversely, the expected error becomes very small with an indefinite increase in area at finite SNR.

The second term is contributed by the variance in the measurement of the receiver noise component $N_o$. The severity of this error depends on the relative gain $g_i$ and is most severe near the edges of the illuminating beam ($g_i \ll 1$). This factor reflects the reality that receiver noise voltages are not modulated by the antenna gain pattern ($g_i \lesssim 1$) as are the scintillating signals from the diffuse scattering surface of the terrain.

The third term is the error from faulty calibration of $K_{rad}$; Equation (4):

$$K_{rad} = \frac{P_T G_o^2 \lambda^2 d_r d_a \Gamma_r}{(4\pi)^3 R_s^4 L_{AT} L_{SYS} \text{SIN}\phi} N_{pc}^2 N_{pulses}^2$$

The product of transmitter power and receiver gain, $P_T \Gamma_r N_{pc}^2 N_{pulses}^2$, is updated at frequent intervals by the pilot mode calibration routine. The $K_{rad}$ factor is updated at infrequent intervals with data from a corner reflector farm. This calibration is especially important since it updates the antenna peak gain factor $G_o$ and the propagation loss factor $L_{AT}$.

The final factor involves the antenna orientation components $g_i$; their contribution depends on knowledge of antenna pointing and antenna pattern parameters (beamwidths). Calibration for these parameters are updated with the infrequent visits to the corner reflector farm. The $g_i$-set errors $\delta_i$ vary systematically from cell-to-cell and look-to-look during $\sigma_o$-measurement. The errors in the $g_i$-parameter sets from look-to-look are minimal if the antenna illumination pattern is symmetrical for the four looks. Thus, the effects of errors in azimuth angle pointing knowledge and antenna beamwidth are minimized with image formation chosen for symmetry in azimuth. The cell-to-cell variations in $g_i$ for elevation are small because of the small fraction of the vertical beamwidth subtended by the image area averaged in the N measurements. This essentially fixed error component is accordingly sensitive to location of the imaged area relative to the swath center; minimum error is obtained with an antenna pattern very nearly flat ($g_i \approx 1$) over a large portion of the swath. The error sensitivity for a uniform weighted array is severe at swath positions outside the middle third of the elevation illumination pattern, both with respect to knowledge of vertical antenna pointing accuracy (look angle) and of pattern (beamwidth). The advantages of a shaped vertical illumination pattern are apparent, as discussed below in consideration of error budgets.

## 4.2 MEASUREMENT ALGORITHMS

Performances of three different $\sigma_o$ algorithms are described and statistically compared in this section. The algorithms differ in terms of the required number of computations and the required a priori knowledge of several system parameters. In general, given the correct system parameters, the more complex the algorithm, the better its performance. When the system parameters used contain calibration errors, performance is slightly degraded. These performance losses are discussed in Section 4.3. In this section the algorithms are compared under the ideal condition, in which all the system parameters are perfectly understood. The results will indicate the accuracy of each algorithm without error in calibration, antenna pointing, or noise power measurement.

The problem of determining the correct $\sigma_o$ from the observed number of resolution cells is equivalent to estimating power from a correlated set of I (in-phase) and Q (quadrature-phase) samples of complex signals modulated by the antenna gain and corrupted by receiver noise. Correlation exists because neighboring resolution cells have a finite overlap and because different looks utilize common overlapped data. The observed image set $\{Y_i^u,\ i = 1, \ldots, N\}$ is unnormalized as shown in Table 8. The normalized image is shown in Table 9. The terrain image is normalized so that the signal power is only a function of the gain pattern and the terrain backscatter coefficient.

TABLE 8. UN-NORMALIZED $Y_i^u$-SIGNAL STRUCTURE

$Y_i^u = X_i^u + Z_i^u$ (Terrain plus noise)

$E\left|X_i^u\right|^2 = K_{rad}\, g_i^2\ \sigma_o$

$g_i$ Normalized antenna power pattern (i.e., $G_i/G_o$)

$\sigma_o$ Terrain backscattering coefficient (to be measured)

$$K_{rad} = \frac{P_T G_o^2\, \lambda^2\, d_a d_r\ \Gamma_r}{(4\pi)^3\, R_s^4\, L_{AT} L_{SYS} \mathrm{SIN}\,\phi}\, N^2_{\text{pulse comp}}\, N^2_{\text{pulses}}$$

(Same for all cells)

$E\left|Z_i^u\right|^2 = N_o^u$ (Receiver noise power appearing at $i^{th}$ cell, same for all cells)

TABLE 9. NORMALIZED IMAGE

| Component | Normalization by $\sqrt{K_{rad}}$ (*) | Average Power Normalized Signal |
|---|---|---|
| Total Image ($Y_i$) | $Y_i = \frac{Y_i^u}{\sqrt{K_{rad}}}$ | $E\|Y_i\|^2 = g_i^2 \sigma_o + N_o$ |
| Terrain ($X_i$) | $X_i = \frac{X_i^u}{\sqrt{K_{rad}}}$ | $E\|X_i\|^2 = \frac{E\|X_i^u\|^2}{K_{rad}} = g_i^2 \sigma_o$ |
| Receiver Noise ($Z_i$) | $Z_i = \frac{Z_i^u}{\sqrt{K_{rad}}}$ | $E\|Z_i\|^2 = \frac{N_o^u}{K_{rad}} = N_o$ |
| *$K_{rad}$ is part of the radar calibration procedure. | | |

The $\sigma_o$-measurement algorithms are given in Table 10. The baseline algorithm computes a weighted power estimate of the terrain image by compensating for the antenna gain pattern and removing the power contribution of noise. The near optimum alternate pre-whitens the data and also computes a weighted power estimate by also compensating for the antenna gain and removing the bias term caused by noise power. The near optimum algorithm corresponds to the maximum likelihood estimate within the signal-to-noise power ratio regions of interest (S/N ≥ 4 dB). The marginal alternate algorithm computes a simple power average which does not compensate for the gain variations and correlation. This algorithm is the most commonly used power estimate and is optimum when there is no gain variation and statistical independence exists.

The complexity of each algorithm is determined by the number of computations and the a priori knowledge of the system parameters it requires. The parameters required in the computation of a particular algorithm are given in Table 11. All the algorithms require measurement of the normalization parameter $K_{rad}$ and noise power term $N_o$. In addition, the

## TABLE 10. $\sigma_o$ MEASUREMENT ALGORITHMS

| Algorithm Classification | Type Algorithm | $\hat{\sigma}_o$ Algorithm | |
|---|---|---|---|
| | | Matrix Form | Summation Form |
| Baseline | Weighted Power Averaging | $\frac{\overline{y}' D_g^{-2} y - \hat{N}_o \operatorname{tr} (D_g^{-2})}{N}$ | $\frac{1}{N} \sum_{i=1}^{N} g_i^{-2} \left[ \lvert y_i \rvert^2 - \hat{N}_o \right]$ |
| Near Optimum Alternate | Pre-Whitened and Weighted Power Averaging | $\frac{\overline{y}' (D_g R D_g)^{-1} y}{N} - \frac{\hat{N}_o \operatorname{tr} (D_g^{-1} R^{-1} D_g^{-1} R)}{N}$ | $\frac{1}{N} \sum_{i}^{N} \sum_{j}^{N} a_{ij} (y_i \overline{y}_j - \hat{N}_o r_{ji})$<br>$\left[ a_{ij} \right] = \left[ D_g R D_g \right]^{-1}$ |
| Marginal Alternate | Simple Power Averaging | $\frac{\overline{y}' y}{N} - \hat{N}_o$ | $\frac{1}{N} \sum_{i=1}^{N} \left[ \lvert y_i \rvert^2 - \hat{N}_o \right]$ |

TABLE 11. $\sigma_o$ MEASUREMENT PRELIMINARY
PARAMETER MEASUREMENTS

| $\sigma_o$ Measurement System | Estimated Parameters | Related Notation |
|---|---|---|
| Baseline | $K_{rad}$<br>$g_i$ (Antenna Pattern)<br>$N_o$ (Normalized Noise Power) | $D_g = \begin{bmatrix} g_1 & 0 & 0 & \cdots & 0 \\ 0 & g_2 & 0 & \cdots & 0 \\ 0 & 0 & g_3 & \cdots & 0 \\ \vdots & \vdots & \vdots & \ddots & \\ 0 & 0 & 0 & & g_N \end{bmatrix}$ |
| Near Optimum Alternate | $K_{rad}$<br>$g_i$<br>$N_o$<br>R (Correlation Matrix) | $R = \left[\int_A \int h_i(x, y)\, h_j(x, y)\, dx\, dy\right]$<br>$h_i(x, y)$ is the normalized 2-dimensional impulse response function for $i^{th}$ cell |

baseline and the near optimum algorithm require knowledge of the antenna gain pattern and pointing angles. The near optimum algorithm requires the a priori knowledge of the covariance matrix so that data can be pre-whitened. Computationally, the near optimum alternate performs a weighted double summation of complex numbers. The baseline and marginal alternate perform a single summation of real numbers with an additional premultiply by the inverse of the gain pattern.

The performance of the $\sigma_o$-algorithms is summarized in Figures 26 through 30. The performance described here reflects the accuracy of the algorithms alone and not the effects of calibration, antenna pointing or noise power measurement accuracies. The Cramer-Rao bound, illustrated in most of these figures, theoretically is the smallest standard deviation possible for the $\sigma_o$ measurements and, therefore, a lower bound to measurement

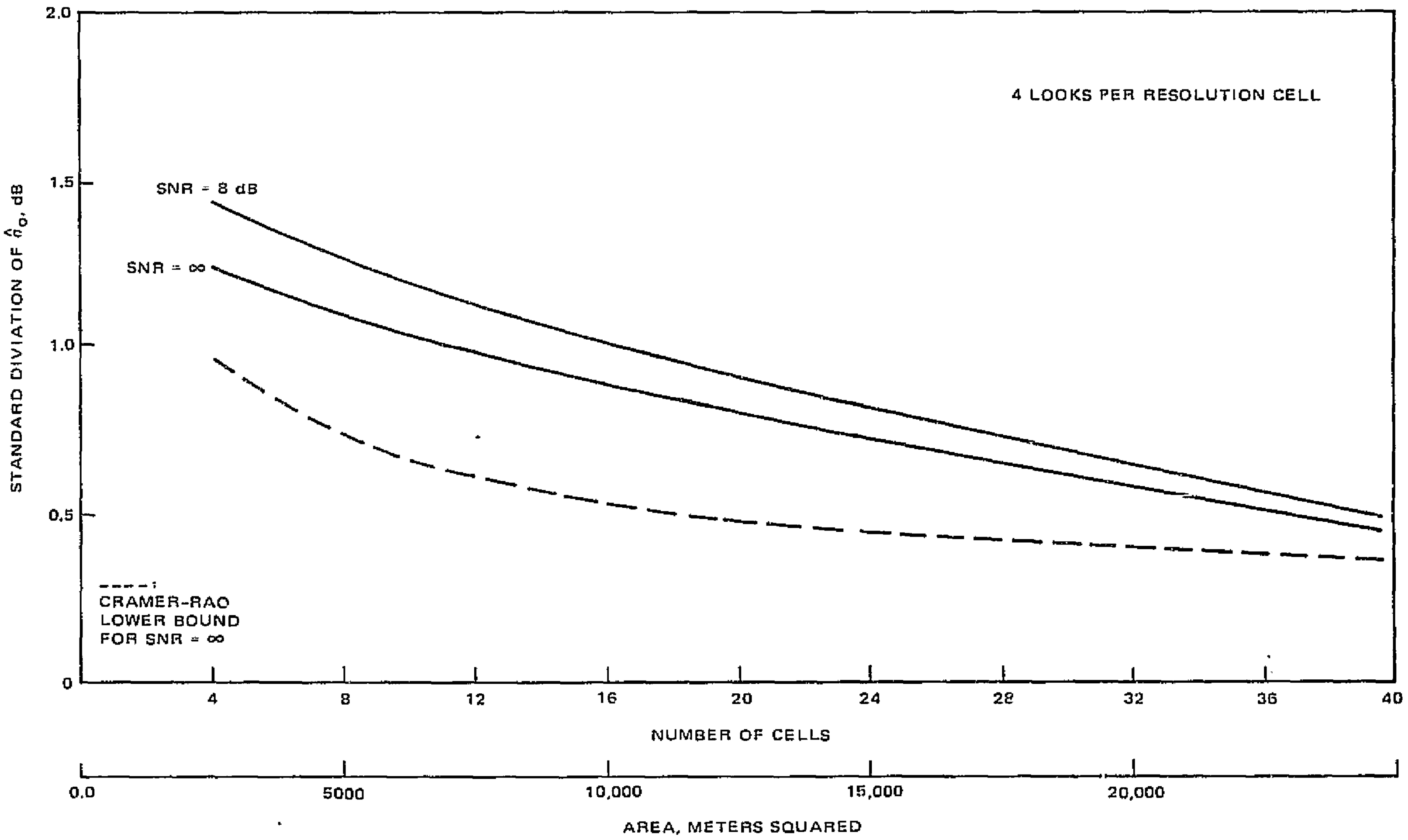

Figure 26. Baseline $\sigma_o$ algorithm performance

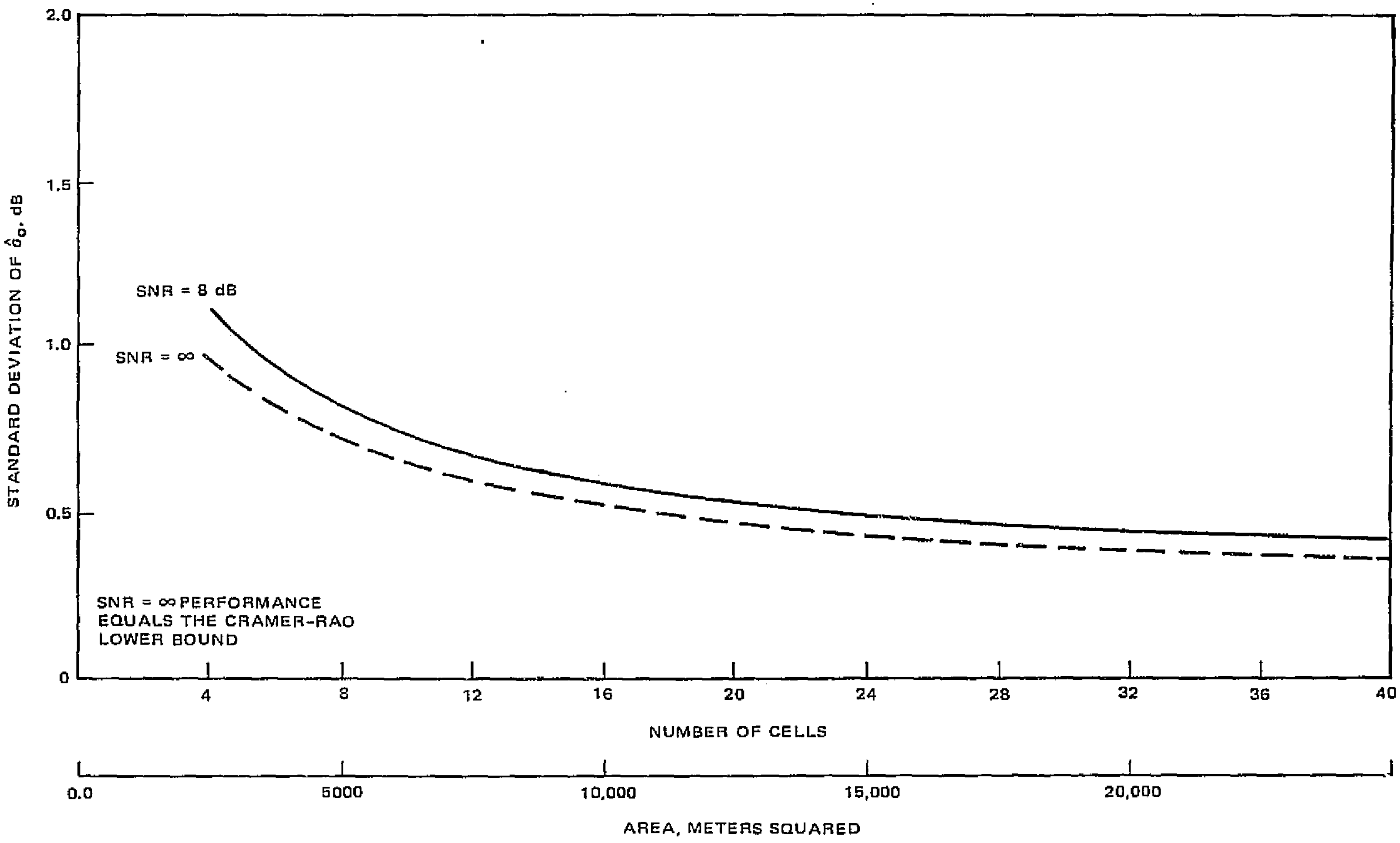

Figure 27. Performance of near optimum $\sigma_o$ algorithm, four looks per resolution cell.

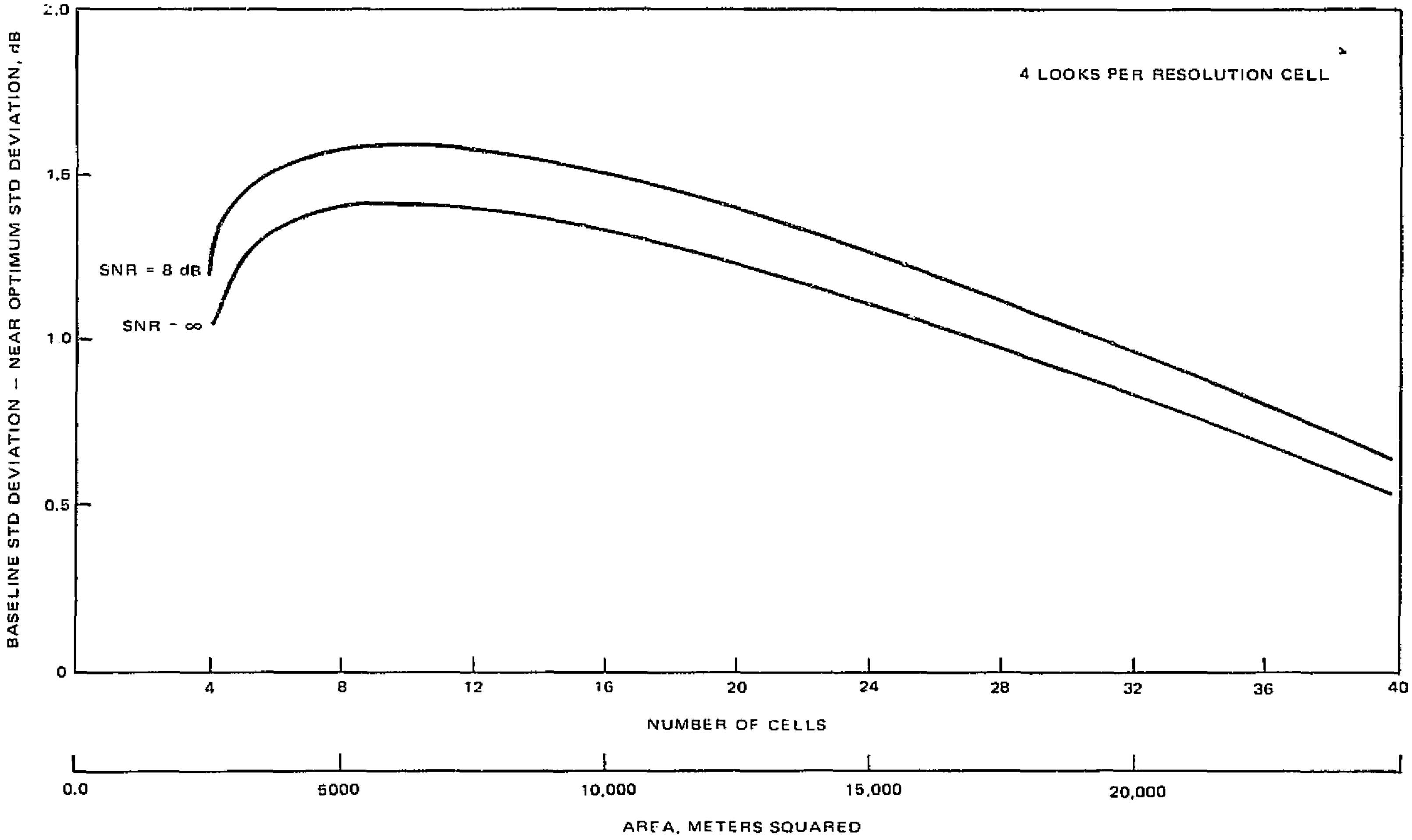

Figure 28. Near optimum versus baseline $\sigma_o$ algorithm performance

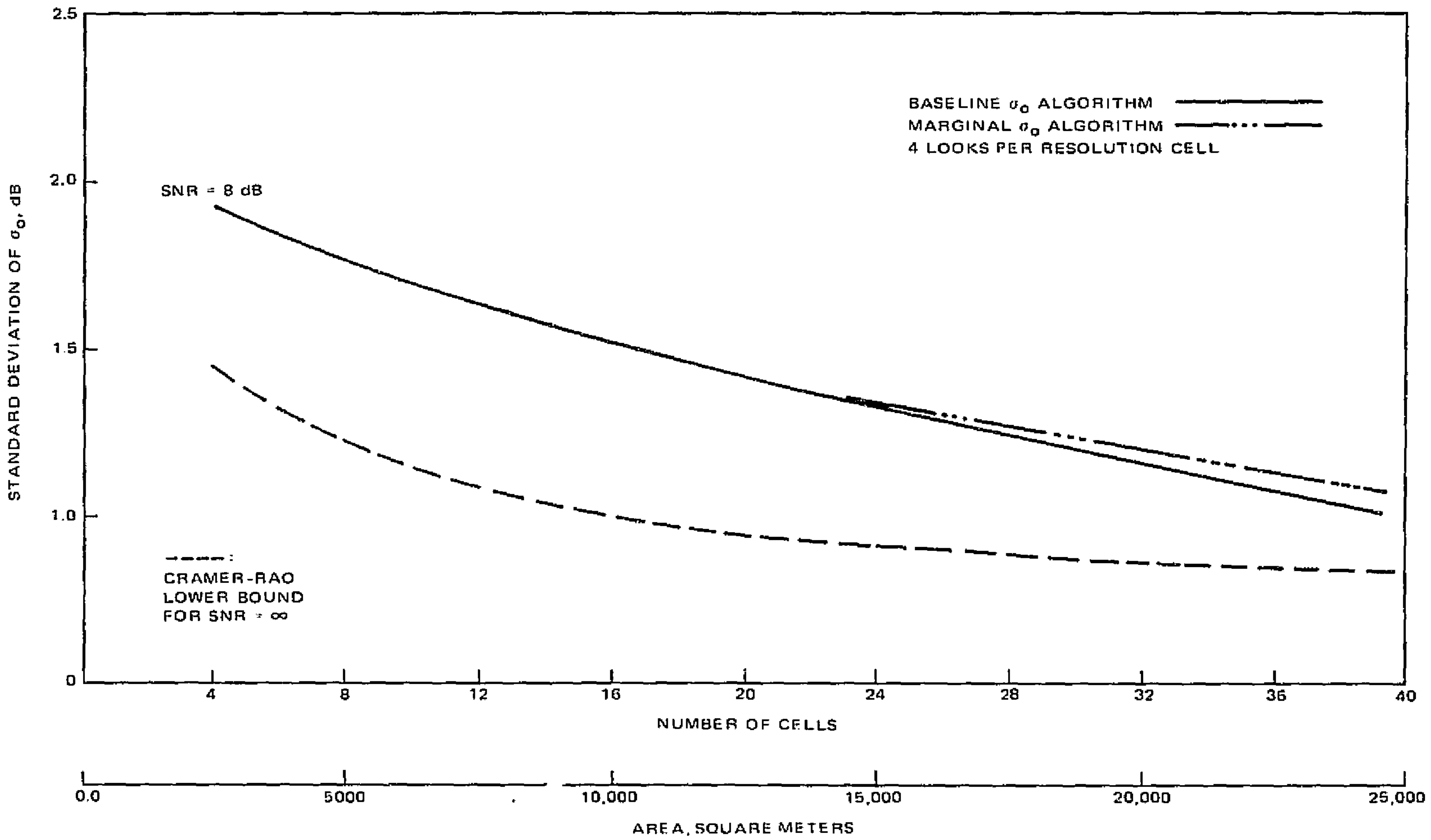

Figure 29. Comparison of baseline to marginal algorithm.

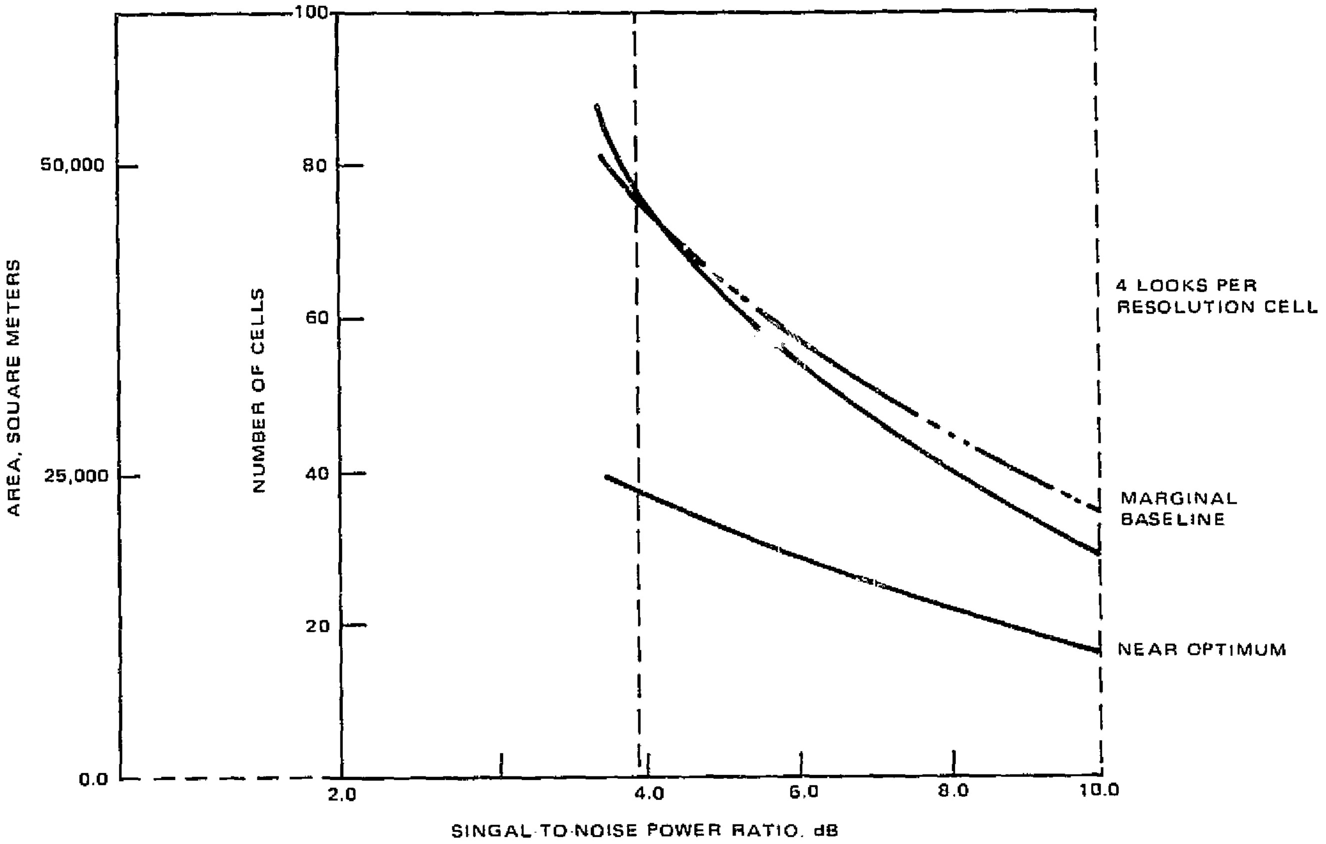

Figure 30. Algorithm cor. parisons

accuracies. It should be noted that four looks per resolution cell are assumed for all these performance curves. Figures 26 and 27 show e standard deviation of the baseline and near optimum alternate algorithms as a function of number of cells (area) for signal-to-noise power ratio of 8 dB and infinity. The near optimum performance is superior and coincides with the Cramer-Rao (CR) bound for given SNR ratios. The near optimum alternate attains this bound because, for the SNR region of interest, this algorithm is the "maximum likelihood estimate" (MLE) of $\sigma_o$. On the other hand, even at infinite SNR, the baseline algorithm standa.d variation differs considerably from the CR bound and the MLE algorithm.

The relative performance differences of the baseline to the near optimum algorithm for SNR of 8 dB and infinity is shown in Figure 28. The baseline standard deviation is subtracted from the near optimum standard deviation and then converted to dB. The figure shows that the maximum difference occurs when nine resolution cells are used. Beyond nine cells, the difference diminishes monotonically as the number of cells are increased. For 8 dB SNR, the maximum difference is near 0.5 dB.

The marginal alternate algorithm forms a biased estimate of scattering coefficient $\sigma_o$. The bias can be removed by estimating the sum of the antenna gain pattern coefficients squared (Table 11). The comparative performance of the baseline is shown in Figure 29 versus the marginal algorithm when the bias from the marginal algorithm is removed. The curve shows that the standard deviation at 8 dB SNR for both algorithms are the same for small numbers of resolution cells, and deviation from each other becomes more pronounced as the cells are increased.

All the algorithms are compared in Figure 30 in terms of the required number of cells and the signal-to-noise ratio (SNR) to achieve an estimation error (standard deviation) of a 0.5 dB. At SNR of 4 dB, the baseline and the marginal algorithm require essentially twice as many cells to process as the near optimum. For SNR of 10 dB, the marginal still requires twice as many cells, whereas the baseline requirement is reduced to only 1.5 as many cells. In all the cases, the number of cells required is monotonically reduced as SNR is increased. For example, the near optimum algorithm requires 40 cells at SNR of 4 dB and 20 cells at 10 dB; comparable requirements are 78 cells at 4 dB and 36 cells at 10 dB SNR for the baseline algorithm. The near optimum performance is superior under every condition. The algorithms with system parameter errors included are compared in a later section.

## 4.3 ERROR BUDGET

### 4.3.1 Calibration Error Budget

Calibration errors are budgeted in terms of three correlation time components ($\epsilon_{mission}$, $\epsilon_{10\ sec}$, $\epsilon_{independent}$) one each of three broad categories, of error: radar parameter sources of error ($K_{rad}$), the antenna orientation error sources ($g_i$) and the noise measurement errors ($N_o$).

The radar parameter $K_{rad}$ is, in turn, budgeted in terms of three major components:

$C_s$ = sensor components periodically updated with the pilot mode calibration routine, essentially the transmitter power and receiver gain product $P_T \Gamma_r$.

$C_G$ = sensor components infrequently calibrated with corner reflector farm data, essentially the peak antenna gain and any system losses not included in $C_s$.

$C_{R,\phi}$ = sensor components which depend on geometry and atmospheric attenuation.

The error components comprise three correlation time components:

$\epsilon_{mission}$ = components highly correlated over the period of a mission (5 - 30 days)

$\epsilon_{10\ sec}$ = components highly correlated over a 10-second period, corresponding to a ground path distance of 75 km.

$\epsilon_I$ = "independent" components of error which are uncorrelated for periods of time and distances as great as 10 seconds and 75 km; i.e., components of calibration error highly correlated only for multilook images and neighboring cells used for areal smoothing.

The calibration error budget is summarized in Table 12. The component errors are tabulated in units of the standard deviation, expressed in decibels:

$$\sigma_\epsilon (dB) = 10 \log (1 + \sigma_\epsilon), \ \sigma_\epsilon^2 = Var (\epsilon)$$

The independent component has only two contributors:

1. At X-band, a component of error caused by propagation loss variations with spatial distance.

## TABLE 12. CALIBRATION ERROR BUDGET

| Calibration Component | Mission Error, dB $\sqrt{Var(\epsilon_{MIS})}$ | Correlated Over 10 seconds, dB $\sqrt{Var(\epsilon_{10\ sec})}$ | Independent Component, dB $\sqrt{Var(\epsilon_I)}$ |
|---|---|---|---|
| $K_{rad}$: $C_s$ ($P_T \cdot$ Rec Gain ... ) | 0.25 | 0.15 | -- |
| $C_G\left((\lambda G_o)^2/L_{SYS}\right)$ | 0.31 | 0.21 | -- |
| $C_{R,\phi}\left(\frac{d_a d_r}{L_{AT} R^4 \mathrm{SIN}\phi}\right)$ L-Band:<br>X-Band: | 0.10<br>0.10 | 0.22<br>0.27 | <br>0.15 |
| $K_{rad}$, RSS: L-Band:<br>X-Band: | 0.41<br>0.41 | 0.34<br>0.37 | --<br>0.15 |
| $g_i$: (Antenna Pattern, Pointing) | 0.26 | 0.24 | 0.20 |
| $N_o$: (Receiver Noise)* | -- | 0.02 | -- |
| Net RSS: L-Band<br>X-Band | 0.49<br>0.49 | 0.42<br>0.44 | 0.20<br>0.25 |
| TOTALS: | L-Band: | 0.67 | |
| | X-Band: | 0.70 | |

*NOTE: Noise measurement accuracy ≤ 0.12 dB, SNR ≥ 2 dB, and receiver gains scaled with 0.12 dB accuracy or better.

2. Antenna orientation, $g_i$, component error caused by fluctuations in antenna pointing knowledge. These components arise because of scintillation noise in the measurement of antenna pointing angles and variations in terrain geometry (primarily altitude, used in the determination of vertical angles).

The independent component of calibration error is a variable, a function of external factors that are not assessable to direct calibration by sensor instrumentation. Topographical data can be used to supplement ephemeris and/or altimeter data for terrain clearance altitude; it is assumed that provision will be made for terrain profile data in ground processing. Similarly, weather data from ground and satellite sources (e.g., Nimbus, or an auxiliary sensor) can serve for estimating cloud cover in terms of average propagation loss for short wavelength (X-band) SAR $\sigma_o$-measurements. Ground processing should factor propagation loss data into the measurement algorithms for the short wavelength band (X-band) SAR processing. In all cases, basic temporal and spatial variation of propagation losses must be recognized, and some estimate of the expected impact on measurement accuracy must be made to best utilize the cloud cover penetration capability of the SAR sensor. An effective modeling of variations in terrain altitude with geographical location is also needed to improve the precision of measurements.

The receiver noise calibration error contribution is very small, essentially insignificant, at meaningful signal-to-noise ratios (SNR $\geq$ 2 dB). The tabulated error is equivalent to a measurement accuracy for the noise factor $N_o$ of 0.12 dB made on 1200 independent samples of the receiver noise and scaled to the appropriate receiver gains with equivalent accuracy (0.12 dB). Without the removal of bias caused by noise, the expected measurement error is $\leq 1$ dB for SNR $> 5.8$ dB. The independent component of receiver noise is a function of SNR and the scintillation smoothing for $\sigma_o$-measurement. This component is not properly a part of the calibration error budget but rather of the $\sigma_o$-measurement accuracy treated in the following section. The noise component of calibration to remove measurement bias errors is a vital component of $\sigma_o$-measurement algorithms.

The antenna orientation factors, $g_i$, include two related component errors: one attributed to antenna pattern errors and the other to errors in antenna pointing knowledge. The error components caused by antenna pointing knowledge are functions of data processing algorithms and of the antenna patterns. These errors have correlation times that are short in comparison to an orbit period and have a mean error over the duration of a mission that is very close to zero. The antenna pattern errors, on the other hand, tend to vary slowly and have correlation times that are large in comparison to 10 seconds. Thus the estimates for antenna pattern factors are included in the mission error category of correlation times while pointing accuracy estimates are based on short correlation times. The pattern factors are updated with calibration algorithms using the corner reflector farm data. The pointing accuracies are functions of some form of doppler sensing in azimuth and depend, in part, on the form of the algorithm used to derive these data; sensor data alone do not suffice. The estimates for antenna pointing are based on standard derivations of pointing equivalent to 5 percent the azimuth beamwidth, about 0.14 mrad at X-band (antenna length of 10.7 at 9.0 GHz).

The accuracies of look angle pointing knowledge are about ±2 percent of the vertical beamwidth for uniform illuminated antennas and an error in $g_i$ of ±0.2 dB at the beam edges. Thus an accuracy of about ±0.2 degree in look angle knowledge is needed for an antenna vertical beamwidth of 10 degrees. The needed accuracy is greatly reduced with shaped illumination functions for the vertical beams. Figure 31 is an example of a nearly flat topped pattern obtained with truncated sin (Bx)/x illumination functions. Antennas of this type are practical for the SIR sensor.

The radar parameter $K_{rad}$ errors, which constitute the major portion of the overall calibration errors, are budgeted for the three factors: $C_S$, $C_G$, and $C_{R,\phi}$. The factor $C_{R,\phi}$ includes two factors, $L_{AT}$ and $\sin \phi$, which depend on the propagation medium altitude and terrain slope. An allowance of 0.2 dB for temporal errors in the sine of the incidence angle $\phi$ is included in the budget. Errors due to local slope variations, which contribute an independent component of error, are not included in the budget. Thus, errors caused by rough terrain are treated as part of the characteristic reflectivity

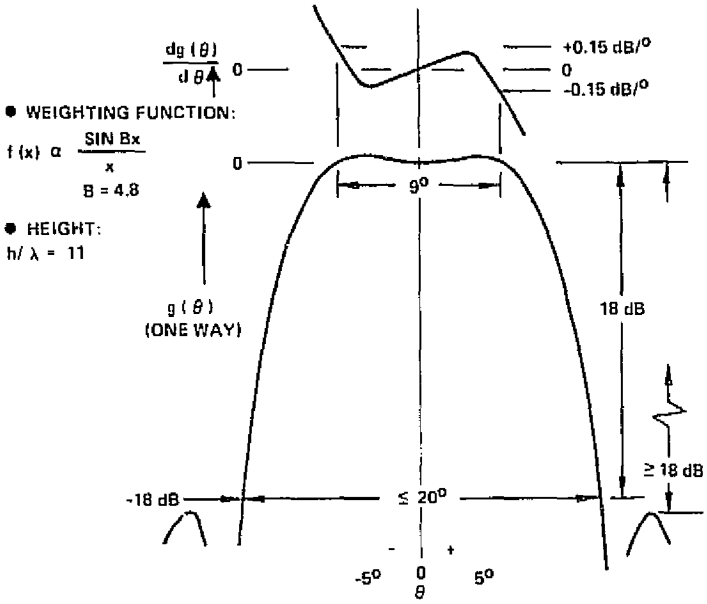

Figure 31. Antenna weighting to control gain slope

of the terrain. The effects of errors in this term are most severe near vertical incidence (small look angle $\beta$), as shown in Figures 32 and 33 and Table 13. The atmospheric loss factor $L_{AT}$ in $C_{R,\phi}$ is relatively insignificant at L-band but is a relevant contributer at X-band and shorter wavelengths, especially for operations with cloud cover. Propagation loss variations with spatial and temporal distribution of condensed water vapor in the cloud cover contribute the independent component of error for X-band. The loss factor estimates assume compensations for propagation losses with accuracies of ±0.2 dB at X-band for areas roughly 100 km square. The mean error of the compensation is estimated to be near zero over the duration of a mission.

Propagation losses are shown in Figure 34 for several models of Southeast Asia and Central Europe weather conditions.[*] These models substantiate the propagation loss estimates; they show reasonable expectations (annual occurrence rates of at least 15 percent) for weather conditions (e.g.,

---

[*] Capt. P. J. O'Reilly, "Adverse Weather Models," USA Environmental Technical Application Center Report 6467, October 1970.

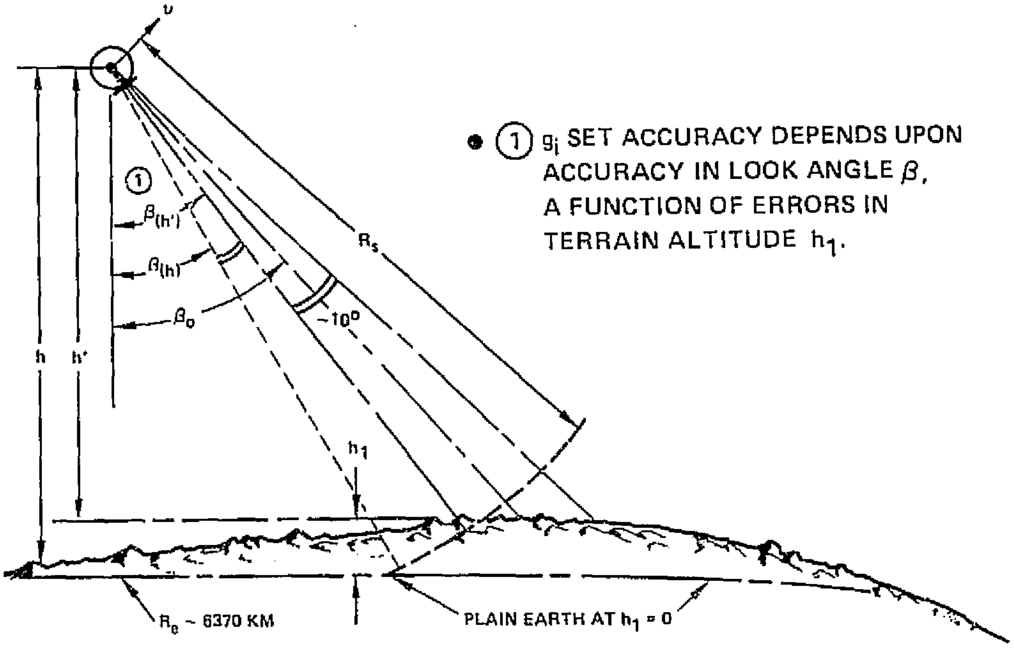

● ① $g_i$ SET ACCURACY DEPENDS UPON ACCURACY IN LOOK ANGLE $\beta$, A FUNCTION OF ERRORS IN TERRAIN ALTITUDE $h_1$.

Figure 32. Terrain altitude and slope errors

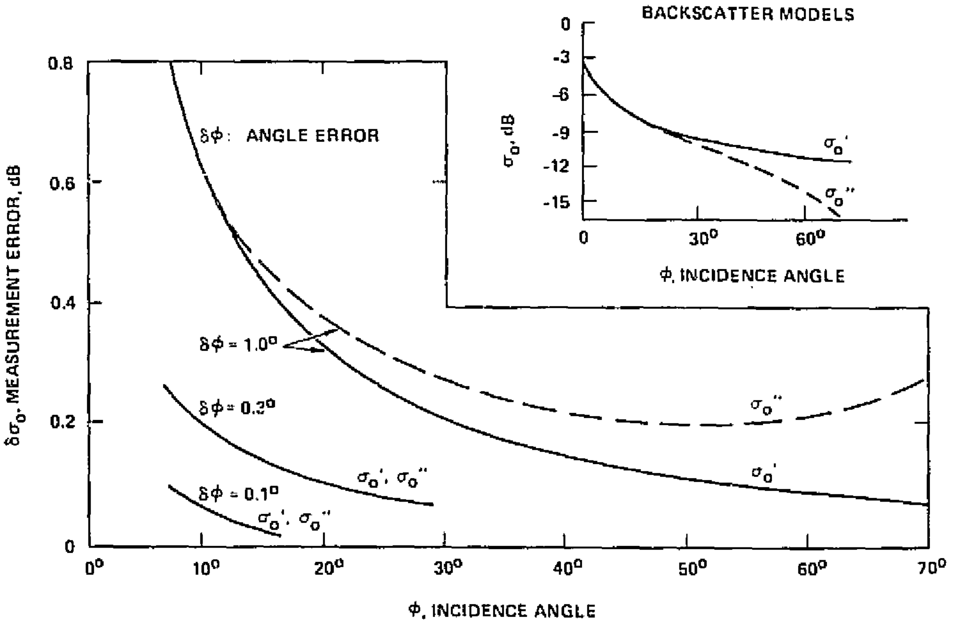

Figure 33. Error in $\sigma_0$ measurement caused by errors in incidence angle

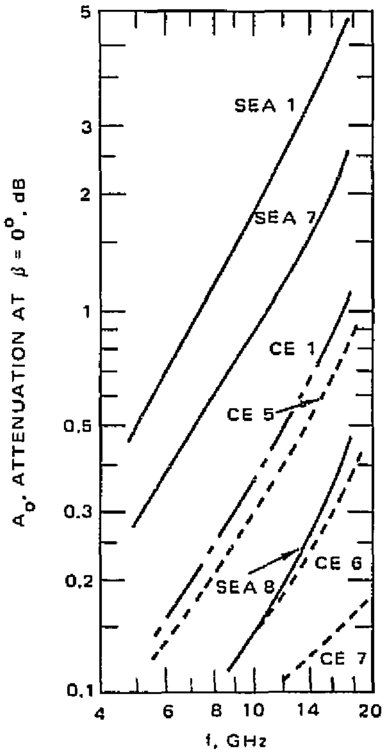

NOTES:

MODELS:

| | |
|---|---|
| SEA 1 | LIGHT TROPICAL RAIN (~5%) |
| SEA 7 | MOIST LOW STRATUS CLOUDS (~15%) |
| SEA 8 | CLEAR (SOUTHEAST ASIA 8-14%) |
| CE 1 | LIGHT RAIN (CENTRAL EUROPE, ~5%) |
| CE 5 | THIN MOIST STRATUS CLOUDS (15-20%) |
| CE6 | THIN STRATUS CLOUDS AND LIGHT FOG (~17% |
| CE7 | CLEAR, DRY WITH HAZE AND SMOKE (24-38%) |

TWO-WAY PATH ATTENUATION:

$A$ (dB) $\simeq A_o$ SEC $\beta, \beta$: VERTICAL

LOOK ANGLE

AT $\beta = 40^o$ (H = 200 KM):

$A \simeq 1.33\ A_o$, dB

Figure 34. Propagation loss for southeast Asia and Central Europe weather models

### TABLE 13. TERRAIN ALTITUDE AND SLOPE ERROR CONSTRAINTS

AT ORBIT ALTITUDE 200 km:

NEED: 1. $\Delta\beta \leqslant 0.3^\circ$ $\beta < 20^\circ$,; $\Delta\beta \leqslant 0.1^\circ$ $\beta > 40^\circ$

2. $\Delta(\mathrm{SIN}\ (\phi)) \leqslant$ 5% (0.2 dB):

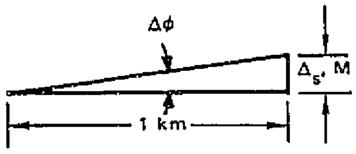

| LOOK ANGLE, $\beta$, DEGREES | $\Delta h_1$ FOR: | | SLOPE ERROR $\Delta s$ FOR SIN ($\phi$) ERROR = 0.2 dB |
|---|---|---|---|
| | $\Delta\beta = 0.3$ | $\Delta\beta = 0.1^\circ$ | |
| 10 | 185m | -- | 8.1 m/km |
| 20 | 361m | 120m | 16.7 m/km |
| 40 | 675m | 225m | 39.1 m/km |
| 60 | -- | 302m | 86.1 m/km |

DESIRED KNOWLEDGE:

1. ALTITUDE ACCURACY: ± 200m
2. SLOPE ACCURACY: ± 12m/km, $\beta < 20^\circ$
   TO ± 40m/km, $\beta > 40^\circ$

moist cloud cover) with significant propagation losses for SAR carrier frequencies above 6 GHz.

System parameters of wavelength $\lambda$, pulse-repetition frequency PRF, pulse compression bandwidth, and range are determined to the precisions of stable reference frequencies used in the SAR sensor. The contributions of these sources to error in the $C_{R,\phi}$ parameter are estimated at 0.1 dB for the mission and for the temporal ($\epsilon_{10\ sec}$) components. The equivalent accuracy for range determination is a standard deviation of roughly 200 m (orbit altitude = 200 km). Resolution parameters should be determined with accuracies of 0.5 percent or better.

The $C_S$ component of the radar parameter $K_{rad}$ is determined with the pilot mode calibration routine, discussed in Section 3.1. The pilot mode routine uses precise instrumentation, which is tested and certified for accuracy in situ and which uses thermal control as necessary to ensure stable measurement data for transmitter power-receiver gain products. Measurements are performed at adequate signal-to-noise ratios (at least 13 dB) and with a sufficient number of sample points (at least 100) to ensure a standard deviation less than 0.1 dB for each set of calibration data. The pilot mode calibration routine is repeated at sufficiently short (e.g., 5 minutes) intervals to account adequately for any uncompensated drifts. Transmitter power data are recorded concurrently with SAR sensor data to permit compensation for temporal variations in this factor. The temporal component of this source of error is estimated at 0.15 dB. The in situ calibrations of the pilot signal generator, performed before and after each mission, are estimated to be accurate to ±0.25 dB RMS.

The $C_S$ component of the radar parameter $K_{rad}$ is essentially antenna peak gain $G_o$. $C_G$ is calibrated with SAR sensor data from a corner reflector farm or equivalent facility. This calibration with SAR sensor data is supplemented by analysis based on known properties of the antenna and thermal and mechanical test data.

The accuracies that can be expected of this parameter without calibration (using corner reflector farm data) are uncertain and depend on the type of antenna, thorough thermal and mechanical designs and extensive ground test data. The performance of the antenna can be estimated only after study of detailed designs of the antenna structure, its operational (deployed) configurations, and relevant shuttle and space environmental factors.

Repeated calibrations with corner reflector farm data are needed to provide knowledge of the antenna gains throughout a mission. The precision of calibration with the corner reflector farm data is estimated below at ±0.63 dB RMS, for one corner reflector and four independent looks.

Calibration precision of 0.3 dB for $C_G$ is possible with data from a corner reflector farm of 16 standard cross section targets and planar array antennas. The temporal error in antenna gain is estimated at 0.2 dB, compensated as needed for known thermal stresses.

## Calibration Accuracies with Corner Reflector Farm Data

The factors $C_S C_G$ in $K_{rad}$ are measured with corner reflector farm data. Consider the square of the amplitude measured with four looks for a single corner reflector of cross-section $\sigma_k$:

$$\overline{E}_k = \frac{P_T(\lambda G_o)^2 \Gamma_r \sigma_k \sum_{i=1}^{4} g_{i,k}^2}{L_{SYS}\,(4\pi)^3 R_k^4 L_{AT}} N_{pc}^2\, N_{pulses}^2 \qquad (30)$$

where the radar parameter symbols stand for transmitter power (peak) $P_T$, receiver gain $\Gamma_r$, peak antenna gain $G_o$, relative gain for the i-th look at the k-th corner $g_{i,k}$, wavelength $\lambda$, system losses $L_{SYS}$, propagation loss $L_{AT}$, and range $R_k$. $N_{pc}$, $N_{pulses}$ are the number of received signal samples processed for pulse (range) compression and for the SAR azimuth compression, respectively. Let

$$G_k^2 = \sum_{i=1}^{4} g_{i,k}^2$$

then

$$\overline{E}_k = \frac{C_S C_G G_k^2 \sigma_k}{(4\pi)^3 R_k^4 L_{AT}} \qquad (31)$$

and the estimate $\overline{C_S C_G}$ for the parameter $C_S C_G$ is

$$\frac{(\lambda G_o)^2\, P_T \Gamma_r\, N_{pc}^2\, N_{pulses}^2}{L_{SYS}} = \frac{(4\pi)^3}{16} \sum_{k=1}^{16} \frac{R_k^4\, L_{AT}\, \overline{E}_k}{\sigma_k\, G_k^2} \qquad (32)$$

Estimated errors for measurements with data from a single corner reflector are tabulated in Table 14. Component errors are caused by measurement noise, target position and motion relative to image cell coordinates, also to faulty compensation for background clutter plus receiver noise bias, and the error in the estimate of the radar cross section of the corner reflector.

The measurement error, estimated at 0.31 dB, is limited by the finite signal-to-total noise (clutter + receiver noise) with which each of the four looks at the corner reflector can be made. The cross section of the corner reflector is specified at 5000 $m^2$ to realize an effective measurement SNR of 20 dB in practical clutter backgrounds ($\sigma_o \leq -12$ dB for reasonably smooth surfaces).

TABLE 14. STANDARD TARGET MEASUREMENT ERRORS

| Measurement: Apparent Radar Cross Section: | | |
|---|---|---|
| | Budgeted Error, dB | |
| Source of Error | Total RMS | $\sqrt{\text{Variance}}$ |
| Measurement of Power* | 0.31 | 0.31 |
| Position in Cell | 0.15 | 0.15 |
| Migration in Cell | 0.15 | 0.15 |
| Background Measurement Error** | 0.04 | 0.04 |
| Corner Reflector Cross Section Error# | 0.5 | 0.2 |
| Net RSS | 0.63 | 0.43 |

*4 independent measurements per target at signal-to-(clutter + noise) ratio = 20 dB

**Background $\sigma_o$-measurement from area 150 x 150 m minimum with measurement accuracy ≤ 2.8 dB at 80 percent confidence

#Corner cross section ≥ 5000 $m^2$, symmetry axis aligned to ±10 degrees (two planes)

The error in the estimate for $\sigma_k$ includes components caused by faulty knowledge of target position in the resolution cell and uncompensated motion of the target relative to the image cell. These components of error are minimized by positioning the cell at the target coordinates throughout the measurement. The errors in positioning and migration compensation are estimated at ±15 percent of the resolution (25 x 25 m) for positioning and 10 degrees quadratic phase error for migration.

The background clutter and receiver noise bias errors are compensated with residual errors that are essentially zero at reasonable signal-to-total noise ratios and for practical accuracies in the estimation of the bias component. The estimate is made in a region of at least six by six resolution cells surrounding the target cell.

The apparent radar cross-section of the corner reflector includes errors caused by imprecision in the corner reflector construction and calibration and survey errors. The corner reflectors should be aligned with their symmetry axes in the direction of SAR viewing and the aspect presented by the corner reflectors accurately surveyed to allow for any misalignment. Alignment should be no worse than ±10 degrees to minimize the contribution of uncompensated alignment errors.

The parameters $G_k^2$ are estimated with the data for the 16 corner reflectors, using the method described in Section 3.2.

The errors given in Table 14 are independent with respect to measurement of peak antenna gain and related factors in the parameters $K_{rad}$. This statistical independence is assured by spacing the nearest neighbor corner reflectors at many resolution cells, about 30 cells or 750 m for the proposed corner reflector farm.

The estimated resultant measurement accuracies for the factors $C_S C_G$ using the corner reflector farm of 16 standard cross section targets are 0.28 dB at L-band and 0.34 dB at X-band, assuming measurements are made with an error in propagation loss estimates for X-band. The calibration accuracies for these factors are approximately 0.3 dB for measurements made in clear atmospheres. In all cases, local atmospheric and

and terrain conditions relevant to measurement accuracy are appropriately monitored. The estimated measurement accuracies are given below:

Independent component errors $\frac{E_k}{\sigma_k}$ @ 0.64 dB:--0.17 dB

| | | |
|---|---|---|
| Correlated errors $L_{AT}$, $R_k$, $G_k$: | L-band<br>X-band | 0.23 dB<br>0.30 dB |
| Net RSS for $(\lambda G_o)^2 P_T \Gamma_r / L_{SYS}$: | L-band<br>X-band | 0.28 dB<br>0.34 dB |

## Measurement Accuracy

Measurement accuracy is the aggregate of two accuracies. One is the accuracy of $\sigma_o$-measurement caused by finite signal-to-noise ratio and area, discussed in Section 4.2 for a near optimum algorithm and the baseline algorithm. The second is the accuracy attributable to calibration. Comparisons of the two algorithms are presented for two areas: 100 by 100 m (four by four cells of 25 m resolution) and 150 by 150 m (six by six cells). In both cases, four looks at 45 percent overlap and a peak signal-to-noise ratio of 8 dB are assumed. The results are given in Table 15.

The independent component of error includes the scintillation component caused by receiver noise and the finite, diffuse scattering surface for the $\sigma_o$-measurement. The accuracies are expressed in dB as 10 log (U/L) where the intervals U to L are the 80 percent confidence intervals of mathematical statistics:

$$\frac{U}{L} = \frac{1 + 1.282\ \sigma_x}{1 - 1.282\ \sigma_x} \qquad (33)$$

---

*The L-band error caused by Faraday rotation in the ionosphere is negligible for low orbit altitudes of 200 km. At low L-band frequencies near 1 GHz, compensation for Faraday rotation is necessary for orbit altitudes greater than about 500 km, at least for daylight hours.

TABLE 15. $\sigma_o$ MEASUREMENT ACCURACY AT 8 DB S/N

| $\sigma_o$ Measurement Algorithm | Ground Region Dimension, m | $\sigma_o$ Measurement Accuracy ($\frac{U}{L}$ at 80 Percent Confidence, dB) | | | | |
|---|---|---|---|---|---|---|
| | | Absolute Accuracy, dB $V_{ar}(\overset{\omega}{\sigma}_o)$ | | Mission Component, dB $V_{ar}(\epsilon_{MIS})$ | Independent Component, dB $V_{ar}(\epsilon_I)$ | |
| | | L-Band | X-Band | L and X-Band | L-Band | X-Band |
| Baseline | 100 x 100 | 3.9 | 4.0 | 1.3 | 3.1 | 3.1 |
| Baseline | 150 x 150 | 2.6 | 2.7 | 1.3 | 1.6 | 1.7 |
| Near Optimum | 100 x 100 | 2.7 | 2.8 | 1.3 | 1.7 | 1.8 |
| Near Optimum | 150 x 150 | 2.36 | 2.44 | 1.3 | 1.27 | 1.34 |

where

$$\sigma_x(\mathrm{dB}) = 10 \log (1 + \sigma_x)$$

$$\sigma_x^2 = \mathrm{Var}\,(\overset{\omega}{\sigma}_o)_{4m}$$

and m is the number of cells in the area imaged at 4 looks for $\sigma_o$-measurement. The factor 1.282 is the units of standard deviation required for 80 percent confidence. The variance $\sigma_x^2$ is the sum of the variance for ideal data (perfect calibration) and the variance due to the calibration error.

The mission component is simply the calibration error expressed in terms of the 80 percent confidence interval for calibration error ($\sigma_x = 0.49$ dB). It represents the very best absolute accuracy that can be expected with 80 percent confidence for the aggregate of $\sigma_o$-measurements from all available terrains of common $\sigma_o$ imaged during a single mission.

The absolute accuracy is the aggregate of the variances for the independent component, the mission component and the temporal component errors:

$$\sigma_{XA}^2 = \sigma_{XI}^2 + \sigma_{XMIS}^2 + \sigma_{XT}^2$$

The slight difference in $\sigma_o$-measurement accuracy between X- and L-band is caused by the inclusion of an atmospheric propagation loss error (0.2 dB) at X-band. This error occurs because of the needed compensation of propagation losses at X-band for average expected atmospheric conditions over a substantial area (e.g., about 10,000 square kilometers); errors also accrue from the inevitable local variations in cloud thickness, moisture content, etc. It is noted that the effect of this error is barely perceptible in the aggregate calibration error, a net RSS error of 0.67 dB at L-band and 0.70 dB at X-band. Under more adverse conditions that include moisture laden clouds the situation degrades; with moderate to heavy precipitation, the X-band accuracy suffers greatly (see Figure 34).

The advantage of the near optimum algorithm as compared to the baseline algorithm for $\sigma_o$-measurement is evident for the 1 hectare area (100 x 100 m), which has an 80 percent confidence accuracy of 2.7/2.8 dB for the near optimum compared to 3.9/4.0 dB for the baseline; or, in terms of area, 2.25 hectares for the baseline compared to 1 hectare ($10^4 m^2$) for the baseline algorithm. At the larger area of 2.25 hectares (150 x 150 m), the advantage of the near optimum algorithm is less but still significant. The independent component of errors exhibits comparable advantages.

# 5.0 IMPLEMENTATION

Precision space calibrator equipments and standard radar cross section targets must be developed to implement the baseline calibration systems recommended for the shuttle imaging radar. One or more sites for the corner reflector farm should be developed and surveyed as well.

The space calibrator equipments should be developed and fully evaluated well before they are integrated with the shuttle sensor. The evaluation should be thorough and should consider both accuracy and thermal characteristics. The space calibrator hardware should be calibrated in situ before the first mission, and the relevant calibration parameters should be certified.

The standard cross section targets and their mountings should be carefully designed, with careful attention to cross section accuracy. The corner reflectors must be rugged and precise and be stable with respect to effective radar cross section. Radar cross sections are ideally identical; each target should be calibrated and the cross section should be certified for use in shuttle calibration operations. Provision should be made for precise orientation of the corner reflectors relative to calibration geometry. The corner reflectors and their mountings should be designed to facilitate survey and inspection services appropriate to shuttle calibration operations.

Task descriptions and estimated schedules for the development of the elements of the baseline calibration systems are presented below.

## 5.1 TASK DESCRIPTIONS

### Space Calibrator

The space calibrator devices that require development and evaluation are listed below:

1. A power measurement device, for comparing two power sources and for setting a reference power level. This device should perform the equivalent power measurement and set functions described in Section 3.1.
2. A device for generating range delayed pilot signals, which are precise replicas of an input reference waveform. This device should perform the equivalent pilot signal record data source functions described in Section 3.1.

The critical tasks are listed below:

1. Develop the power measurement and pilot signal generator devices described above.
2. Develop, evaluate and calibrate the input and output hardware required to integrate the calibration devices into the SIR sensor.
3. Evaluate the thermal characteristics and the accuracy limitations of the developed devices.
4. Develop a practical thermal control system to use with the SIR calibration devices.
5. Produce and evaluate serviceable models of the calibration devices.
6. Perform and certify calibration of the service models of the calibration devices.

### Corner Reflector Farm

The corner reflector farm tasks that must be performed for implementation of the baseline calibration subsystems are given below:

1. Select candidate sites for corner reflector farms. The sites must be free of elements that could be the source of substantial threats to the integrity of calibration of the target radar cross sections. They should permit locating targets in regions of low reflectivity where they are free from interference (i. e., no villages, farm buildings, radar sites, etc.). Atmospheric conditions should be generally stable and reliable estimates of tropospheric propagation losses should be available.

2. Develop electrical and mechanical designs of standard cross section targets. Radar cross sections should be 1000 $m^2$ minimum (about 5000 $m^2$, preferably) at the assigned wavelengths; cross section stability should be assured with suitably rugged construction. The targets should be portable and mounted to facilitate alignment and inspection.
3. Develop designs for mounting fixtures. The designs should facilitate alignment and inspection. Multi-path interference should be precluded; target heigth and a mounting base of suitable configuration may be useful for this purpose, as described in Section 3. 3.
4. Construct and calibrate the standard cross section targets.
5. Install the corner reflectors in assigned sites and determine locations.

Corner reflectors should be aligned, with the target axis of symmetry colinear with the radar line of sight, before each calibration. Survey data of target coordinates, radar cross section, and orientation should be certified for use in SIR radar parameter calibrations.

## 5.2 SCHEDULES

### Space Calibrator

It is estimated that the development of the space calibrator devices described above will require nine months, including time needed for calibration and certification of service models. An implementation schedule is shown in Figure 35.

### Corner Reflector Farm

Implementation of a corner reflector farm is expected to require six months, including time for installing the standard targets in a selected site. Separate sets of 16 targets are needed for each wavelength of dual L-, X-band SIR sensors, as discussed in Section 3. 3. An implementation schedule for the corner reflector farm is given in Figure 36.

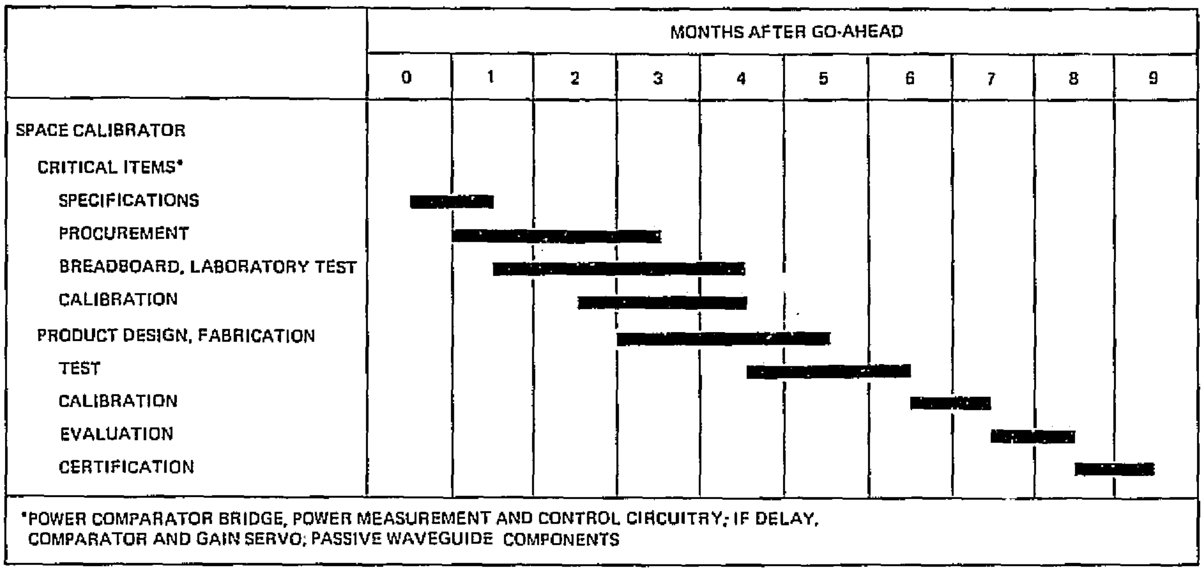

Figure 35. Space calibrator implementation schedule

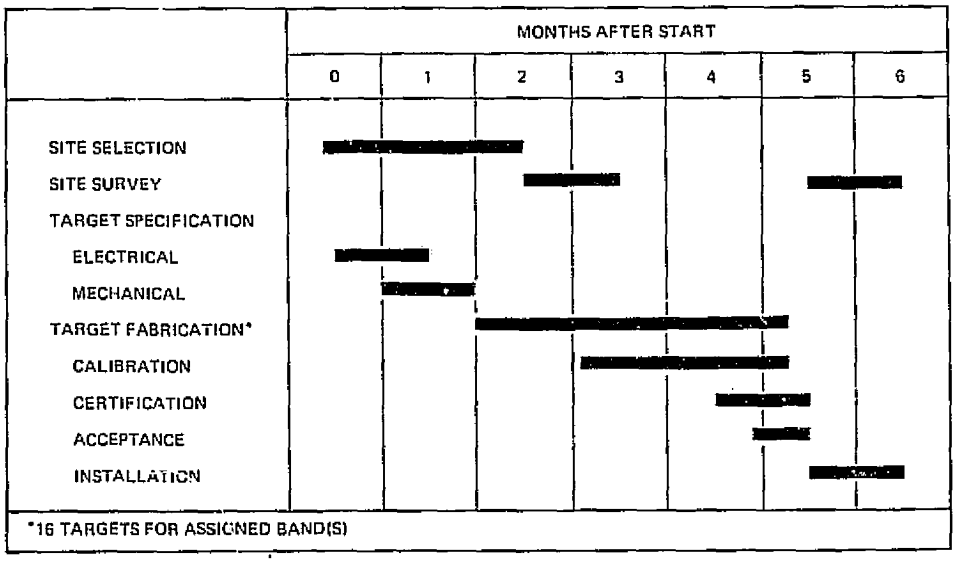

Figure 36. Corner reflector farm implementation schedule